Long-term morphological response of tide-dominated estuaries

Ilaria Todeschini

UNIVERSITÀ DEGLI STUDI DI TRENTO
Dipartimento di Ingegneria Civile
e Ambientale

2006

Doctoral thesis in **Environmental Engineering** (XVIII cycle)
Faculty of Engineering, **University of Trento**
Year: **2006**
Supervisor: **Prof. Marco Tubino**

Università degli Studi di Trento
Trento, Italy
2006

Contents

1 Introduction

Estuaries have been important to mankind for a long time, either as places of navigation or as locations on their banks for towns and cities. For millennia, in fact, estuaries have been sites of intensive human settlement and of large-scale irrigated agriculture and, more recently, they have encouraged the growth of large urban and industrial centers. Given the extent of this development, it is not surprising that estuaries exhibit many environmental problems related to the effluent of industrial processes or domestic waste; moreover they are prime sites for reclamation in order to create further land for industry or agriculture. Against this background, other functions of estuaries have attracted the attention of biologists: they can be seen as vital feeding areas for many species of birds, locations of coastal fisheries or fascinating areas that represent a challenge to understand how animals and plants are able to adapt in these environments (McLusky, 1989). The are characterized by a constantly changing mixture of salt and fresh water and by the presence of fine sedimentary material, carried into the estuary from the sea and from the rivers, that accumulates inside the estuarine channel to form mudflats. The mixtures of salt and fresh water represents an obstacle for many species of animals whose physiology is not able to adapt to. Moreover the mudflats contain areas that are very rich in food but law in oxygen or in some cases even anoxic. Despite these peculiarities that seem to hinder the development of the ecosystem, the estuaries have been claimed to be the most productive natural habitats in the world. They are characterized by having abundant populations of animals but with relatively few species.

These natural characteristics and the relationship with the human presence explain the great interest that has been reserved to the understanding and the analysis of these particular environments. The study of their morphology appears to be a very interesting issue: on the one hand, the intense human activities to which estuaries have often been subject have strongly influenced their morphological behaviour. On the other hand such systems have had a strong impact on human activities; an example is the case of the city of Bruges, formerly an important commercial harbour, which lost its commercial role

during the fifteenth century when the tidal channel joining the city to the sea filled in with sediments.

The prediction of the morphological evolution of these environment is a very complex subject since it involves many different spatial and temporal scales. The scale cascade introduced by de Vriend (1996) provides a classification for the morphological features at different levels:

Micro-scale is the level typical of the smallest-scale morphological phenomena as the ripple and the dunes.

Meso-scale is the level that characterizes the principal morphological features as channels and shoals, in which typically the temporal time scale is of the order of years and the spatial scale of the order of the channel width.

Macro-scale is the level at which these features interact.

Mega-scale is the level that characterizes the main elements of the entire system, in which the temporal scale is of the order of centuries and the spatial scale of the order of the entire length of the system.

The problem of the long-term morphological response of estuarine channels is the subject of this thesis. The study is tackled at the mega-scale level in order to investigate the morphodynamic evolution of the entire estuary. The existence of equilibrium configurations is quite a relevant subject because it has strong practical implications in the management of these tidal systems.

Many contributions have been proposed to investigate the morphological evolution of estuarine channels (Friedrichs and Aubrey, 1994; Lanzoni and Seminara, 1998; Schuttelaars and de Swart, 1999; Schuttelaars and de Swart, 2000; Lanzoni and Seminara, 2002). The attention has been mainly focused on the case of well-mixed, tide-dominated estuaries, characterized by a given funnel shape, negligible river discharge and mild bottom slope. The interest for the study of such class of estuaries is motivated by the fact that, in nature, many estuaries display a typical funnel shape. Several important harbours in Europe are located on tide-dominated estuaries (Antwerp, Hamburg, Bordeaux, London). Nevertheless, in spite of its relevance and of the interest that has been reserved to it, the problem of the morphological evolution of a tide-dominated estuary still awaits for a complete investigation. In particular, it is well known that channel convergence may strongly affect the hydrodynamics of estuaries (Friedrichs and Aubrey, 1994; Friedrichs et al., 1998; Lanzoni and Seminara, 1998; Toffolon et al., 2003). Its role on the morphological evolution of tidal channels, which was neglected in previous morphological analyses, like that of Schuttelaars and de Swart (2000), has been highlighted by Lanzoni and Seminara (2002)

though the limited number of simulations they consider does not allow one to fully recognize the role of the different parameters which characterize the system (e.g. the tidal forcing, the length of the system, the degree of convergence).

In the first part of this thesis, in order to study the propagation of the tidal wave into a convergent channel and to analyse its consequent morphological evolution, a one-dimensional model is adopted. This kind of schematization is typically used to describe the behaviour of well-mixed systems with regular channels where the flow can be supposed to occur along one preferential direction. One-dimensional models have the advantage of simplicity and imply a smaller computational time with respect to two- and three-dimensional schemes. They appear to be a useful tool to investigate the morphological evolution of a tidal channel if the flow conditions are not complex.

In this analysis the estuary is schematized as a rectangular cross-section channel with fixed banks. This simplifying schematization may be rather rough, since it implies that the model is unable to account for topographically driven effects on the flow field as well as to include the role of shallow areas adjacent to the main channel. For a more refined approach, the one-dimensional global model should be coupled with a "local" model based on a characteristic length scale of the order of channel width in which the above effects can be considered. Otherwise the presence of tidal flats flanking the main channel can be accounted for with a modification of the continuity equation (Speer and Aubrey, 1985; Shetye and Gouveya, 1992). The one-dimensional model is used to investigate the effect of the different external parameters on the equilibrium bottom profiles of a convergent channel. Moreover the influence of the boundary conditions is analyzed.

The fixed bank model provides interesting results that are useful to understand the equilibrium configurations of convergent channels but it is obviously unable to explain the reasons for the planimetric funnel shape of tide-dominated estuaries. Therefore, in the second part of the thesis, the hypothesis of fixed banks is removed in order to identify the conditions under which the exponential law for width variation, which is so often observed in nature, is reproduced. In literature most of the models are based on the assumption of fixed banks. Various attempts to reproduce the equilibrium cross section of tidal channels have been pursued (Fagherazzi and Furbish, 2001; Gabet, 1998); the above analyses mainly focus on the local scale, hence the full coupling with the morphological evolution of the channel is not taken into account. On the other hand, several contributions already exist in the case of rivers. In order to obtain a single model that, although very simple, is able to couple the morphological evolution of the bottom and of the banks profiles, a lateral erosion law for width variation is introduced. The equilibrium configurations of bottom

and width profiles and the role played by the parameters that characterize the system is examined in detail.

1.1 Thesis Structure

This thesis is organized as follows: in Chapter 2 an introduction to the definitions and the classifications of estuaries is reported; moreover the bathymetries of some real tide-dominated estuaries are analyzed to point out the peculiarities of this class of estuaries. In Chapter 3 a brief review of some of the most significant papers related with the study of the morphological evolution of tidal channels is presented. For convenience, they have been grouped in a few broad topics: the hydrodynamics and the propagation of the tidal wave into the estuarine channel, the relationship between asymmetries in tidal currents and sediment transport and the morphological evolution, simplified models to simulate the morphological behaviour of a tidal basin and finally the problem of the channel cross-section evolution. In Chapter 4 the adopted one-dimensional model and the corresponding numerical scheme are described; the problems connected with the choice of the boundary conditions are introduced. The results of the model in the case of a convergent estuary with fixed banks are shown in Chapter 5 where the influence of the initial and boundary conditions and of the external parameters is pointed out. The numerical results obtained when the width variation is taken into account are presented in Chapter 6. Also in this case, the influence of the external parameters on the bottom and banks profile is analyzed. Finally, in Chapter 7 some concluding remarks about the present model and the possible developments are made.

2 Estuaries: definitions and classifications

Estuaries are ephemeral features on geological time scales, having an average life of at most a few tens of thousand of years and generally much less; most of them developed during the latest post-glacial rise of sea-level, which inundated coastlines and drowned the mouths of river valleys. Despite this fact, they have been extremely important in the world's development given the high fertility of their waters and the navigational access they provide. Estuaries exist in many shapes and sizes, from the vast areas at the mouths of the Nile and Amazon rivers, to the narrow inlets along the steep, green coastline of the Pacific Northwest. Given this great diversity, no two estuaries are alike; besides, their river flow, tidal range and sediment distribution are continually changing and so it is very difficult to formulate general principles.

In the last decades many definitions of estuaries have been suggested; a sufficiently comprehensive definition which seems generally acceptable has been proposed by Perillo (1995): "an estuary is a semi-enclosed coastal body of water that extends to the effective limit of tidal influence, within which sea water entering from one or more free connections with the open sea, or any other saline coastal body of water, is significantly diluted with fresh water derived from land drainage and can sustain euryhaline biological species for either part or the whole of their life cycle". This definition in particular excludes costal lagoons and brackish seas: the first ones do not usually have a free connection with the open sea and may only be inundated with sea water at irregular intervals, while the second ones, as the Caspian Sea, do not experience the regular fluctuations of salinity due to tidal effects. Furthermore, the use of the term "semi-enclosed" serves to exclude coastal marine bays. In this way, estuaries is emphasized as a dynamic ecosystem having a free connection with the open sea through which the sea water can enter according to the twice-daily rhythm of the tide (McLusky, 1989). The dilution process between the sea water and the fresh water flowing into the estuary from rivers strictly depends on the volume of fresh water, the range of tidal amplitude and the extent of evaporation from the water within the estuary.

2.1 Classifications of estuaries

In literature many classifications of estuaries have been proposed in order to compare the different existing types and to set up a framework of general principles within which the prediction of their characteristics may be attempted. The possibilities in the choice of the scheme are various depending on the criteria that are used. Topography, river flow and tidal action are important factors that determine the mixing of salt and fresh water and consequently the density structure; in turn the presence of stratification influences the water circulations. These causes and effects are interlinked and it would be difficult to take account of them all in one classification system. In this section a brief review of some of the most common ones is presented.

Physiographic classification Pritchard (1952) proposes a classification according to their geological origin and distinguishes four classes: drowned river valleys, bar-built estuaries, fjords and tectonic estuaries (Perillo, 1995; Dyer, 1997).

- Drowned river valleys

  These estuaries were formed by the flooding of Pleistocene-Holocene river valleys following the sea level rise by about 100-130 m during Flandrian transgression (roughly 15000-18000 years ago). They are typically characterized by a funnel shape, depths of the order of 10 m, increasing towards the mouth and V-shaped cross sections (Figure 2.1). They are generally restricted to temperate latitudes, where the amount of sediment discharged by the river is relatively small. River flow is generally small if compared with the volume of the tidal prism. Most estuaries of the world belong to this category, as Delaware, Chesapeake Bays, the Thames and the East Alligator River (Figure 2.2).

- Fjords

  Fjords were formed in areas covered by Pleistocene ice sheets; the pressure of the ice overdeepened and widened the pre-existing river valleys. They are typically extremely deep (several hundred meters), U-shaped and bounded by steep rock walls (Figure 2.3). Because of overdeepening, fjords have a small width-to-depth ratio and steep sides. River discharge is small if compared with the total fjord volume. A shallow sill is typically present at the mouth of the estuary and constrains the tidal exchange between the estuary and the sea. Sediments are coarse at the head of the

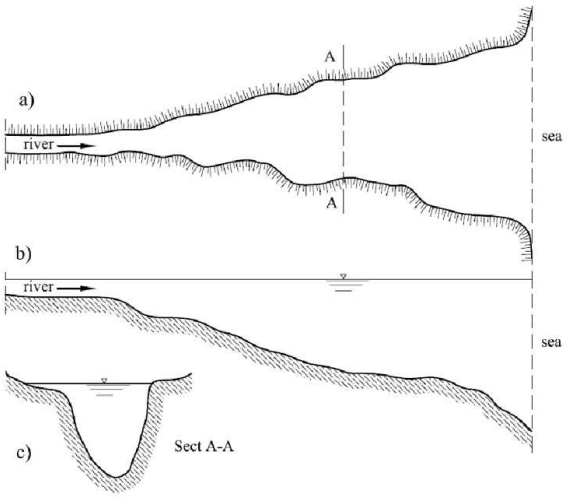

Figure 2.1: Schematic diagram of a drowned river valley estuary: a) plan view, b) longitudinal profile, c) cross-section profile (from Seminara et al., 2001).

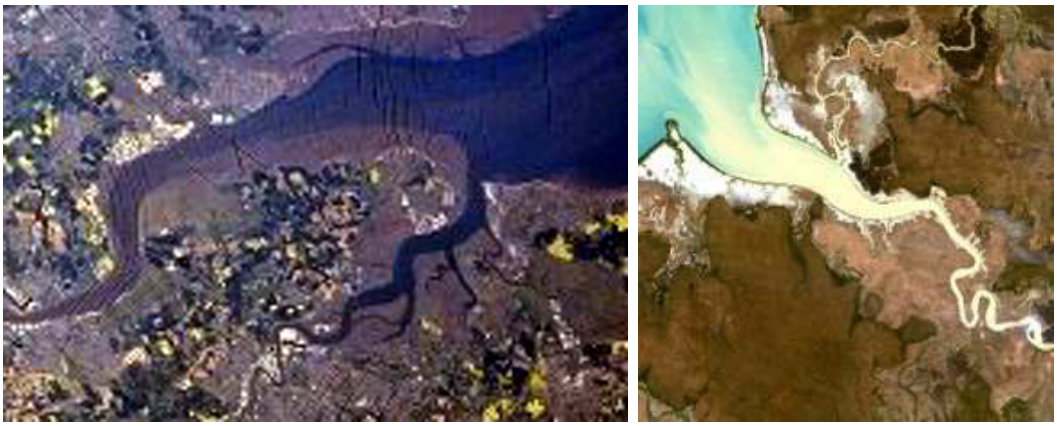

Figure 2.2: Plan view of the Thames, UK (on the left) and of the East Alligator River, Australia (on the right).

estuary, near the main river entrance, while the absence of significant water circulation leads to deposition of the fine suspended fraction along the muddy bottom. Examples of this type of estuaries are found in high latitude mountainous regions like Alaska, Norway (Figure 2.4) and New Zealand.

- Bar-built estuaries

  Bar-built estuaries are formed by the same processes as the drowned river valleys. The difference is that sedimentation has kept pace with inundation, with a character-

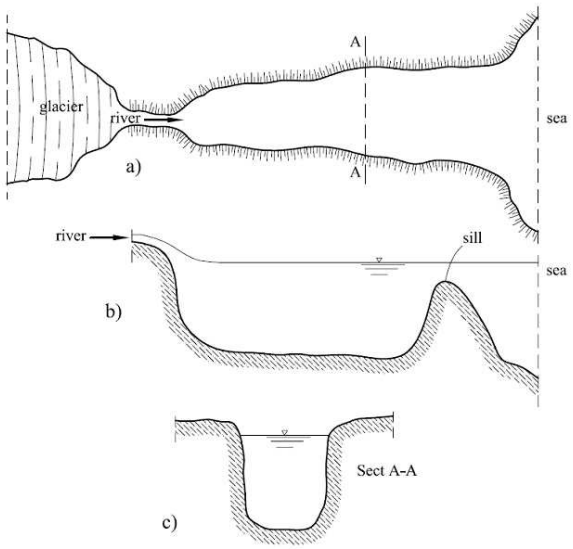

Figure 2.3: Schematic diagram of a drowned glacial valley estuary: a) plan view, b) longitudinal profile, c) cross-section profile (from Seminara et al., 2001).

Figure 2.4: Areal views of two Norwegian fjords: Stavanger (from www.fjordman.de, on the left) and Aurlandsfjord (from www.norvegiaviaggi.com, on the right).

istic bar, aligned to the coastline, forming at the mouth. Associated with depositional areas, bar-built estuaries are shallow with extensive lagoons and waterways inside the mouth (Figure 2.5). Entrance velocities can be quite high but quickly diminish as the estuary widens. They are influenced by littoral transport and wind action which plays an important role comparable with that associated with tidal motion. The embayment is most commonly bounded by tidal flats and salt marshes, dissected by

highly sinuous tidal creeks. The river flow is large and seasonally variable and large volumes of sediment are river-borne at times of flood. This type of high sediment volume estuary is most often found in tropical or active coastal deposition areas. An important example of bar-built estuary is the lagoon of Venice (Figure 2.6).

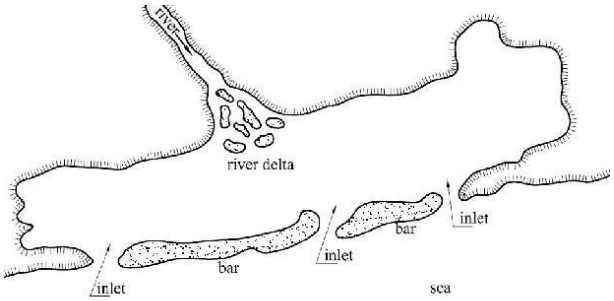

Figure 2.5: Schematic diagram of a bar-built estuary (from Seminara et al., 2001).

Figure 2.6: Plan view of the Venice Lagoon (from http://www.tu-berlin.de).

- Tectonically formed estuaries

  All the estuaries which cannot be clearly recognized as belonging to any of the

other three classes are included in this category; in particular tectonically produced estuaries, formed by faulting, landslides and volcanic eruptions. An example of this category is the San Francisco Bay, where the lower reaches of the Sacramento and San Joaquin Rivers have been drowned by movements on faults of the San Andreas fault system (Figure 2.7).

Figure 2.7: Plan view of the San Francisco Bay (from http://www.sfbayquakes.org).

Classification by tidal range Another classification, based on the tidal range, has been proposed by Hayes (1975). The intensity of the tidal currents, which are increasing functions of the tidal range, determine the intensity of the transport processes.

- Microtidal estuaries

  When the tidal range is smaller than 2 m, the estuary is described as microtidal. It is dominated by wind and wave action. When sediments and water discharge are significant, they can trigger the rapid evolution of the feature towards a deltaic environment; this type of estuaries can be associated to the bar-built estuaries of Pritchard (1952) where the principal depositional form are flood deltas, wave built features and river deltas. They are generally shallow and wide. Microtidal estuaries are generally wide (typically 10 Km) and shallow (typical depth 1 m).

- Mesotidal estuaries

When the tidal range falls between 2 and 4 m, the estuary is described as mesotidal. As form-generating agent, tidal currents are dominant over other marine, fluvial or climatic agents. A composite delta develops, which includes a landward side (called flood-tide delta) and a seaward side (called ebb-tide delta) while salt marshes and tidal flats take place at the boundaries of the estuary. The upstream reaches are usually strongly meandering. This kind of estuaries is the most common and widely studied in the world.

- Macrotidal estuaries

  When the tidal range is larger than 4 m, the estuary is described as macrotidal. It is dominated by strong tidal currents whose effect can be felt for hundreds of kilometers. Their morphology is characterized by elongated tidal bars and by a typical funnel shape; they can be associated to the drowned river valleys of Pritchard (1952).

Classification by salinity structure The mixing process between fresh water and salt water driven by the interaction between the river flow and the tidal currents is another important parameter which provides a framework for the classification of estuaries. Such mixing process also has as a great influence also on sediment transport (Dyer, 1997).

- Highly stratified or salt wedge estuaries

  When the tidal motion is small if compared to the river flow, as in the case of microtidal estuaries, the salt water forms a wedge that intrudes into the river and is separated from the upper fresh water layer by a sharp interface, which strongly inhibits the mixing between the two layers (Figure 2.8). This interface, which would be horizontal in absence of friction, becomes blunted and the water surface will slope more steeply in the seaward direction; a weak landward residual current of sea water is formed (Seminara et al., 2001). For this type of estuary, the ratio of width-to-depth ratio is relatively small. An example of highly stratified estuary is the Mississippi River.

- Partially mixed estuaries

  In partially mixed estuaries the tidal range is generally mesotidal; the spring tide currents favour the turbulent exchanges of salt and fresh water consequently reducing the stratification. The two layers are separated by a less sharp interface and both display a longitudinal salinity gradient with salinity decreasing towards the head of the estuary. The form of the vertical salinity profile does not change much along the

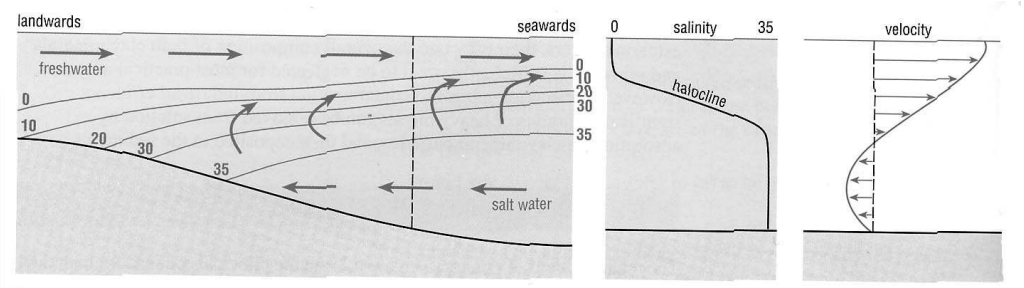

Figure 2.8: Sketch of a highly stratified estuary (The Open University, 1989).

estuary; there is normally a zone of high salinity gradient at about mid-depth and the surface and bottom layers are quite homogeneous (Figure 2.9). Seasonal variations of the degree of stratification often occur in this type of estuary. Examples of partially mixed estuary are the Mersey and the James River.

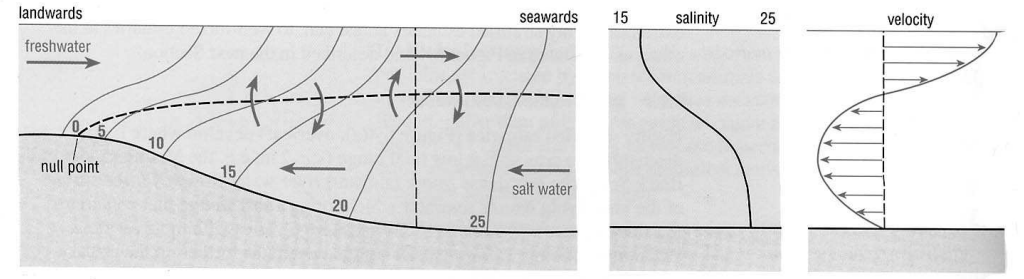

Figure 2.9: Sketch of a highly stratified estuary (The Open University, 1989).

- Well mixed estuaries

  When the tidal range is relatively large with respect to the overall water depth, especially in macrotidal conditions, turbulent energy is high enough to ensure a complete mixing within the water column such to produce vertically homogeneous salinity distribution (Figure 2.10). Lateral variations of salinity and of velocity are also induced when the width to depth ratio of the channel is sufficiently large to drive a significant secondary circulation: there can be the separation between flood and ebb dominated channels. The lower reaches of the Delaware and Raritan are examples of this type. On the contrary, when the width is smaller, lateral shear may be sufficiently intense to create laterally homogeneous conditions. Salinity increases evenly towards the mouth and the mean flow is seawards throughout the cross-sections.

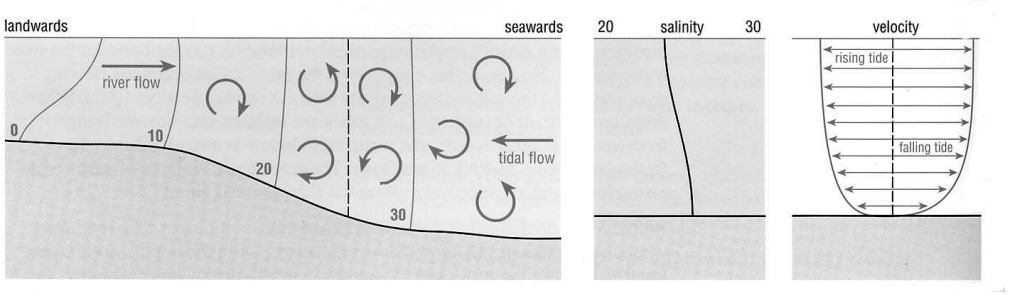

Figure 2.10: Sketch of a highly stratified estuary (The Open University, 1989).

Obviously some correspondence between the results of classification on topographical and salinity structure bases esists; but it is clear that the limits of each estuarine type are never well defined and they can be considered just a stage on a continuous sequence. The ratio between river flow and tidal flow determines to a certain extent this sequence. Dyer (1997) points out that when this ratio is equal or greater than one the estuary is highly stratified, when it is about 0.25 the estuary can be defined as partially mixed while for values smaller than 0.1 it is well mixed. This is a very general assertion that cannot be true for all the estuaries. Variations in the estuarine type are possible from section to section since near the head of the estuary, where the tidal action is reduced, a salt wedge is able to form. Downstream the velocities can increase until a partially mixed structure is realized. Also the seasonal changes can drastically influence the flow ratio and consequently the estuarine type.

In the end, the topographic differences deeply influence the flow ratio: a widening or an increase in the water depth are able to change the salinity structure of an estuary.

Evolutionary classification Dalrymple et al. (1992) propose a classification that combines the relative importance of river outflow, waves and tides with time (see also Perillo, 1995). The result is a triangular prism that represents the different coastal environments associated to these three essential parameters (Figure 2.11a). Every section of the prism corresponds to a time-independent triangle that correlates the percentage of each environment given a particular sea-level condition (Figure 2.11b). Deltas, which are dominated by rivers, are located at the fluvial apex while strand plains and tidal flats are positioned along the wave-tide side. Estuaries occupy an intermediate position because they have a mixed sediments source and the difference among them can be expressed in terms of wave or tidal dominance. The evolutionary aspect is portrayed by the third dimension, relative time, that in Figure 2.11a is expressed in terms of transgression and progradation. Thus

during progradation the estuaries are filled and they are converted into deltas or strand plain or tidal flats, while during transgression the river valleys are flooded and they are converted into estuaries.

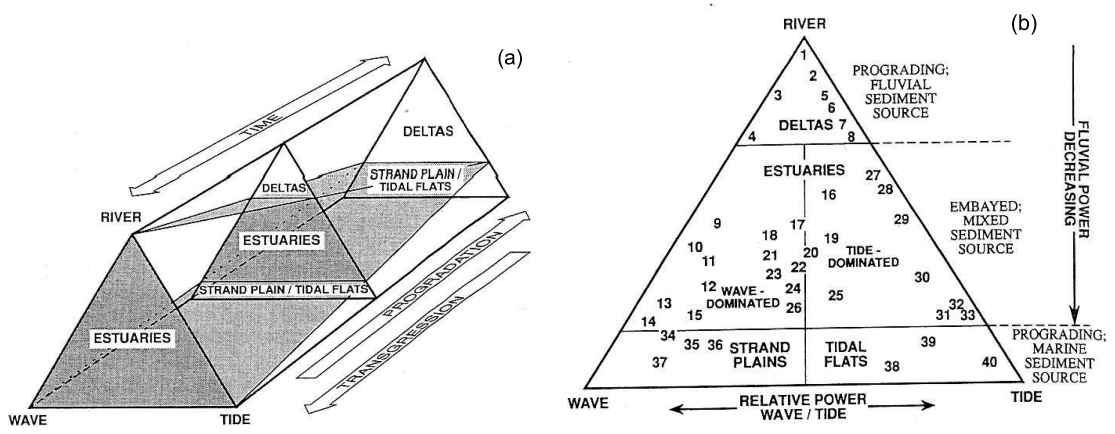

Figure 2.11: Classification of coastal environments associated to estuaries according to Dalrymple et al. (1992): (a) general classification on the basis of the relative importance of river input, wave and tidal processes and their variation in time (sea level changes); (b) a cross-section of (a) showing the classification of estuaries in wave- and tide-dominated.

- Wave-dominated estuaries

  At the mouth of a wave-dominated estuary waves are strongly dominant producing littoral transport and normally developing some kind of barrier that partially closes the mouth. This barrier prevents most of the wave energy from entering the estuary, consequently only internal generated waves are present behind the barrier. In Figure 2.12 the distribution of the dynamic processes along the estuary and of the major morphological components is illustrated. Tidal influence is limited to the seaward part of the channel and it is able to maintain open the inlet. The total energy profile shows two maxima, one at the mouth caused by the wave energy and one at the head due to river currents, while in the central zone a pronounced minimum can be found. The facies distribution are those typical of a bar-built estuary or microtidal estuary from other classifications. Flood deltas can be found near the mouth while in the central part the sedimentation of the fine sediments is dominant. At the head the river forms a delta as it enters the basin.

- Tide-dominated estuaries Tidal dominance does not require necessarily strong tidal currents or large tidal ranges; in fact sometimes a microtidal estuary with a simple

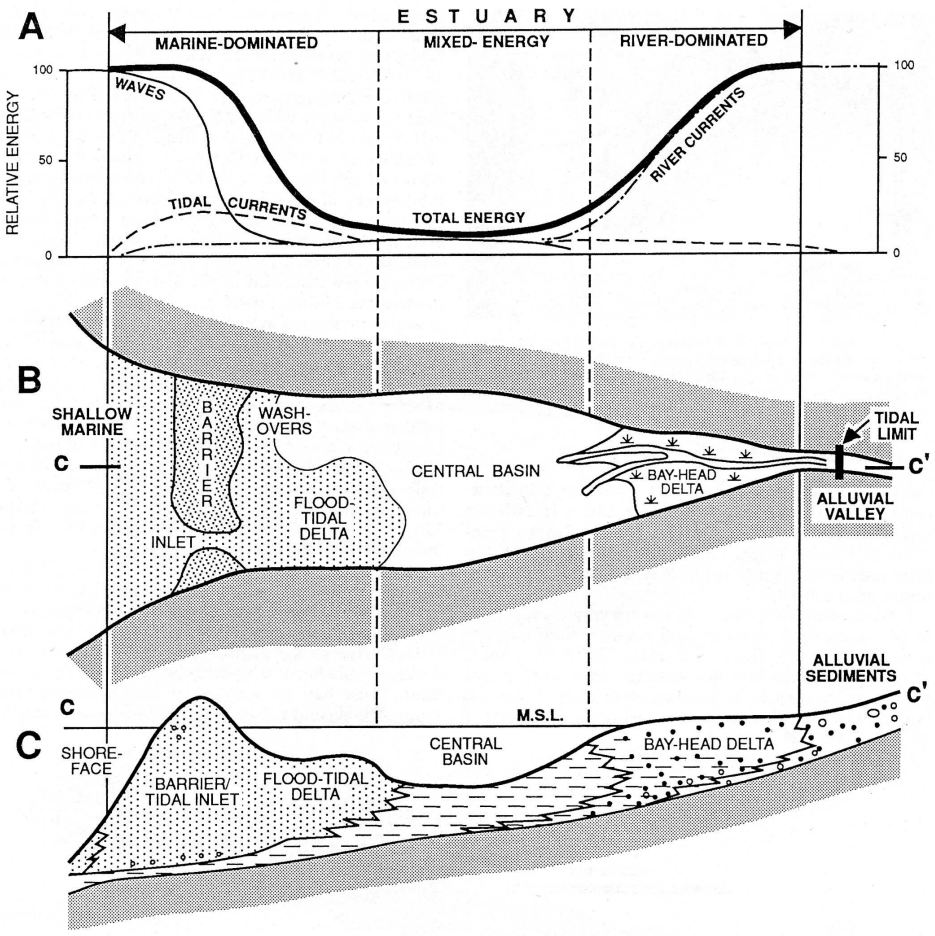

Figure 2.12: Wave-dominated estuaries: distribution of energy types **(A)**, morphological components in plan view **(B)** and sedimentary facies in longitudinal section **(C)** (from Dalrymple et al., 1992).

lack of wave activity can be tide-dominated. Near the mouth, the energy of tides and waves can be similar, but usually the tidal currents are dominant and elongate sand bars are formed; these bars dissipate the wave energy causing it to decrease with distance up the estuary. In the middle and in the upper estuary tides are absolutely dominant, as it can be seen in Figure 2.13. The total energy is about the same all along the estuary and sand sediments and facies are found to be distributed all along the estuary. The larger concentrations are located near the mouth and are reduced moving landward. Close to the minimum energy point, finer sands can be found.

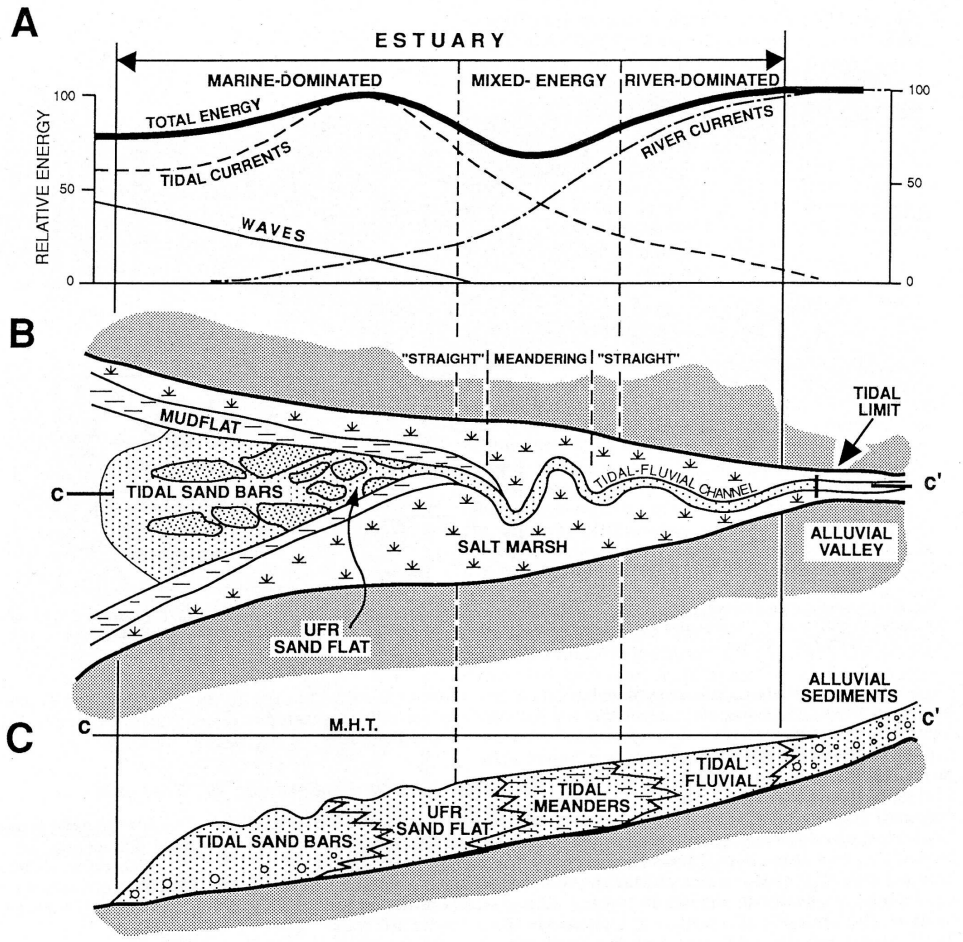

Figure 2.13: Tide-dominated estuaries: distribution of energy types **(A)**, morphological components in plan view **(B)** and sedimentary facies in longitudinal section **(C)** (from Dalrymple et al., 1992).

2.2 Tide-dominated estuaries

In this thesis the attention is focused on the category of tide-dominated estuaries. The first reason is that most estuaries of the world are influenced by tides. The tidal action, in fact, is a fundamental mechanism for mixing riverine and estuarine waters, resuspending and transporting sediments and creating bedforms. The role of tide is very complex but less studied than many other aspects that characterize the estuarine processes; this fact represents a further incentive to examine more closely this category of estuaries. Even the definition of a tide-dominated estuary, however, is not a trivial issue. In fact, tidal dominance cannot be determined only on the basis of the tidal range, given that some

macrotidal estuaries are not tide-dominated while some microtidal ones show the features of tide-dominated channels. Trying to describe them in the simplest terms, tide-dominated estuaries are those in which tidal currents play the dominant role in determining the fate of the river-borne sediments and in which density driven circulations are nearly absent because strong tidal effects are able to destroy vertical stratification. The volume of water exchanged in a tidal period in this kind of estuaries, the so-called "tidal prism", is typically an order of magnitude larger than the corresponding volume associated with the river discharge. In the section of the coastal classification prism reported in Figure 2.11b tide-dominated estuaries are located on the right side; each number corresponds to a different estuary which is briefly described in Table 2.14.

The morphology of tide-dominated estuaries is characterized in plan view by a funnel-shaped geometry with a high width-to-depth ratio. The width of the estuarine section tends to decrease rapidly upstream well approximating an exponential law (Figure 2.16). Moreover they generally exhibit non-significant bottom slopes. As one moves along the estuary, the funnel shape is replaced by an upstream pattern of sinuous channels, as it is sketched in Figure 2.15.

An important process that conditions the sediment dynamics in tide-dominated estuaries is the distortion of the tidal wave as it propagates into the channel, due to non linear effects. Flood phase is characterized by larger velocities and by a shorter duration with respect to the ebb phase. Because of the funnel shape, both the water depth and the width decrease landward and the amplitude of the tidal wave, as it propagates through progressively smaller cross-sectional areas, tends to increase. However, friction plays a counteracting effect and tends to decrease the tidal amplitude. In tide-dominated estuaries the effects of convergence usually exceed frictional dissipation and the system is defined as hypersynchronous (Wells, 1995). Tidal currents reach their maximum speed in the upper part of the estuary, until the tidal energy is exhausted and both amplitude and speed vanish in a region called the tidal node.

The asymmetric shape of the temporal velocity distribution, enhanced by channel convergence, determines a net upstream sediment flux which continues to the point where the tidal wave is damped by friction and transport is controlled only by fluvial processes. As a result of this asymmetry, the flood phase is followed by longer periods of slack water which favour deposition in the upstream part of the estuary. Usually the tidal influence becomes negligible where the typical funnel shape gives way to an upstream sinuous channel.

Tide-dominated estuaries are very common in nature; observed tidal and geometric

Number	Location	Tide	Wave	River	Reference
Deltas					
1	Mississippi Delta, USA	Low	Low	High	Wright 1985
2	Chang Jiang Delta, China	Mod	Low	High	Chen et al. 1982
3	Ebro Delta, Spain	Low	Mod	High	Maldonado 1975
4	Sao Francisco Delta, Brazil	Low	High	Mod	Coleman and Wright 1975
5	Mahakam Delta, Indonesia	Mod	Low	High	Allen et al. 1979
6	Klang-Langat Delta, Malaysia	High	Low	Mod-High	Coleman et al. 1970
7	Fly River Delta, New Guinea	High	Low	High	Harris et al. 1992
8	Colorado Delta, Mexico	High	Low	Mod-High*	Meckel 1975
Wave-dominated Estuaries					
9	San Antonio Bay, USA	Low	Mod	Mod	Donaldson et al. 1970
10	Hawksbury Estuary, Australia	Low	High	Low-Mod	Roy et al. 1980; Roy 1984
11	Lavaca Bay, USA	Low	Mod	Low-Mod	Wilkinson and Byrne 1977
12	Miramichi River, Canada	Low-Mod	Mod	Low	Reinson 1977; unpublished observations
13	Lake Macquarie, Australia	Low	Mod-High	Low	Roy et al. 1980; Roy 1984
14	Mgeni Estuary, South Africa	Low	High	Low	Cooper 1988
15	Eastern Shore estuaries, Nova Scotia, Canada	Low	High	Low	Boyd et al. 1987; Honig and Boyd 1992
Mixed-energy Estuaries					
16	St. Lawrence River, Canada	Mod	Low-Mod	High	d'Anglejan and Brisebois 1978
17	Gironde River, France	Mod-High	Mod-High	Mod	Jouanneau and Latouche 1981; Allen 1991
18	Raritan River, USA	Low-Mod	Low-Mod	Mod	Ashley and Renwick 1983
19	Humber River, GB	Mod-High	Mod	Mod	unpublished observations
20	James River, USA	Mod	Low-Mod	Mod	Nichols et al. 1991
21	Ogeechee River, USA	Mod	Mod	Mod	Dörjes and Howard 1975; Greer 1975
22	Chesapeake Bay, USA	Low-Mod	Low-Mod	Low-Mod	Biggs 1967; Colman et al. 1988
23	Delaware Bay, USA	Low-Mod	Low-Mod	Low-Mod	Knebel et al. 1988
24	Willapa Bay, USA	Mod	High	Low-Mod	Clifton 1983; Clifton et al. 1989
25	Oosterschelde Estuary, The Netherlands	Mod	Low	Low	Yang and Nio 1989
26	Corio Bay, Australia	Mod-High	High	Low	unpublished observations
Tide-dominated Estuaries					
27	Cook Inlet, Alaska	High	Low-Mod	Mod-High	Bouma et al. 1980; Bartsch-Winkler and Ovenshine 1984
28	Ord River, Australia	High	Low	Mod-High	Wright et al. 1973, 1985; Coleman and Wright 1978
29	South Alligator, Daily and Adelaide Rivers, Australia	High	Low	Mod	Woodroofe et al. 1989
30	Severn River, GB	High-Ext	Mod	Low-Mod	Hamilton 1979; Harris and Collins 1985
31	Broad Sound Australia	High-Ext	Low-Mod	Low	Cook and Mayo 1977
32	Cumberland Basin, Canada	Ext	Low-Mod	Low	Amos et al. 1991
33	Cobequid Bay-Salmon River and Avon River, Canada	Ext	Low	Low	Lambiase 1980; Dalrymple and Zaitlin 1989; Dalrymple et al. 1990
Prograding Strand Plains					
34	Senegal "Delta"	Low	High	Low-Mod	Coleman and Wright 1975; Wright 1985
35	Shoalhaven River, Australia	Low	High	Low	Roy et al. 1980; Wright 1985
36	Yaquina Bay, USA	Low-Mod	High	Low	Kulm and Byrne 1967
37	Nayarit, Mexico	Low	High	Low	Curray et al. 1969
Prograding Tidal Flats					
38	Mont St. Michel Bay, France	High	Mod	Low	Larsonneur 1988
39	Head of the German Bight	High	Low-Mod	Low-Mod	Reineck and Singh 1980
40	East coast, Taiwan	High	Low	Low	Reineck and Cheng 1978

* Before human interference.

Figure 2.14: Characteristics of the tidal systems presented in Figure 2.11 (from Dalrymple et al., 1992).

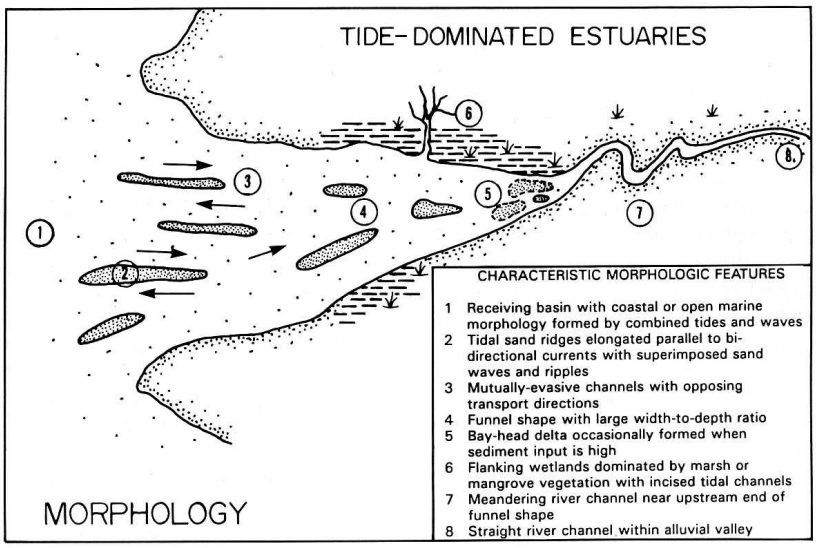

Figure 2.15: Diagram showing the morphology of a tide-dominated estuary (from Wells, 1995).

properties of some of them are reported in Table 2.1 (from Lanzoni and Seminara, 1998): despite the natural differences that can be discovered among them, their main recurring feature is the significant degree of convergence. In fact, as it will be better explained in the following chapters, the funnel shape is approximated by an exponential law and the width B^* can be described as:

$$B^* = B_0^* \exp\left(-\frac{x^*}{L_b^*}\right) \tag{2.1}$$

where L_b^* is the convergence length and B_0^* the width at the channel mouth. If it is scaled with the value at the mouth, it becomes:

$$\frac{B^*}{B_0^*} = \exp\left(-\frac{x^*}{L_b^*}\right) \tag{2.2}$$

The smaller is the convergence length, the more convergent is the channel.

2.2.1 Bathymetries of real estuaries

In order to observe the morphology of tide-dominated estuaries more closely, it is useful to examine the bathymetries of real estuaries. Although the large number of estuaries that has been analyzed thoroughly and the big amount of measurements that has been made in

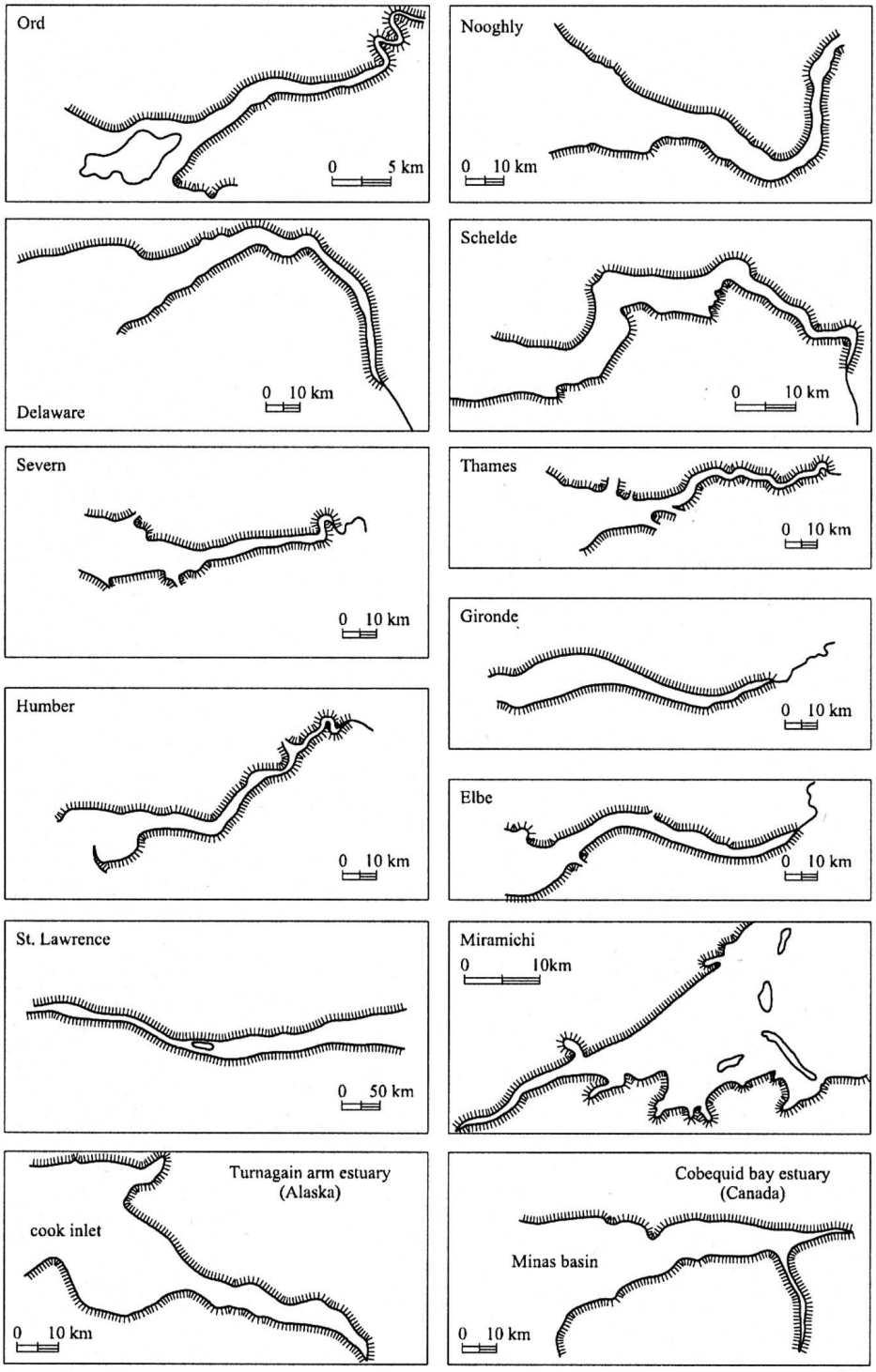

Figure 2.16: Funnel shaped estuaries (from Seminara et al., 2001).

Estuary	$a_0^*[m]$	$D_0^*[m]$	$L_e^*[km]$	$L_b^*[km]$	$U_0^*[m/s]$	C_0	$T_0^*[hours]$
Bristol Channel	2.60	45.0	80	65	1.0	20.0	12.4
Columbia	1.00	10.0	240	25	1.0	18.0	12.4
Conwy	2.40	3.0	22	6.3	0.5	14.0	12.5
Delaware	0.64	5.8	215	40	0.6	21.8	12.5
Elbe	2.00	10.0	77	42	1.0	20.0	12.4
Fleet	0.60	1.5	12.5		0.4	22.4	12.5
Fraser	1.50	9.0	108	215	1.0	14.4	12.4
Gironde	2.30	10.0	77	44	1.0	18.0	12.4
Hoogly	2.10	5.9	72	25.5			12
Hudson	0.69	9.2	245	140	0.7	30.9	12.4
Irrawaddy	1.00	12.4	124	35			12
Khor	1.30	6.7	90	20.6			12
Ord	2.50	4.0	65	15.2	2.0	20.0	12
Outer Bay of Fundy	2.10	60.0	190	230	1.0	21.0	12.4
Potomac	0.65	6.0	187	54	0.9	24.0	12.4
Rotterdam Waterway	1.00	11.5	37	56	0.7	21.0	12.4
Scheldt	1.90	8.0	77	54	0.5	16.5	12.4
Severn	3.00	15.0	110	41	1.5	20.0	12.4
Soirap	1.30	7.9	95	34			12
St. Lawrence	2.50	7.0	330	183	1.0	28.8	12.4
Tamar	2.60	2.9	21	4.6	0.5	25.0	12.5
Tees	1.50	7.5	14	5.5	0.4	16.0	12
Thames	2.00	8.5	95	25	0.6	14.1	12.3

Table 2.1: Values of tidal amplitude a_0^*, average tidal depth D_0^*, channel length L_e^*, convergence length L_b^*, cross sectional averaged velocity U_0^*, flow conductance C_0 and tidal period T_0^* for various estuaries, reported by Lanzoni and Seminara (1998)

many years of studies, it is not easy to obtain these data and the possibility to elaborate them. On the other hand a comparison with field data is extremely important to better understand the models that deal with this category of estuaries.

The U. S. National Ocean Service provide the Digital Elevation Models (DEM, at one arc second resolution) for all the estuaries in the United States (available at the web-site http://sposerver.nos.noaa.gov/bathy/finddata.html). The estuaries which display the typical characteristics of the tide-dominated class have been selected and analyzed in detail. Some of them are present in the list presented in Table 2.1, as the Columbia River, the Delaware Bay, the Potomac and the Hudson River. Two other estuaries have been chosen: the St. Helena Sound and the St. Andrew Sound which are located in the South Atlantic coast of the United States. Their DEM have been imported in GRASS, which is one of the most widely used GIS, and transformed in raster maps. For each raster map, GRASS allows to trace cross-sectional profiles that can be exported and elaborated.

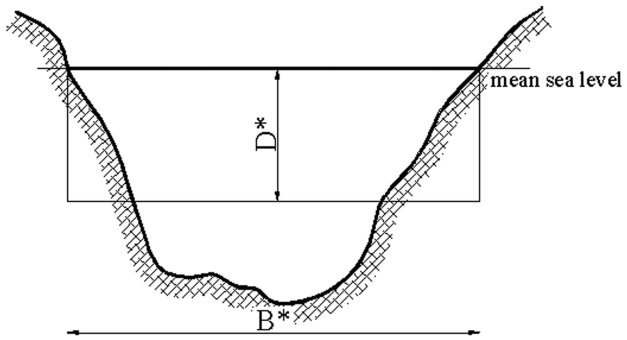

Figure 2.17: Example of a generic cross-section and of its equivalent rectangular section.

An example of a generic cross-section is shown in Figure 2.17. The width B^* is defined as the width corresponding to the mean sea level and the cross-sectionally averaged depth is defined as the depth of the equivalent rectangular section $D^* = \Omega^*/B^*$ where Ω^* is the cross-section area; at last the average bottom elevation η^* is defined as the difference between the mean sea level and the average depth $\eta^* = H^* - D^*$. The profiles of these four parameters D^*, η^*, Ω^* B^* are reported in Figure 2.19, 2.21 and 2.23; the variables are scaled with their values at the mouth of the estuary and refer to tidally averaged conditions. The width scaled with its value at the mouth is equivalent to the right hand side of equation 2.2.

As it can be seen from the plan views of these estuaries and from their bathymetries

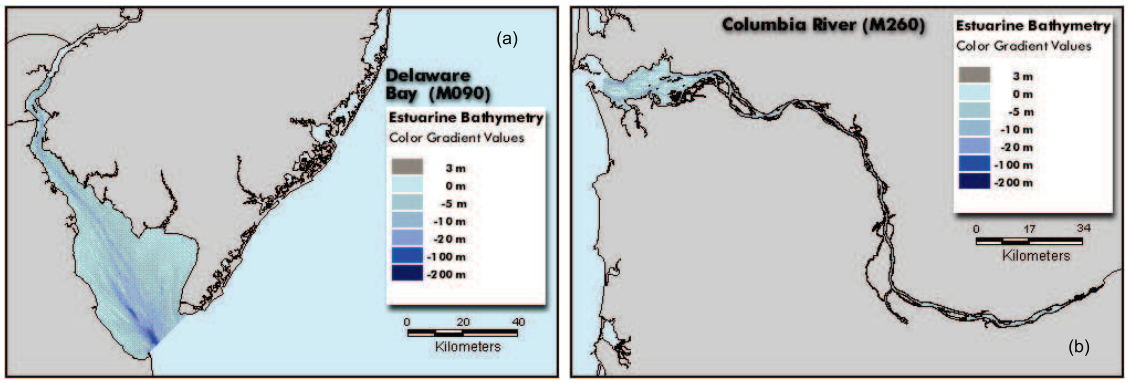

Figure 2.18: Plan view of the Delaware Bay (a) and the Columbia River (b) estuaries (from http://sposerver.nos.noaa.gov/bathy/finddata.html).

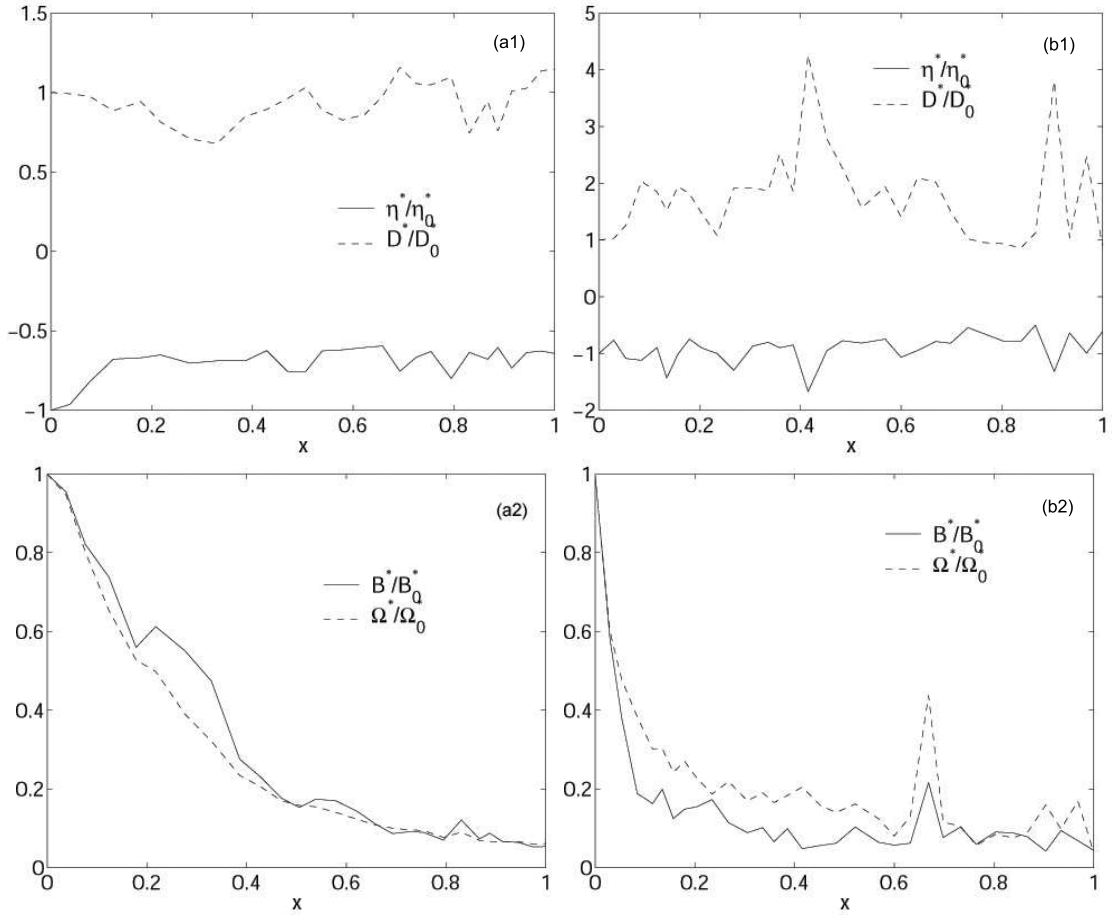

Figure 2.19: Bottom, average depth, width and average cross-sectional area profiles in the Delaware Bay ($a1$) and ($a2$) and in Columbia River ($b1$) and ($b2$).

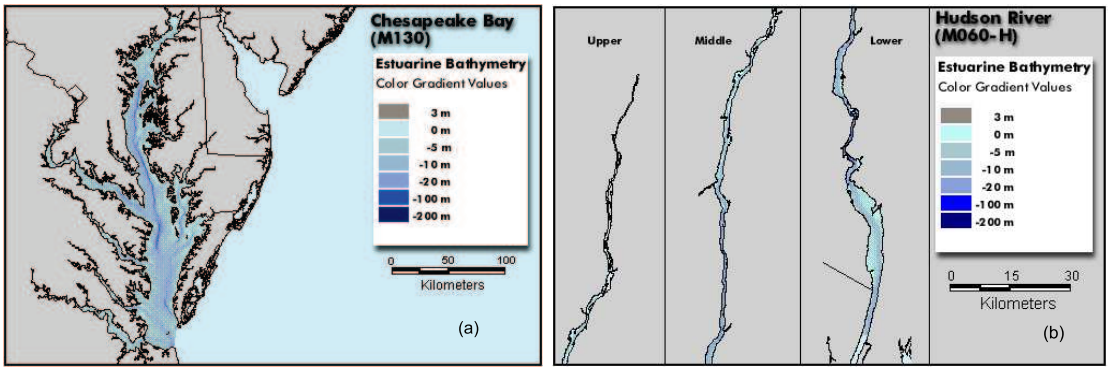

Figure 2.20: Plan view of the Potomac (a) and the Hudson River (b) estuaries (from http://sposerver.nos.noaa.gov/bathy/finddata.html).

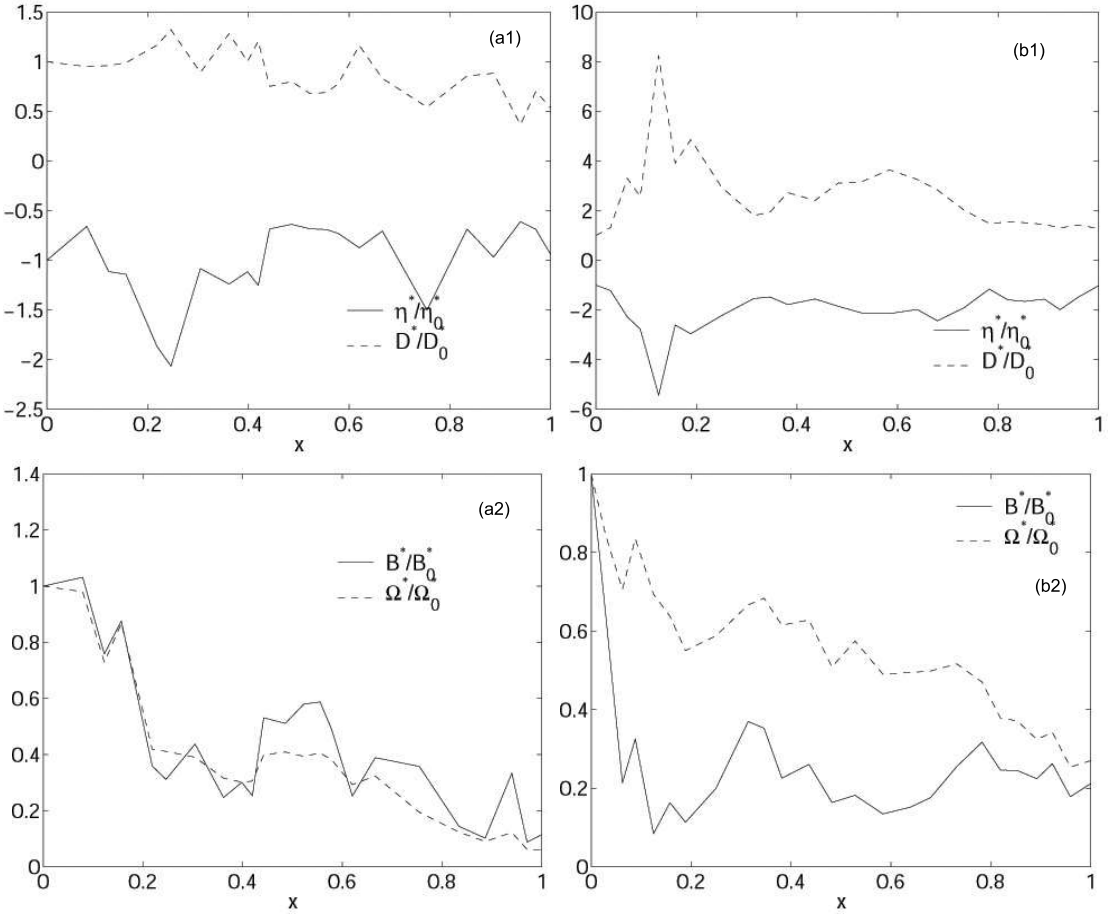

Figure 2.21: Bottom, average depth, width and average cross-sectional area profiles in the Potomac ($a1$) and ($a2$) and in Hudson River ($b1$) and ($b2$).

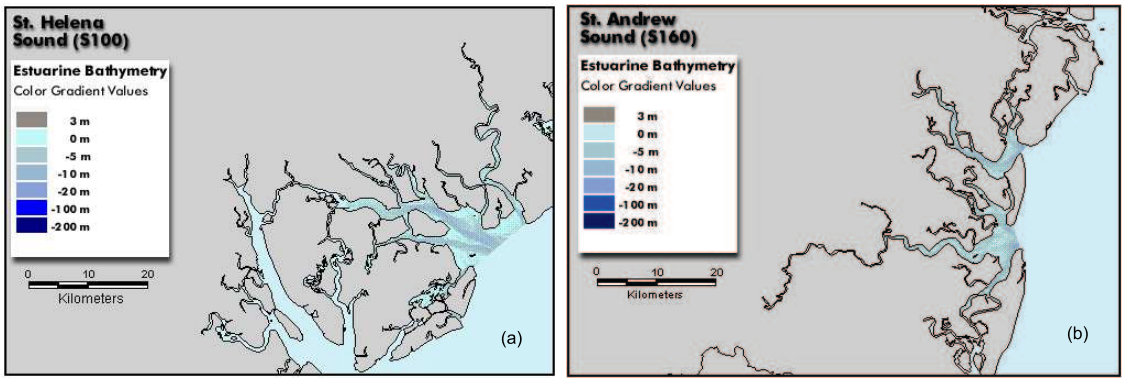

Figure 2.22: Plan view of the St. Helena Sound (a) and the St. Andrew Sound (b) (from http://sposerver.nos.noaa.gov/bathy/finddata.html).

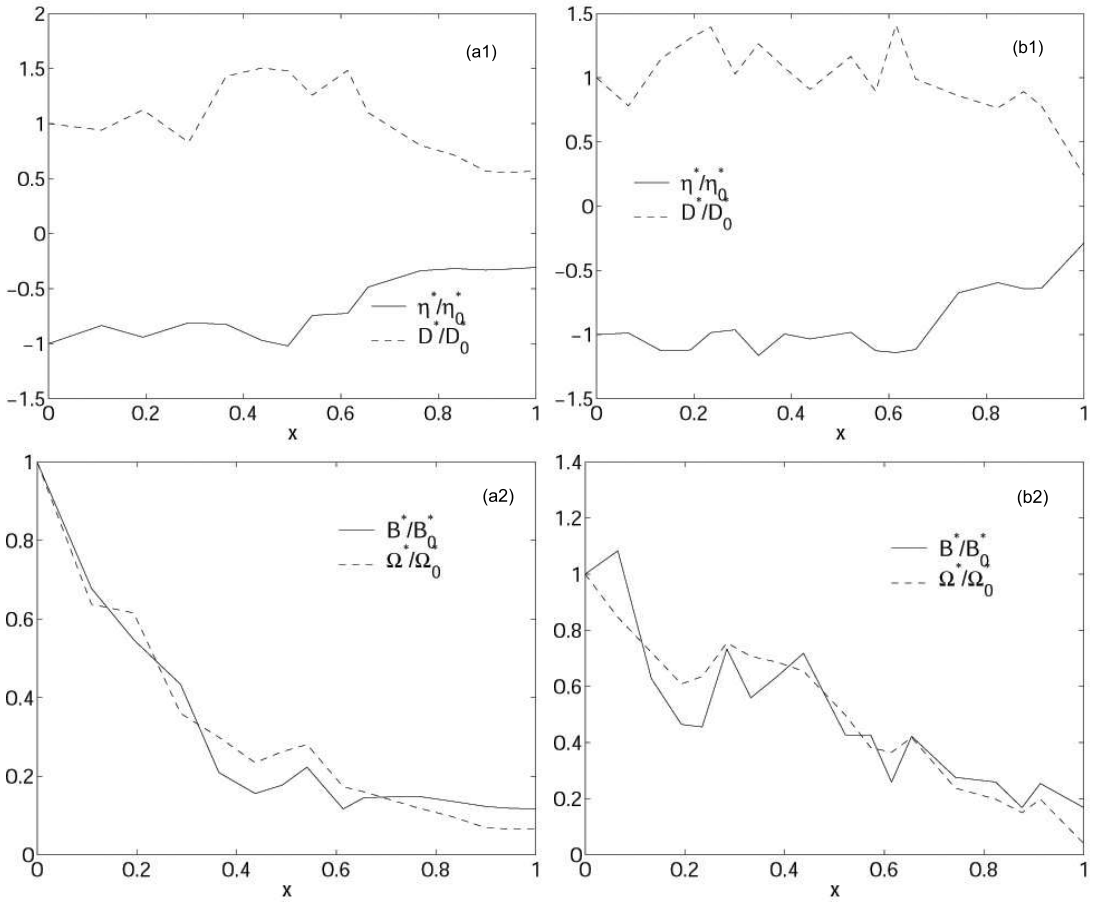

Figure 2.23: Bottom, average depth, width and average cross-sectional area profiles in St. Helena Sound ($a1$) and ($a2$) and in St. Andrew Sound ($b1$) and ($b2$).

(Figure 2.19, 2.21 and 2.23), the bottom slopes of the estuaries are quite mild and in some cases almost negligible.

Moreover, although the obvious variations from the theoretical law, as one moves upstream, the width decreases in an almost exponential way.

2.2.2 Estuarine sediments

In the description of estuarine morphology the characterization of the estuarine sediments becomes very important since it determines the sediment flux on which the morphodynamic evolution of the estuary strictly depends.

Fine sedimentary deposits, or muds, are an important characteristic feature of estuaries. Sedimentary material is transported into the estuary from rivers or sea or it is washed in from the land surrounding the estuarine channel. In most North European and North American estuaries the sea is the main source of sedimentary material which is carried into the estuary as suspended sediment flux or as bedload transported in the bottom inflowing currents that characterize salt wedges. Whatever the source of the sediments, their deposition within the estuary is controlled by the speed of the currents and the particle size of the sediments. In fast-flowing rivers or in strong tidal currents at either end of the estuary all sizes of sedimentary particles may be eroded and transported. As the currents begin to slacken within the estuary, the coarser sediments and sands will be the first to be deposited and the finer silt and clays will remain in suspension. In the calmer middle and upper reaches of an estuary where the river and the tidal currents meet, especially in the slack water at high tides, also the mud can be deposited.

Tide-dominated estuaries are composed by sediments that derive from both fluvial and offshore sources and the grain size varies from gravel to mud. Finer sands and muds have a fluvial origin, coarser sands originate from the the shelf or from erosion of the shoreline (Perillo, 1995). Although each estuary is sedimentologically unique, some structures are shared by a great variety of estuaries. In the estuarine channel there is the dominance of sand, while in the adjacent tidal flat deposit a dominance of silt and clay is found. Sands are coarsest near the mouth and near the head of the estuary. In Figure 2.24 the grain size distribution of the Western Scheldt is reported to exemplify the characteristics of sediments in tide-dominated estuaries.

Sediments can be transported as wash load, suspended and bed load. The first mechanism involves only the finest fraction (clay particles): the vertical concentrations profiles of wash load are fairly homogeneous. Suspension occurs as the result of two counteracting mechanisms, namely the ability of turbulence to raise sediment grains and their tendency

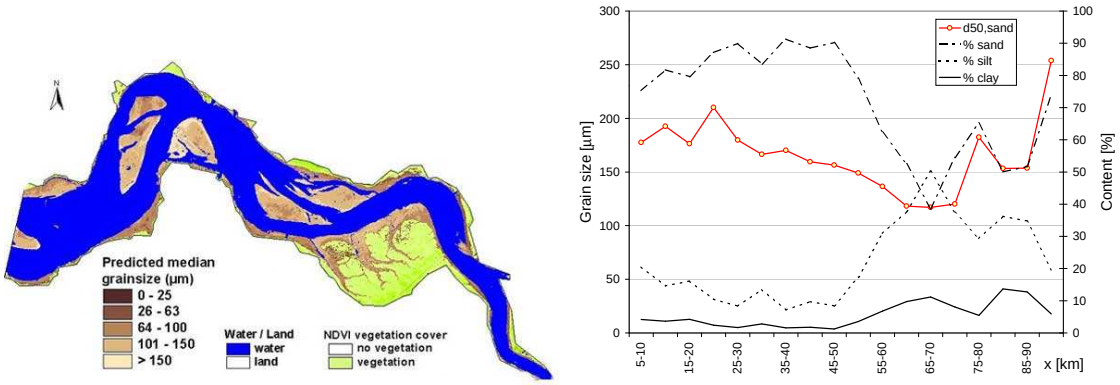

Figure 2.24: Sediment grain size distribution in the Western Scheldt (Toffolon, 2002) .

to settle due to gravity. Grains smaller than 0.15 mm can be entrained into suspension as soon as they begin to move, while larger grains move dominantly as bed-load at low values of flow velocity and then go into suspension when velocity attains higher values during the tidal cycle.

3 State of art

Given the great variety of tidal systems and complexity of the processes related to them, many different approaches have been developed to study these kind of environments. As common in other branches of earth sciences, it is possible to distinguish between *data-based models* that use measured data to describe phenomena, *empirical models* that use statistical relationships between the variables derived from the analysis of field data, *semi-empirical long-term models* that describe the interaction between large elements of the system with empirical relationships, *process-based models* that are mathematical models using physical principles and *formally-integrated long-term or idealized models* that are also based on physical principles but focus on a specific morphodynamic process by simplifying the equations in an appropriate way (de Vriend, 1996).

There is a wide range of contributions concerning this subject; it is convenient to group them in a few broad topics depending on the approach that is used and on the problem that is investigated. Given that the main objectives of this thesis are the study of the morphological evolution of a tide-dominated estuary and the characterization of a model for width change, the topics that are mainly related with them have been selected. The first issue deals with the investigation of the hydrodynamics and the propagation of the tidal wave into the estuarine channel which is fundamental to tackle the problem of morphodynamics. Another important issue concerns with the relationship between asymmetries in tidal currents and sediment transport in order to predict the morphological evolution. It is also possible to find simplified models that simulate the morphological behaviour of a tidal basin. Finally, the problem of the channel cross-section evolution is tackled. In the following paragraphs, a brief review of some of the most significant papers is presented.

3.1 Estuarine hydrodynamics: propagation of the tidal wave

A large number of scientific contributions have been proposed to investigate the hydrodynamics of tidal channels. The understanding of the hydrodynamical behaviour is not only important for its conceptual relevance but also because it is the starting point to predict the morphodynamical evolution.

Speer and Aubrey (1985) focus their attention on the generation of tidal asymmetries, through the use of numerical integration of the one-dimensional equations in narrow channels with tidal flats, that are typical in shallow estuaries. A trapezoidal geometry is used to represent estuarine channels where width increases with elevation above the bottom. Only the first component of the tide, M_2, is considered. It is pointed out that channels without tidal flats develop a time asymmetry characterized by a longer falling tide. This behaviour is enhanced by strong friction and large channel cross-sectional area variability over a tidal cycle. Resulting tidal currents have a shorter but more intense flood phase and a longer but weaker ebb phase, so these estuaries are termed flood-dominated. The presence of tidal flats can produce a longer rising tide and stronger ebb currents, e.g. ebb-dominated estuaries, when the tidal area is large enough to overcome the effects of time-variable channel geometry. In fact, the asymmetry reflect the conflicting effects of time-variable channel geometry in continuity and momentum equations tending to drive a longer falling tide and the presence of tidal flats in continuity driving a longer rising tide. For example, a channel with a rectangular cross-section and a small value of the tidal amplitude with respect to the water depth requires small tidal flats to become ebb-dominated. Some studies show that the magnitude of this asymmetry increases upstream in an estuary, implying that it is generated within the estuary. Looking at tides as the sum of discrete sinusoidal variations, tidal asymmetry has been interpreted to imply generation of higher harmonics within the estuary (Speer and Aubrey, 1985). So trying to understand this asymmetry due to flood/ebb dominance is equivalent to understand how higher harmonics are generated in the estuary that is forced only by a semi-diurnal tide and what controls the phase difference between them. Shetye and Gouveya (1992) restrict their attention to the case of flood dominance, often observed in shallow, narrow estuaries in which the fresh water discharge is negligible. Through the derivation of analytical solutions obtained with perturbation techniques, they establish a link between tidal asymmetry and channel geometry. Neglecting the local advection, the momentum equation becomes a balance between the pressure term and friction, which is linearized;

substituting this equation into the continuity equation, they obtain a single equation for sea level oscillation. The "tidal diffusion coefficient" in this equation, indeed, depends on the channel geometry, so in this way a relationship between the cross-section and the tidal asymmetry is established.

Friedrichs and Aubrey (1994) tackle the subject of the tidal wave propagation, applied to shallow, strongly convergent channels and derive first and second order analytic solutions. Scaling the governing equations, at first-order, gradients in cross-sectional area dominate velocity gradients in the continuity equation and the friction term dominates acceleration in momentum equation. The dominant role of friction is in contrast with previous classic solutions for cooscillating tides in prismatic channels, which often neglect friction entirely. Other analytical approximations that consider convergence in channel geometry exist, but they usually treat friction and local acceleration at the same order. Applying this scaling, the first-order governing equation for elevation in strongly convergent estuaries becomes a first-order wave equation, in contrast to the classical second-order equation which results from low friction and prismatic channels. A first-order wave allows propagation only in the incident direction and is inconsistent with the presence of a reflected wave. The first-order solutions for elevation and velocity are both constant amplitude waves with a phase between them of 90 degrees. Unlike classical wave, the dynamic balance is strongly frictional. Furthermore, the solutions are independent from the length of the estuary, in contrast to the length-sensitive quarter-wave resonance of classical tidal estuary theory. Also the second-order solutions are unidirectional waves and have the same phase. However, their amplitude is modulated by an exponential factor; it contains a growing factor which can be positive if inertia is finite and the convergence strong or negative if inertia is weak and the convergence limited, causing a decay in the amplitude with distance. This factor determines the decay or the growth also for velocity, so for a morphodynamically stable estuary it should be negligible. When this happens, the wave speed is exactly equal to the frictionless wave speed, as it can be obtained from the second-order solution. This explains why the wave speed is usually close to this value in convergent channels, despite the dominance of friction at first-order. Another observation is possible: flood dominance will cause sediment to collect in the inner portion of the estuary, that cannot be stable over the long term unless a physical mechanism simultaneously exists which favours seaward sediment transport. A slightly positive amplitude growth factor may provide such a mechanism, since velocity amplitude tends to increase and scour and settling lag favour seaward sediment transport.

Lanzoni and Seminara (1998) revisit the subject of tide propagation in convergent channels, identifying four limit regimes characterized by different degree of convergence and relative importance of friction compared with local inertia. In weakly dissipative estuaries the effect of convergence can be incorporated in the context of classical perturbation expansion approach, adequate to weakly non-linear processes. The cascade generation of overtides and their evolution landward is described, showing that the tidal wave is increasingly distorted as channel convergence increases. A non-linear generation of a seaward directed residual currents and a character of ebb-dominance emerge. In strongly dissipative estuaries, the highly non-linear nature of the frictional term cannot be modelled by perturbation expansions. So a non-linear parabolic model results suitable to strongly dissipative systems, provided local inertia is sufficiently small while channel convergence is sufficiently strong. The distortion of the current profile typical of strongly dissipative estuaries has been invariably found to be associated with flood dominance. In this model, the role of intertidal flats and of a river discharge has been neglected.

A simple analytical expression to describe tidal damping or amplification is proposed by Savenije (2001); he derives an explicit relation for the tidal range, consisting on an exponential and a linear term. In alluvial estuaries, characterized by an exponential decreasing width and no apparent bottom slope, there is not exponential amplification of the tidal range along the estuary axis. If there is tidal amplification is almost completely linear. Tidal amplification is dominant in estuaries where there is strong convergence; in estuaries where there is damping, the process is also predominantly linear, in particularly close to the mouth of the channel. Moving landward, the tidal range decreases and gradually the exponential term becomes dominant.

A method to calculate the flow field in a short bidimensional embayment is presented by Fagherazzi (2002), assuming that the water level oscillates synchronously in the whole basin. The continuity equation, under this hypothesis, becomes a Poisson equation, which can be solved at each instant of the tidal cycle.

3.2 Tidal asymmetry, sediment transport and channel morphodynamics

The propagation of the tidal wave into a channel strongly influences its morphological evolution. Actually the long term erosion/deposition process in tidal channels is determined by the residual sediment transport, which is mainly related to the degree of asymmetry between the flood and the ebb peak values of flow velocity, due to the non-linear depen-

dence of sediment transport on flow velocity. This is well pointed out by Dronkers (1986), who compares some field observations in two tidal basins in the Netherlands with these general principles.

In literature, several studies relate the flow along a tidal channel and the cross-sectional morphology. Many authors suggest a nearly proportionality law between the cross-sectional area and either the tidal prism or the peak discharge. A possible explanation for this proportionality turns to the concept of maximum entropy, but the relation between the minimum work and the equations that govern tidal flow and sediment motion is not so evident. Another theory suggests that the cross-sectional area adjusts until a characteristic cross-sectionally averaged velocity makes the bottom shear stress capable to remove material from channel bed and banks. Others consider a propensity toward plane bed flow. With the intent to define a more robust method, Friedrichs (1995) uses a physically-based mechanism, the stability shear stress, that is defined as shear stress just necessary to maintain a zero gradient in net along-channel sediment transport. A theoretical lower bound for this stress is the critical grain shear stress necessary for initiation of sediment motion or, for cohesive sediment, the critical erosion shear stress typically observed above mud bottoms. At equilibrium, a linear relationship between the cross-sectional area and discharge emerges, which is well confirmed by observations. It is possible to notice how the critical shear stress depends on the spring tidal range: high values of this parameter may favour flood-dominance and so enhance shoaling while small values may favour ebb-dominance and the correspondent flushing of sediment. If the seaward part of a tidal channel is flood-dominated while the landward part is ebb-dominated, the consequent spatial convergence in the direction of maximum discharge causes a localized increase in sediment concentration. This process in known as “tidal ‘turbidity’ maximum”. Seaward of this point, the flood dominance induced by a large tidal range-to-depth ratio, favours landward movement of sediments; on the contrary landward of the same point the ebb dominance induced by the fresh water discharge favours seaward movement of sediments. This resulting turbidity maximum migrates along the channel following the seasonal variations in the fresh water discharge. Close to this point, a net deposition is possible and so a reduction of the cross-section area and a local increase in velocity until the stability shear stress is large enough to prevent further deposition. This kind of scheme is found to be observed in several natural channels.

The problem of interaction between tidal currents, sediment transport and bedform changes is tackled by Schuttelaars and de Swart (1996) who introduce a simple one dimensional model restricting their attention to the case of short embayments, whose length is

smaller than the tidal wavelength, such that the system is far from resonance. Moreover, they consider a rectangular cross section channel with constant width, closed at one end (i.e. no river discharge is considered) and connected at the mouth with a tidal sea. The sediments are supposed to be noncohesive and may be transported both as suspended load and bedload. Relatively deep channels are considered for which the frictional time scale is at least of the order of the tidal period, so this model is not applicable to highly frictional embayments. Since the tidal time scale is much shorter than the morphodynamic time scale, they apply the method of averaging to describe separately the water motion and the bottom. At the first order of approximation, they find that the free surface oscillation is spatially uniform, since it is affected neither by inertia nor by friction. If no overtide is considered and the suspended load transport dominates, the equilibrium profile that satisfies all the boundary conditions represents a constantly sloping bottom with vanishing water depth at the landward boundary. In the case of bedload transport, the equilibrium profile reduces to a flat bottom. These profiles all result stable. If an overtide is introduced, the equilibrium bottom profiles in the suspended load model can be concave or convex, depending on the ratio of advective and diffusive transports. The most significant differences with the case of no overtide is in the bedload transport model, because the bottom profile becomes linear. Also in this case the profiles result all stable.

Starting from the same geometric scheme, Schuttelaars and de Swart (1999) investigate the stability of these equilibrium states with respect to bidimensional perturbations. The presence of friction appears to be a necessary condition for instability, since bottom frictional torques and vorticity are produced and cause the tidal velocity to decrease above the shoals and to increase in the channels. If their effect is stronger than the continuity effect, the bottom perturbation can grow. Introducing a bedslope term in the total load sediment flux, it is possible to observe the damping of short-scale modes. A critical lateral wavenumber, depending on the length and on the width, is found, when the constantly sloping bottom profile becomes unstable for the first time. Three regions can be identified in the embayment, between which no sediment exchange can be seen.

With an extended version of the non-linear one dimensional model, Schuttelaars and de Swart (2000) try to investigate the morphodynamic equilibria of tidal channels with arbitrary lengths. This allows to consider phenomena as tidal propagation, tidal resonance and the generation of overtides by advective processes and depth-dependent frictional forces in the momentum equations; actually, increasing the embayment length, the advection term becomes dominant in the momentum equation. The bottom friction in the momentum equation is linearized. At the closed end, which is a moving boundary, a

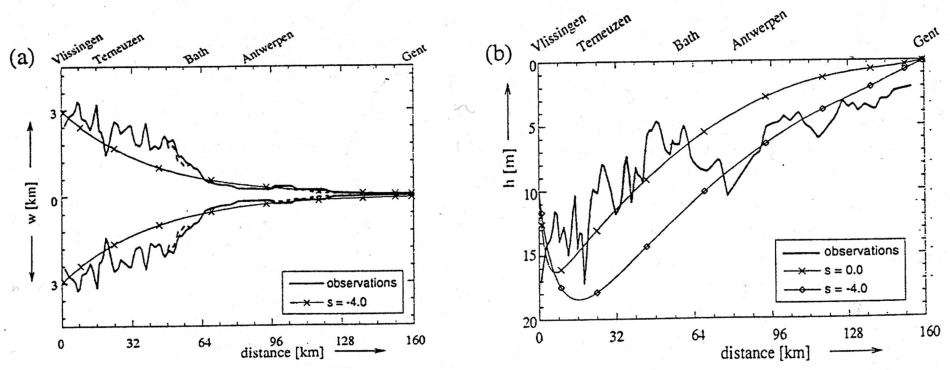

Figure 3.1: Averaged depth and width profiles of the Western Scheldt compared with field observatios, as shown by Schuttelaars and de Swart (2000).

kinematic condition is posed while at the entrance the bed is fixed. An equilibrium bed profile is obtained when the net sediment flux throughout the embayment is zero. The solution is obtained by applying continuation methods, starting from the known solution valid for short embayments. They find that morphodynamic equilibria exist if the embayment length is not short compared with the tidal wavelength, but also if not longer of the frictional length-scale of the predominant tide. This is because longer channels tend to full up at the landward side until the maximum length is reached. If an externally prescribed overtide is added to the forcing, more than one equilibrium can be reached. For length smaller than the overtide resonance length scale, the bottom profiles are concave and the water motion looks like a standing wave. For longer embayments another type of equilibrium appears: it is characterized by a weakly concave profile and a travelling wave. If the amplitude of the of the overtide is sufficiently high, multiple equilibria are possible. The maximum value of length for which morphodynamic equilibria cease to exist decreases with increasing influence of external overtide and bottom friction (see Figure 3.1 as example).

Friedrichs et al. (1998) consider an infinite funnel-shaped channel with exponentially decreasing width and a rectangular cross-section. To solve the tidal variations in depth integrated suspended sediment concentration, the advection/dispersion equation is used. At the lower order, the balance is between erosion and deposition. Analytical solutions show that tidally averaged sediment transport is due to three dominant effect: flood-dominant tidal asymmetry, seaward river flow, settling/scour lag made effective by along-channel width convergence. The third effect represents a new mechanism for the maintenance of the turbidity maximum. The model is able to predict changes in direction of tidally av-

eraged sediment transport in a good way if compared with some observations. Differently from Schuttelaars and de Swart (1999), where a short channel with constant width is considered, in these systems the along-channel variation in water depth does not play a role in the equilibrium sediment budget.

Following an approach different from these models that want to find whole-estuary solutions, Prandle (2003) proposes a localized analytical solution for the propagation of a single predominant tide in estuaries characterized by a strongly convergent triangular cross-section. Dyer (1997) shows how frictional and energy conservation effects can combine in funnel-shaped bathymetry to produce a 'synchronous estuary' with constant tidal elevation amplitudes. The role of the advective term is neglected and the friction term is linearized. By deriving this cross-sectionally averaged solutions, many relationships between the dynamics and the bathymetry are established.

Lanzoni and Seminara (2002) consider again a funnel-shape estuary, with rectangular cross section, closed at one end and investigate its morphodynamic equilibrium configuration that is reached if the net sediment flux vanishes everywhere (since at the landward boundary an impermeable barrier is supposed to exist). Differently from Schuttelaars and de Swart (1996), the friction term is not linearized, since the linearization could produce an incorrect steepening of the tidal wave in strongly convergent estuaries. Besides, they describe the wetting and drying portion of the flow domain, while Schuttelaars and de Swart (2000) consider a fixed landward boundary where a "kinematic condition" is imposed. The equilibrium bed profiles obtained by Lanzoni and Seminara are very different from the peculiar bed profiles, characterized by large scour, inflection points and the possibility of multiple solutions of Schuttelaars and de Swart (2000): a possible explanation could be the fact that they force the bottom elevation at the mouth to keep constant. They found that the morphological evolution is characterized by the formation of a sediment front which migrates landward until it reaches the end of the domain and is completely reflected. It can be seen that a very shallow area forms in the inner part of the estuary as confirmed also by experimental observations of Bolla Pittaluga et al. (2001) (see also Bolla Pittaluga, 2002); the bottom profile grows until a vanishing net sediment flux realizes all along the channel. An example of temporal evolution of their bottom profiles can be seen in Figure 3.2. A nearly constant value of the maximum and minimum flood/ebb speed is reached. They also report the relationship between the tidal prism and the minimum cross-sectional flow area. In absence of a net import of sediment either from the sea or from the river, a power law is progressively attained as the bottom evolves. A break in this law characterizes the smaller cross-sectional areas in the inner part of the estuary, where probably wetting and

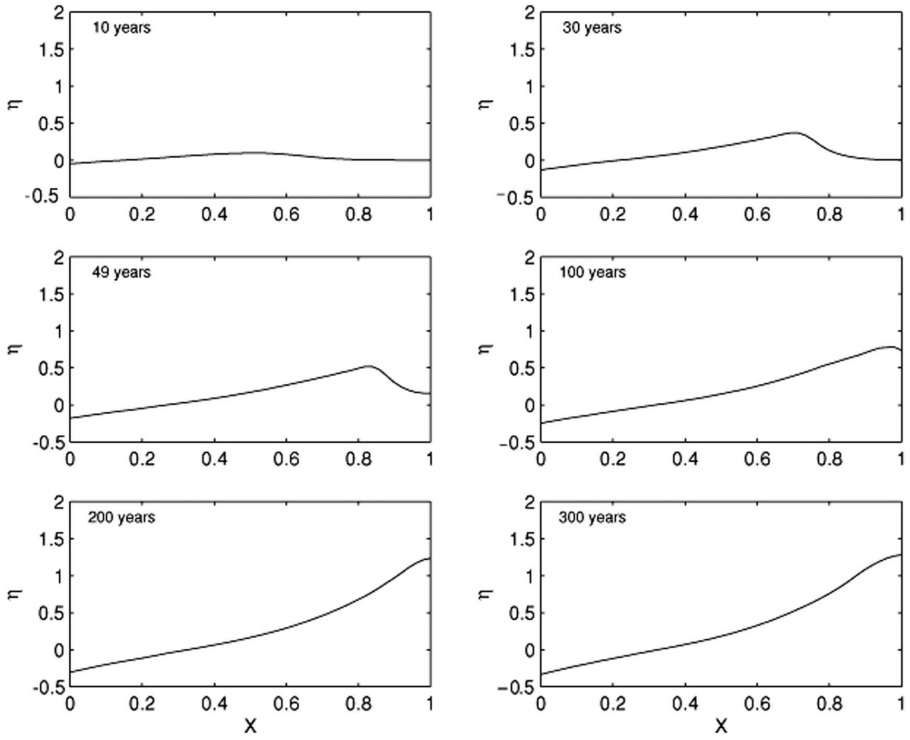

Figure 3.2: Example of temporal evolution of the bottom profile in a strongly convergent channel as shown by Lanzoni and Seminara (2002).

drying affect heavily the dynamics of sediment transport.

3.3 Morphometric analysis of tidal networks

Myrick and Leopold (1963) analyse some of the relationships between the water stage and the discharge existing in literature, comparing them with the measurements made at various locations and at different stages in the tidal cycle in a marsh near the Potomac River. The width, the depth and the velocity are related with the discharge through simple power functions. They find a good agreement between the field data and the theoretically derived values; it emerges that an estuarine channel changes more rapidly in width and less rapidly in depth as discharge changes downstream than does a terrestrial channel. Both theory and field data show that in estuaries depths tend to be more conservative that in upland rivers, so that the width to depth ratio varies rapidly downstream: at the mouth, an estuary is wide and relatively shallow, at its head, it is narrow and relatively deep.

Starting from the work of Myrick and Leopold (1963), many morphometric analyses of tidal networks have been carried out in the following years. Some of them use the quantitative procedures proposed for terrestrial rivers. Other works, on the contrary, introduce a simplified approach, since they consider that solving the complete momentum and mass equations cannot be used to describe the evolution over a morphologically reasonable period of time (Rinaldo et al., 1999a; Marani et al., 2003). They simplify the classical two dimensional shallow water equations and describe the hydrodynamics with a Poisson-like mathematical model. They show that it is robust and reliable if compared with the complete models in a large range of cases of interest.

A simple measure that controls the channel morphodynamic evolution is the with-to-depth ratio $\beta = B^*/D^*$ (D'Alpaos et al., 2005; Allen, 2000). Marani et al. (2002) provide many observational values of this parameter for the tidal channels and creeks in the Lagoon of Venice and show its great variability. The great differences in these values are consistent with those shown by Allen (2000) for the various types of channel cross-sections. The same variability can be identified when this ratio is evaluated depending on the channel order (Lawrence et al., 2004). In fact, the basic process that controls the section shape can be very different (D'Alpaos et al., 2005): the presence of vegetation and the sediment cohesion can influence the bank failure mechanism in a significant way and consequently the different erosional process and the type of incision. The salt marsh creeks typically are deeply incised whereas in tidal flats the channels are are less incised, since both the vegetation and the sediment cohesion becomes less important due to the increase in the sand fractions.

The morphometric analysis of these tidal systems tries to identify the possible relationships between the geometric or dynamic parameters and the landscape-forming flowrates. In the systems that are supposed to have reached an equilibrium configuration, a power law between the tidal prism, P and the inlet minimum cross-sectional area A can be pointed out in this form: $A = CP^n$ (O'Brien, 1969; Jarret, 1976), where the coefficient n and C are empirically derived parameters. In fact, Jarret (1976) examines earlier work by O'Brien (1969) for Pacific Coast inlets and establishes relationships for sites along the Gulf and Atlantic coasts. These are perhaps the most common criteria applied to predict the stability of tidal inlets.

A near proportionality between the cross-sectional area and the spring peak discharge, as found in many existing tidal systems (e.g. Myrick and Leopold, 1963), is stated by many authors (Rinaldo et al., 1999b; Lanzoni and Seminara, 2002). Moreover, the empirical relationship that can be established between the channel cross-section area and the its

drainage area can be somehow considered an extension of the Jarret's law where the role of the drainage area were played by the tidal prism or the maximun peak discharge.

However, among the well-defined power law relationships between cross-sectional area, drainage area, tidal prism, channel width, and peak discharge in larger channels, there is a considerable variance, much larger than that reported for corresponding fluvial systems; nevertheless, the linkage of tidal hydrodynamics with the morphology of the tidal networks that is observed in nature holds in a surprisingly robust manner (Rinaldo et al., 1999b).

3.4 Semi-empirical models

Another class of models has been developed in order to simulate the morphological evolution of a tidal basin in a simplified way. Originally, most models regarding the interaction between water motion and the erodible bottom were of empirical or semi-empirical type. In fact the long-term morphological development under the influence of natural processes, e.g. sea level rise or under the influence of human activities, e.g. land reclamation, dredging or dumping, cannot still be predicted by dynamic models which are often too complex and laborious. In practise, the prediction of this development in estuaries still relies on empirical relations, in which the morphological variables, such as the cross-sectional area of channels, are related to integrated hydrodynamic parameter, as for example the tidal prism. Wang et al. (1998) present a mathematical model partly based on process descriptions and partly on empirical relations. The basic idea is that there is no accumulation of sediment or water anywhere in the area if all the elements in the morphological system are in equilibrium. The main difference between this model and a process-based one is that the equilibrium sediment concentration is not directly computed from the hydrodynamic parameters, but through the equilibrium morphological state. The morphological changes occur when the local sediment concentration differs from its local equilibrium. There is a good agreement between these results and those obtained with a process-based model. In addition to the empirical relations defining the morphological equilibrium, the most important parameters determining the behaviour of the model are the overall concentration, the vertical exchange velocity of sediment, the horizontal diffusion coefficient for sediment and the power in the equilibrium concentration formula.

Another example of semi-empirical model is the one realized by van Dongeren and de Vriend (1994), which simulates the morphological behaviour of a tidal basin in response to a change in one or more extrinsic parameters. The system is supposed to be made of three interacting elements, the tidal basin, the outer delta and the adjacent coast

which try to reach a new equilibrium. In this schematization, the tidal basin is composed of two elements, channels and flats, which can be described using three variables: the channel cross-sectional area, the flats surface area and the flats level. These variables are supposed to tend to an equilibrium value determined by bathymetry and extrinsic hydraulic parameters, such as the tidal range or the mean sea level. They consider a constant width channel, characterized by the presence of tidal flats area in the end and not beside the channel as in Speer and Aubrey (1985). A growing tidal flats area conditions the asymmetry in the velocities since the net sediment transport is changed from flood dominant to ebb dominant. Three different scenarios are examined: partial closure, sea level rise and change in tidal range and they are compared with measured data.

3.5 Evolution of the channel cross-section

All the previous morphological models are enable to account for changing channel width through time. In literature several contributions exist that study the evolution of the cross section of a channel. Many of them refer to rivers, as Pizzuto (1990) that provides a numerical model to describe the bank erosion in a straight channel composed of noncohesive sediment. The model predicts the distribution of boundary shear stress, cross-channel sediment transport rates and the evolution of the bed topography. When erosion produces a bank slope larger than the angle of repose, widening occurs by a planar bank failure. Equilibrium channel produced by the model have flat beds and curved bank regions which are similar to the classical cosine stable bank profile. Equilibrium values of dimensionless depth are inversely proportional to the slope as suggested by previous studies.

Darby and Thorne (1996a) develop and test a numerical model or river widening. It is applied to straight, sand-bed streams with cohesive bank materials (differently from Pizzuto, 1990) and nonuniform bathymetry and width in the longitudinal direction. The flow is supposed to be only in the streamwise direction and assumed steady and uniform. So secondary and overbank flows are excluded. By depth-integrating the simplified equation, they obtain an expression for the lateral distribution of the unit discharge and for streamwise and transverse sediment transport fluxes. Numerical solution of the sediment continuity allows temporal variations in bed material size, bed morphology and bank geometry to be simulated. The lateral erosion at the base of the banks is evaluated considering a threshold value for shear stress. Both planar and rotational failures are considered. Channel widening is calculated by coupling bank stability with flow and sediment transport algorithms. A probabilistic approach is used to estimate the longitudinal extent

of mass failures and mixed layer theory is used to model the transport of the resulting bed and bank material mixture. This model considers only banktop widening and not narrowing. In Darby and Thorne (1996b) the model is tested and applied. It emerges that many differences are found between these simulations and those obtained considering a fixed width model, as it is natural to think. An example of the erosion mechanism in riverbanks is reported in Figure 3.3.

A model that simulates the initial channel formation in a youthful saltmarsh environment is proposed by Fagherazzi and Furbish (2001). The model mimics the evolution of the cross section of a channel by coupling calculations of bottom shear stresses caused by tidal motions with erosion, taking into account the deposition of cohesive sediments. For a tidal marsh with a channel closed at one end, they supposed that the tidal flat area pertinent to branched channel does not change with time or water level. Besides, this area is linked to the cross section at the channel mouth and the free surface level is supposed to be uniform. So considering harmonic changes in water elevation as a boundary condition and a salt marsh level sufficiently less than the mean sea level, the discharge flowing in each section can be considered harmonic as well. In particular, the peak discharge repeats at fixed time interval and fixed water elevation with constant magnitude. So their evolution model utilizes an intermittent discharge with constant magnitude to mimic the salt marsh hydrodynamics. The simulations suggest that two mechanisms contribute to the longitudinal widening exhibited by salt marsh channels, which typically is disproportionately greater than that exhibited by river channels. The short duration of the peak discharge (spring tide) and corresponding erosion rates, when compared with deposition rates, prevent the channel from reaching a deep, narrow equilibrium configuration. Furthermore, autoconsolidation of cohesive sediments, often occurring in salt marsh environments, leads to a downward increase in the resistance of the sediment to erosion. As scour occurs locally, the flow encounters more resistant sediment layers, so rather than deepening the channel over a narrow zone, flow and bottom shear stresses become more uniformly distributed leading to a wider channel than would otherwise occur in the absence of autoconsolidation. The hypotheses adopted in this work limit the application to youthful salt marsh development, where the significant reductions in the tidal prism due to increasing bottom elevation above mean sea level are not treated.

A model of tidal network ontogeny is proposed by D'Alpaos et al. (2005) who couple a Poisson-like hydrodynamical model with a morphodynamic model which is able to reproduce the network initiation and the early development on a time scale shorter that those of other landscape-forming processes of tidal systems. The incision is supposed to be led

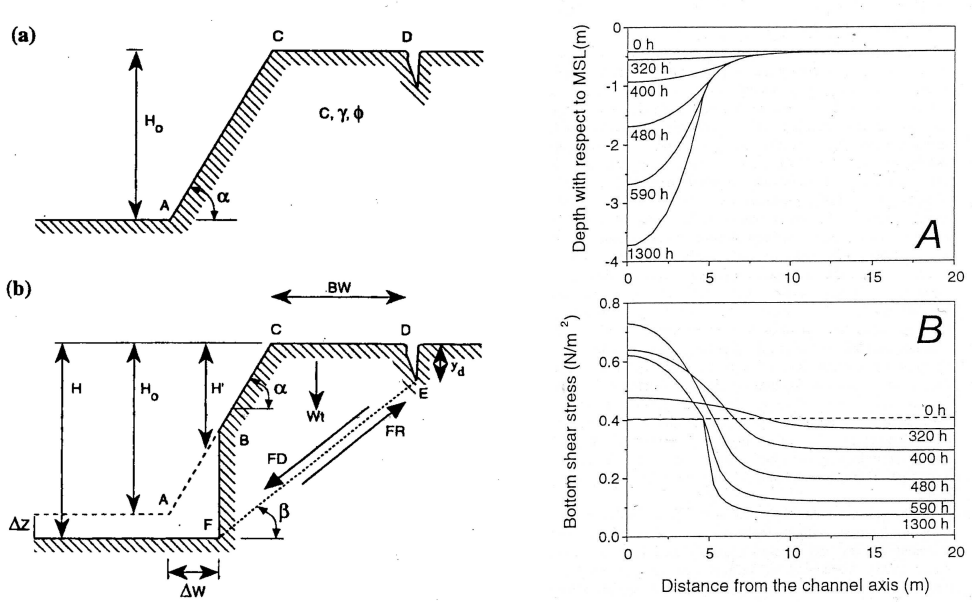

Figure 3.3: Erosion mechanism of the riverbanks as shown by Darby and Thorne (1996a) [left]; example of temporal evolution of the channel geometry (A) and bottom shear stress (B) as shown by Fagherazzi and Furbish (2001) [right].

by the water surface elevation gradients and it occurs when the local shear stress exceeds a threshold value.

A monitoring of a saltmarsh tidal channel in in the San Francisco Bay is described by Gabet (1998), with the aim to solve the paradox for which tidal channels have often been recognized as being stable landscape features, despite highly sinous planforms, severely undercut banks and high rates of bank erosion. The field data are compared with those obtained by the use of a numerical model to predict the rate of lateral migration. When a bank collapses, the slump block induced sedimentation behind it and supports the bank. In this way the bank is protected from attack until the slump block is eventually eroded away. The width of the undercut is determined through a stability analysis, while erosion rates are derived from erosion pin data. The model predicts the lateral migration rate quite accurately.

This brief review certainly does not exhaust the subject of the propagation of the tidal wave into an estuarine channel and its morphological evolution. The main purpose for which it has been presented is to identify the principal subjects which many works deal with and the different methodologies used to tackled them.

4 Formulation of the model

The present study is referred to a tidal channel of length L_e^* with a rectangular cross-section area in order to simulate the behaviour of a real estuary which is sketched in Figure 4.1 along with the relevant notations employed in the present analysis. Note that hereafter the asterisk denotes dimensional quantities and the subscript $_0$ indicates tidally averaged quantities at the mouth of the estuary in its initial configuration. H^* is the free surface elevation, D^* denotes the water depth and a^* the tidal amplitude. B^* indicates the channel width.

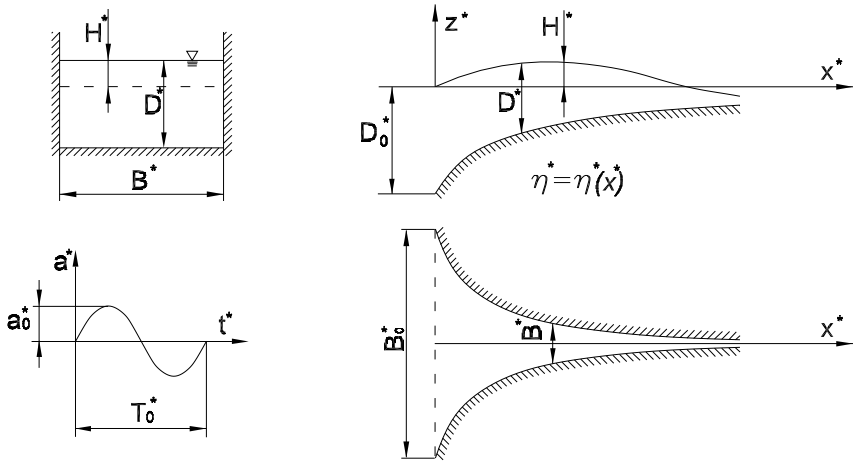

Figure 4.1: Sketch of the estuary and basic notation.

The standard one-dimensional shallow water equations (de Saint Venant) are used; the continuity and momentum equations for water flow read:

$$\frac{\partial Q^*}{\partial t^*} + \frac{\partial}{\partial x^*}\left(\frac{Q^{*2}}{\Omega^*}\right) + g^*\Omega^*\frac{\partial H^*}{\partial x^*} + g^*\Omega^* j = 0\,, \tag{4.1}$$

$$\frac{\partial Q^*}{\partial x^*} + \frac{\partial \Omega^*}{\partial t^*} = 0\,, \tag{4.2}$$

where t^* is time, Q^* the water discharge, Ω^* the area of the cross section and g^* is gravity; furthermore

$$j = \frac{U^*|U^*|}{C_h^2 g^* R_h^*} \tag{4.3}$$

is the frictional term, where C_h is the dimensionless Chézy coefficient, U^* is the cross-sectionally averaged velocity and R_h^* is the hydraulic radius. The morphodynamic evolution of the channel ca be described by coupling the de Saint Venant equations (4.1-4.2) for the flow field with the Exner equation (1925), which represents the continuity equation for the sediments and reads:

$$(1-p)B^*\frac{\partial \eta^*}{\partial t^*} + \frac{\partial \left(B^* q_s^*\right)}{\partial x^*} = \frac{\partial B^*}{\partial t^*} D^* \,. \tag{4.4}$$

In (4.4) p is sediment porosity, B^* is the channel width, q_s^* is the sediment flux per unit width and $\eta^* = H^* - D^*$ is the bottom elevation. The term on the right-hand-side represents the rate of sediments that are eroded from the banks and it is introduced in the Exner equation to assure the conservation of the sediment mass. It accounts for the exchange of sediments volumes between the banks and the bottom of the channel (Figure 4.2); it is of crucial importance for models that allow channel width to vary with time, while it is obviously negligible in the case of fixed banks.

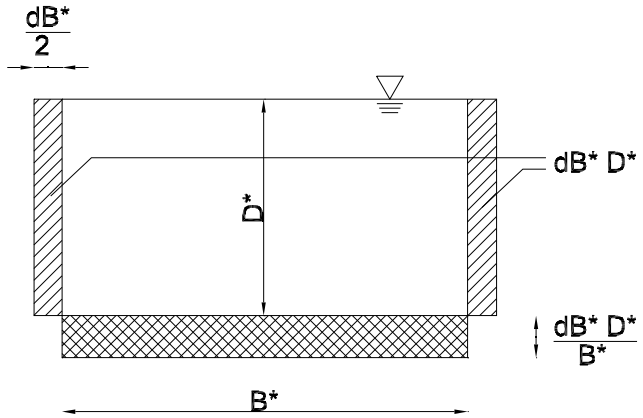

Figure 4.2: Conceptual diagram of sediment exchange between the bottom and the banks of the channel.

The sediment flux per unit width can be written as:

$$q_s^* = \sqrt{g^* \Delta d_s^{*3}}\, \phi(\theta) \,. \tag{4.5}$$

with d_s^* representing the characteristic particle diameter, $\Delta \simeq 1.65$ the relative density of sandy sediments with respect to water and ϕ the dimensionless sediment flux. In all the numerical results presented in the following chapters, a sediment diameter of 10^{-4} m is assumed. ϕ is a function of the Shields parameter, θ that is defined as:

$$\theta = \frac{U^{*2}}{C_h^2\, g^* \Delta\, d_s^*}\,. \tag{4.6}$$

In this thesis, the dimensionless sediment flux ϕ is evaluated using the relationship proposed by Engelund and Hansen (1967)

$$\phi = 0.05\, C_h^2 \theta^{5/2}\,. \tag{4.7}$$

This ia a very simple monomial formula that computes the total load flux and that does not contain a threshold value for the Shields parameter under which the sediment transport vanishes. Alternately the bed load flux could be evaluated by employing the Meyer-Peter and Muller formula and the suspended load flux by the formula proposed by van Rijn (1984).

The problem is conveniently reformulated in dimensionless form, using the length of the estuary L_e^*, the tidal period T_0^*, the width B_0^* and the depth D_0^* at the mouth as representative scales; moreover, a scale U_0^* is assumed for the velocity. Dimensionless quantities are defined as follows:

$$\begin{aligned} t = \frac{t^*}{T_0^*}\,, \quad x = \frac{x^*}{L_e^*}\,, \quad B = \frac{B^*}{B_0^*}\,, \\ (H, \eta, D) = \frac{(H^*, \eta^*, D{*}^*)}{D_0^*}\,, \quad U = \frac{U^*}{U_0^*}\,, \\ Q = \frac{Q^*}{B_0^* D_0^* U_0^*}\,, \quad \Omega = \frac{\Omega^*}{B_0^* D_0^*}\,, \end{aligned} \tag{4.8}$$

The Chézy coefficient C_h is supposed to be a constant.

The sediment flux per unit width can be scaled using the following expression:

$$q_{s0}^* = \sqrt{g^* \Delta d_s^{*3}}\, \phi_0 \tag{4.9}$$

where the coefficient ϕ_0 corresponds to the tidally averaged value of the sediment flux at the mouth and it has been introduced to estimate the order of magnitude of the sediment flux. It depends on the empirical relationship used to evaluate the sediment transport

(4.7) and hence in the present analysis it is obtained by averaging equation (4.7). If the velocity is approximated by a sinusoidal law, $U^* = U_0^* \sin(2\pi t^*/T_0^*)$, this scale of sediment flux, per unit width, can be written in the following form:

$$\phi_0 = 0.05\,\frac{16}{15\,\pi}\,C_h^2\left(\frac{U_0^{*2}}{C_h^2\,g^*\Delta\,d_s^*}\right)^{5/2}. \tag{4.10}$$

A time scale T_b^*, different from the tidal period T_0^*, has been established to describe the morphological evolution. In fact, the erosional/depostional processes are typically slower if compared with the evolution of the flow field and the time scale T_b^* is typically some orders of magnitude greater then the tidal period T_0^*, as it is commonly assumed in literature (e.g. Schuttelaars and de Swart, 1996; Lanzoni and Seminara, 2002). Therefore the following dimensionless variables arise:

$$\tau = \frac{t^*}{T_b^*}\,, \quad q_s = \frac{q_s^*}{q_{s0}^*}\,. \tag{4.11}$$

Using the above scalings, equations (4.1), (4.2) and (4.4) can be written as:

$$\frac{\partial Q}{\partial t} + \frac{1}{S_t}\frac{\partial}{\partial x}\left(\frac{Q^2}{\Omega}\right) + \frac{1}{F_r^2 S_t}\Omega\frac{\partial H}{\partial x} + \frac{\delta}{F_r^2 S_t}\Omega j = 0\,, \tag{4.12}$$

$$\frac{\partial H}{\partial t} + \frac{1}{S_t B}\frac{\partial Q}{\partial x} = 0\,, \tag{4.13}$$

$$\frac{\partial \eta}{\partial \tau} + \frac{q_{s0}^*\,T_b^*}{(1-p)L_e^* D_0^*}\left(\frac{\partial q_s}{\partial x} + \frac{q_s}{B}\frac{\partial B}{\partial x}\right) = \frac{D}{B}\frac{\partial B}{\partial \tau}\,. \tag{4.14}$$

In equation (4.19), the two terms on left-hand-side are of comparable magnitude if:

$$\frac{q_{s0}^* T_b^*}{(1-p)\,L_e^* D_0^*} = O(1)\,, \tag{4.15}$$

an assumption which is equivalent to choose the following morphological time scale:

$$T_b^* = \frac{(1-p)\,D_0^* L_e^*}{q_{s0}^*}\,. \tag{4.16}$$

Substituting this scaling into equation (4.19), the system (4.17-4.18-4.19) can finally be rewritten as:

$$\frac{\partial Q}{\partial t} + \frac{1}{S_t}\frac{\partial}{\partial x}\left(\frac{Q^2}{\Omega}\right) + \frac{1}{F_r^2 S_t}\Omega\frac{\partial H}{\partial x} + \frac{\delta}{F_r^2 S_t}\Omega j = 0\,, \tag{4.17}$$

$$\frac{\partial H}{\partial t} + \frac{1}{S_t B}\frac{\partial Q}{\partial x} = 0\,, \tag{4.18}$$

$$\frac{\partial \eta}{\partial \tau} + \frac{\partial q_s}{\partial x} + \frac{q_s}{B}\frac{\partial B}{\partial x} = \frac{D}{B}\frac{\partial B}{\partial \tau}\,. \tag{4.19}$$

Two dimensionless parameters arise, namely the Strouhal number $S_t = L_e^*/(U_0^* T_0^*)$ and the Froude number $F_r = U_0^*/\sqrt{g^* D_0^*}$. The Strouhal number can be interpreted as the ratio between the estuarine length L_e^*, that is the characteristic length scale, and the distance travelled by a particle characterized by a velocity U_0^* in a tidal cycle. This two lengths may be of the same order of magnitude and consequently $S_t \sim O(1)$; on the other hand this condition assures that the two terms in the continuity equation (4.18) can be compared. The Froude number, given that the typical value of the peak velocity in an estuarine channel is approximately of the order of 1 m/s while the characteristic water depth D_0^* is of the order of 10m, is a small parameter and is always smaller than one.

Since the morphological evolution occurs on a fairly long period of time if compared with the tidal period (Schuttelaars and de Swart, 1996), the morphodynamic problem can be decoupled from the hydrodynamics and solved separately.

4.1 Numerical scheme

The hydrodynamics and the bottom evolution are solved numerically with two different schemes; first the flow field is computed and then the correspondent bottom evolution is evaluated with same time step of the hydrodynamic integration that is very small due to stability reasons.

The differential system (4.17)-(4.18), written in semi-conservative form in terms of the variables Q and H in order to enhance the conservation of mass and momentum, is discretized through finite differences and solved numerically using the explicit McCormack method (Hirsch, 1990a; Lanzoni and Seminara, 2002). This is a two-step predictor-corrector method characterized by a second order accuracy both in space and in time (Figure 4.3). The main advantage of this method is that it is explicit, therefore the solution at time $k+1$ depends only on the solution at time k and on the boundary conditions. Given the differential system:

$$\frac{\partial \mathbf{U}}{\partial t} + \mathbf{A(U)}\frac{\partial \mathbf{U}}{\partial x} = \mathbf{G} \tag{4.20}$$

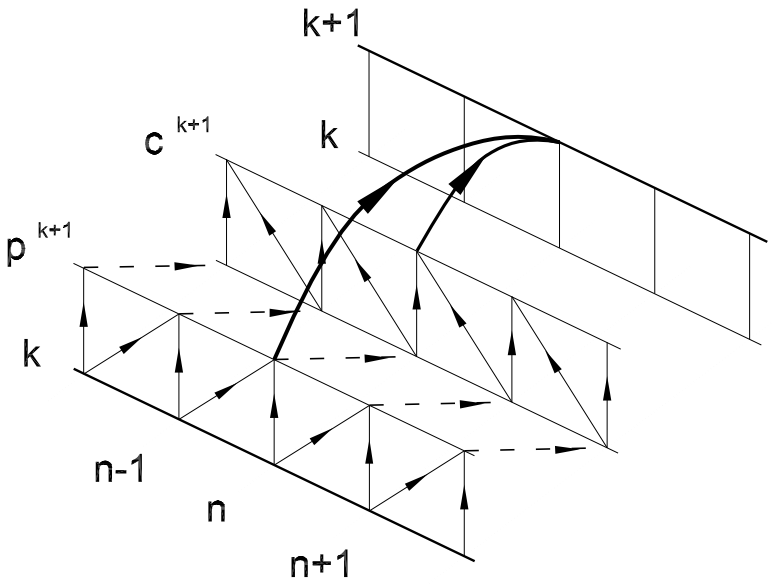

Figure 4.3: Computational stencil for the two-step MacCormack scheme

where the vector of the unknowns **U** is:

$$\mathbf{U} = (H, Q) \tag{4.21}$$

and where the Jacobian matrix of the transformation, **A**, is a function of the unknowns, the predictor and the corrector steps can be written as follows:

$$U_n^p = U_n^k - \frac{\Delta t}{\Delta x} A_n^k (U_{n+1}^k - U_n^k) + \Delta t G_n^k \tag{4.22}$$

$$U_n^c = U_n^k - \frac{\Delta t}{\Delta x} A_n^p (U_n^p - U_{n-1}^p) + \Delta t G_n^p \tag{4.23}$$

in which the index n and k are respectively the spatial and temporal index of the computational grid (see Figure 4.3). The apices p and c indicates the predictor and corrector values of the unknowns **U**. The solution at time $k+1$ is evaluated as the average value between the predictor value and the corrector one:

$$U_n^{k+1} = \frac{1}{2} (U_n^p + U_n^c) \tag{4.24}$$

A suitable artificial viscosity is introduced through a TVD filter (Total Variation Diminishing) in order to remove the spurious oscillations around discontinuities, which may arise since the tidal wave tends to break during its propagation due to friction and convergence. The accuracy of the method remains of the second order, except for the points around these discontinuities where it reduces to a first order. The numerical scheme with the addition of the TVD filter can be expressed as follows:

$$U_n^{k+1} = \frac{1}{2}\left(U_n^p + U_n^c\right) + \frac{\Delta t}{\Delta x}\left(D^k_{n+\frac{1}{2}} - D^k_{n-\frac{1}{2}}\right) . \tag{4.25}$$

The additional term in (4.25) represents the numerical diffusion that is non negligible only when the tidal wave tends to break.

It is possible to demonstrate that the system (4.17-4.18) is hyperbolic and that its two real eigenvalues can be written as to:

$$\lambda_{1,2} = \frac{U}{S_t} \pm \frac{1}{S_t}\sqrt{g^* \frac{\Omega D_0^*}{B U_0^{2*}}} \tag{4.26}$$

In tidal systems these eigenvalues are always distinct and they are characterized by opposite signs, since the Froude number is always smaller the one. The stability condition requires the Courant-Friedrichs-Levi number (CFL) not to exceed the unity:

$$CFL = \frac{\lambda_{max}}{\Delta x}\Delta t \leq 1 \tag{4.27}$$

where $\lambda_{max} = max\left(|\lambda_1|\,|\lambda_2|\right)$ is the leading eigenvalue.

The sediment continuity equation (4.19) is discretized through finite differences and solved numerically using a first-order upwind method, with the same time step imposed by the CFL condition for the hydrodynamic problem.

4.2 Boundary conditions

The choice of the boundary conditions is not a trivial question since different bottom equilibrium profiles can be obtained depending on the way these conditions are posed.

Two boundary conditions are required by the system (4.17-4.18), one for each eigenvalue. Since one eigenvalue is positive and the other one is negative, the two conditions must be imposed at the mouth of the channel and at its landward end.

At the seaward boundary, the free surface level is supposed to be determined only by

the large scale component of the tide. It can be useful to recall that the gravitational effect due to the moon is purely sinusoidal, therefore in the open sea the free surface oscillation is very close to a sinusoidal function (commonly referred to as the M_2 tide). Over-tides originate from non-linear effects of the wave propagation and they are typically present in real estuaries. Although these can be easily accounted for, they are not necessary to identify some distinctive characteristics of the estuarine channel response to tidal forcing (Speer and Aubrey, 1985); hence, the sea level oscillation is characterized with the semi-diurnal M_2 tide, whose dimensional amplitude is a_0^*, and set:

$$H(t)|_{x=0} = \varepsilon \sin(2\pi t)\,, \tag{4.28}$$

where $\varepsilon = a_0^*/D_0^*$.

At the landward boundary two different conditions are tested: in the first case the river discharge is supposed to be negligible, that corresponds to a reflecting barrier condition; in the second case a non vanishing river discharge is fixed.

The Mac-Cormack method consists of two steps: the predictor one corresponds to a first-order forward discretization in space, while the corrector one to a backward first-order scheme. In this way the predictor step is used to estimate the predictor value of the discharge at the mouth of the estuary, while the corrector step permits to calculate the predictor value of the water elevation at the landward end of the estuary. Therefore, in addition to the physically based conditions, corresponding to the two distinct eigenvalues, two further conditions have to be introduced: the predictor value of the water elevation at the landward boundary and the corrector value of the discharge at the mouth of the estuary. They are specified with a first-order extrapolation, since it can be demonstrated that the global order of accuracy of a second-order scheme (Hirsch, 1990b) is not reduced in this case (Figure 4.4).

To solve the Exner equation 4.19, further boundary conditions are needed; they can be imposed directly on the bottom elevation, as it is done by Schuttelaars and de Swart (2000). Since it is arbitrary to fix the bed elevation following a physically meaningful criterion, in this work the conditions are imposed on the sediment flux. Given the finite differences scheme, to evaluate the bottom elevation in the two extreme nodes two fictitious sections are introduced in the computational domain with the same spacing that is fixed between the others.

During the flood phase, two different conditions have been tested: vanishing flux or flux in equilibrium with the hydrodynamical parameters of the first real section. In the

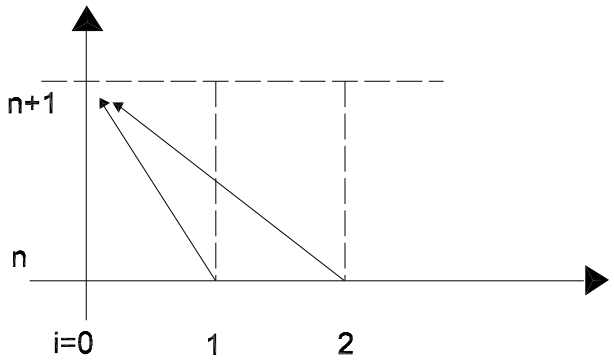

Figure 4.4: First-order in space, zero order in time extrapolation scheme

fictitious section at the mouth of the channel the sediment flux is imposed equal to the one of the first real section. The definition of a suitable boundary condition for the sediment transport near a tidal inlet is still a debated question. A proper formulation would require a detailed analysis of the flow structure close to the inlet, which is beyond the scope of the present work. Notice however that the conditions adopted herein correspond to two extreme situations: in fact, the first condition reproduces the case in which the sediment input from the sea is negligible, while the second condition corresponds to a sediment supply from the sea which is able to compensate the transport capacity of the channelized flow at the inlet. At the landward boundary the sediment flux is supposed to equal the transport capacity. Therefore when a reflecting barrier condition is imposed, the sediment flux is supposed to vanish, that is equivalent to suppose that no sediment can leave the estuary.

During the ebb phase, the outgoing sediment flux in the first section is supposed to be in equilibrium with the hydrodynamic parameters. The same equilibrium relationship is imposed at the landward boundary. The sediment load in the fictitious section at the landward boundary is imposed to equal the one of the last real section. Also at the landward boundary two different conditions are tested: in the first case the river discharge is supposed to be negligible, that corresponds to a reflecting barrier condition, and therefore to negligible sediment flux. In the second case a non vanishing river discharge is fixed and the incoming sediment flux is supposed to equal the equilibrium value corresponding to the transport capacity of the incoming flow, that means that all the sediment load that arrives in the last section leaves the channel.

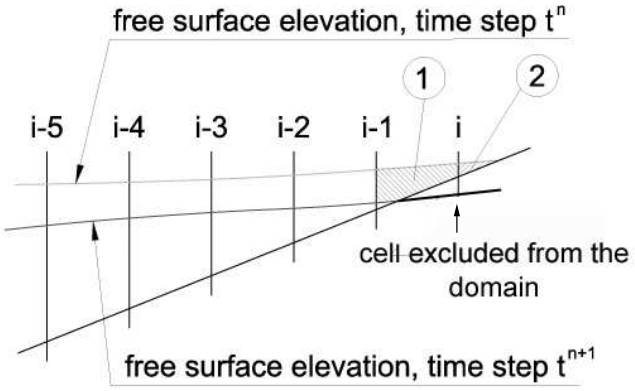

Figure 4.5: Boundary condition in the case of drying area.

4.3 Boundary conditions in the case of drying and wetting

The morphological evolution of the estuary, as it will be shown in the following chapters, is characterized by the formation of a sediment front that migrates landward and tends to emerge. In this way some cells within the estuary may undergo a drainage process during the ebb phase while they can be submerged again during the flood phase.

Different techniques has been developed to tackle this problem and fundamentally two different approaches can be distinguished. The first identifies the partially wet cells and controls the flow over these elements. This kind of methods are strictly related with the adopted numerical scheme. The second approach, on the contrary, introduces a suitable scaling coefficient, which represents the volume of water on each element, in the governing differential equations or alternatively introduces a sub-grid model based on the statistics of bottom topography (Defina, 2000); this latter approach is used by Lanzoni and Seminara (2002). In this thesis a simpler method has been adopted since it requires a smaller computational time and the results are quite similar to those obtained by Lanzoni and Seminara (2002). This method is based on the exclusion from the computational domain of the cells affected by the drying and wetting processes in order to prevent the possibility that negative depths may occur during the simulation (Figure 4.5). In fact, the governing equations (4.17-4.18) exhibit a singularity when the flow depth vanishes. To overcome the above difficulty the computational cells in which the flow depth is smaller than a given small value are excluded from the domain; on the contrary, cells are reintroduced in the computational domain when the rise of free surface occurring in the flood phase leads to new submerged areas (Figure 4.6). The dry cell nearest to the mouth becomes the last active cell at a certain time step. This cell may be located at the end or inside the domain:

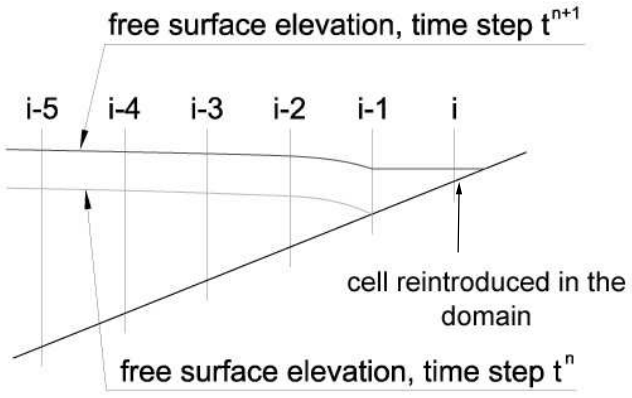

Figure 4.6: Boundary condition in the case of wetting area.

in the latter case all the succeeding cells in the landward direction are excluded from the computation. At subsequent time steps these cells can be flooded, since the free surface is subjected to periodic oscillation; in this case, they are reintroduced in the domain with the same water level of the last active cell and vanishing velocity.

5 Bottom evolution of tide-dominated estuaries with fixed banks

In this chapter, the long-term morphological evolution of a tide-dominated estuary with fixed banks is investigated. The typical funnel shape is described by using an exponentially decreasing function of the longitudinal coordinate x, as assumed by many authors (e.g. Friedrichs and Aubrey, 1994; Lanzoni and Seminara, 1998):

$$B^* = B_0^* \exp\left(-\frac{x^*}{L_b^*}\right) \tag{5.1}$$

where L_b^* is the convergence length and B_0^* the width at the channel mouth. It can be written in a dimensionless form, using the scaling suggested in Chapter 2:

$$B = \exp\left(-x\frac{L_e^*}{L_b^*}\right) \tag{5.2}$$

In the case of fixed banks, only the bed is erodible and the sediment continuity equation (4.19) becomes:

$$\frac{\partial \eta}{\partial \tau} + \frac{\partial q_s}{\partial x} + \frac{q_s}{B}\frac{\partial B}{\partial x} = 0\,. \tag{5.3}$$

since the term on the right-hand-side, which represents the sediment exchange between the bed and the banks related to bank erosion, is neglected. When the width is characterized by an exponential variation law (5.2), it turns out that the solution does not depend explicitly on the width at the mouth B_0^*. In fact in the sediment continuity equation (4.19) the term:

$$\frac{B_{,x}}{B} = -\frac{L_e^*}{L_b^*} = \gamma \tag{5.4}$$

becomes constant and the Exner equation (4.19) can be written as:

$$\frac{\partial \eta}{\partial \tau} + \frac{\partial q_s}{\partial x} - \gamma q_s = 0\,. \tag{5.5}$$

As pointed out in the previous chapters, channel convergence may strongly affect the hydrodynamics of estuaries (see also Friedrichs and Aubrey, 1994 and Friedrichs et al., 1998). Its role on the morphological evolution, which was neglected in previous morphological analysis (e.g. Schuttelaars and de Swart, 2000), has been recently highlighted by Lanzoni and Seminara (2002). At a large spatial scale the morphological evolution of estuaries typically occurs on a fairly long time period, say of the order of centuries, a time span at which geological processes may play a non negligible role. Therefore it is not easy to distinguish between "internal" morphological changes (i.e. those associated with the mutual interactions between the flow field and the bottom surface) and those related to the change in the external conditions (sea level rise, subsidence, etc.). They find that the long term erosional and depositional processes in tidal channels are determined by the residual sediment transport, which is mainly related to the degree of asymmetry between the flood and the ebb peak values of flow velocity. They restrict the analysis to a limited number of situations: in fact they show the bottom evolution of two relatively short channels, the first one convergent, the second one with constant width; this not allow one to fully recognize the role of the different parameters involved.

In this chapter, the one dimensional model formulated in Chapter 4 is used to investigate the long-term bottom equilibrium profiles, starting from an initially horizontal bed. When the width decreases exponentially and the initial bottom profile is flat, the tidal channels are typically flood dominated in a large part of their length and the net flux of sediment is mainly directed landward (Wells, 1995; Lanzoni and Seminara, 2002). This asymmetry causes a net landward sediment flux in many tide-dominated estuaries, as it has been observed in the Ord River estuary in Australia (Wright et al., 1973), in the Salmon River estuary in Canada (Dalrymple et al., 1990) and in the Severn estuary in the UK (Murray and Hawkins, 1977).

Numerical results indicate that, when river discharge is not dominant and a reflecting boundary is assigned at the landward end, a sediment front forms and slowly migrates landward until it leads to the emergence of a beach, which generally inhibits a further development of the channel. The resulting equilibrium bed profile is characterized by an increasing bottom elevation in the landward direction, as it can be found also in previous analyses (Schuttelaars and de Swart, 2000; Lanzoni and Seminara, 2002). The above scenario is confirmed also by the experimental observations of Bolla Pittaluga et al. (2001). In which way are the equilibrium profiles influenced by channel convergence? Does the physical length that is imposed to the system play a role in the determination of the solution? Which is the effect of the initial and boundary conditions? Could the presence

of a freshwater discharge alter this scenario? In this chapter an attempt to answer these questions is made; for this purpose the dependence of the equilibrium length on the relevant physical parameters, such as D_0^*, a_0^*, C_h that characterize the tide and the channel geometry is investigated. Besides, the role of the seaward boundary condition for sediment transport is pointed out. Finally, the role of the river discharge is clarified by comparing the results obtained with a reflecting barrier condition with those obtained with a non negligible river discharge.

5.1 Equilibrium bottom profiles

According to the results of the numerical simulations the morphological evolution of a tidal channel can be described as follows. Starting from an initial horizontal bed profile, a sediment front is formed where the divergence of the sediment flux is larger and negative (see Figure 5.1). The front migrates landward and amplifies until it reaches the last section, where it may be reflected. After a period of time of the order of hundreds of years, the system tends to an equilibrium configuration, which is characterized by a bottom profile displaying an upward concavity, as also found by Lanzoni and Seminara (2002).

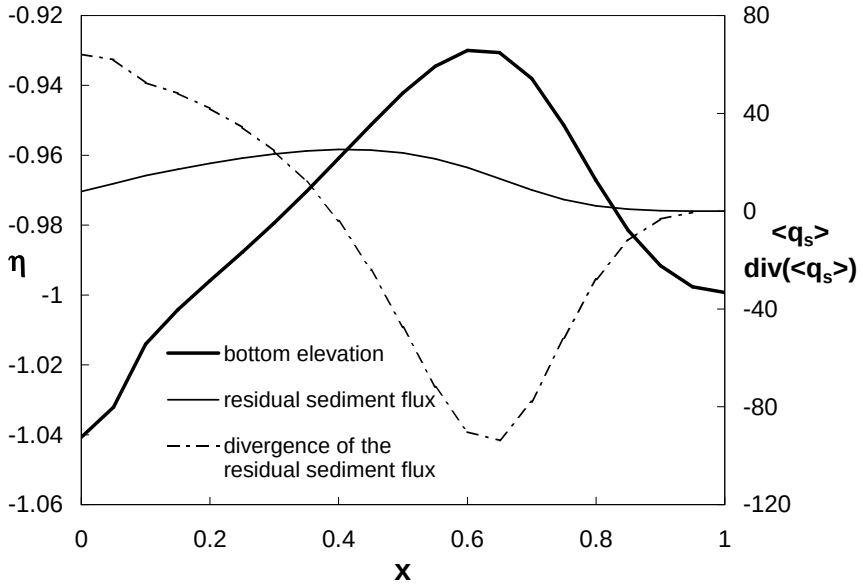

Figure 5.1: Bottom elevation, residual sediment flux and divergence of the residual sediment flux at the beginning of the simulation [$L_e^* = 40km$, $L_b^* = 20km$, $D_0^* = 10m$, $a_0^* = 4m$, $C_h = 20$, $d_s^* = 10^{-1}mm$].

The morphological evolution may follow two different behaviours, depending on the

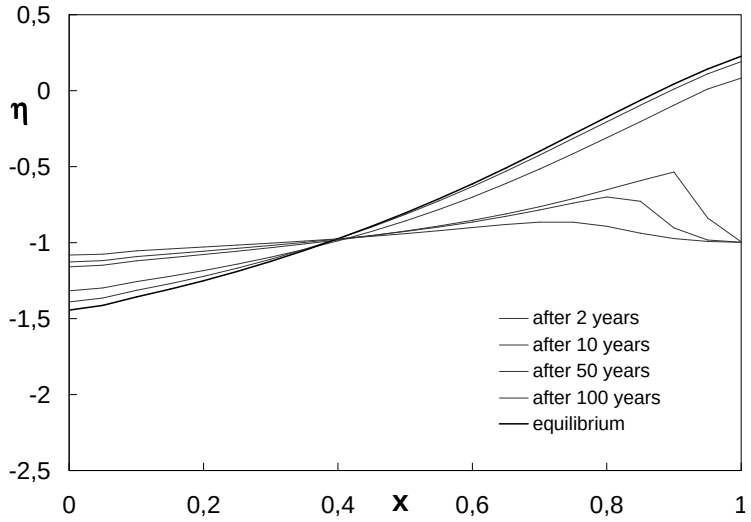

Figure 5.2: The long-term evolution of the bottom profile of a short convergent estuary. [$L_e^* = 160km$, $L_b^* = 120km$, $D_0^* = 10m$, $a_0^* = 4m$, $C_h = 20$, $d_s^* = 10^{-1}mm$].

role of the physical constraint imposed by the finite length of the estuary (notice that in both cases the channel is convergent). Results reported in Figure 5.2 correspond to a relatively short estuary. In this case the asymptotic configuration is characterized by the formation of a beach at the landward end such that the final length coincides with the imposed length of the estuary. This is the case treated by Lanzoni and Seminara (2002). In a longer channel (Figure 5.3) the sediment front migrates landward and stops at a certain distance from the mouth because a beach is formed inside the channel. This condition generally prevents the further development of the channel. In this case the equilibrium bottom profile occupies only a fraction of the total length of the estuary. Hence, for given values of the relevant parameters an equilibrium length of the estuary, L_a^*, can be defined, which is achieved provided the landward boundary condition is located sufficiently far from the mouth. Therefore an estuary is defined "long" when the physical length imposed to the domain is large enough not to influence the morphological evolution of the system and consequently its equilibrium length is determined by the presence of a beach inside the estuary. The channel is defined "short" when the sediment migration is strongly obstructed by the presence of the landward boundary condition that consists of a reflecting barrier and consequently the equilibrium length coincides with the physical length of the domain (see also Todeschini et al., 2003). Notice that results presented herein refer to relatively large values of the initial dimensionless tidal amplitude, $\varepsilon = 0.4$, and hence of flow velocity, which imply a fast evolution of the system.

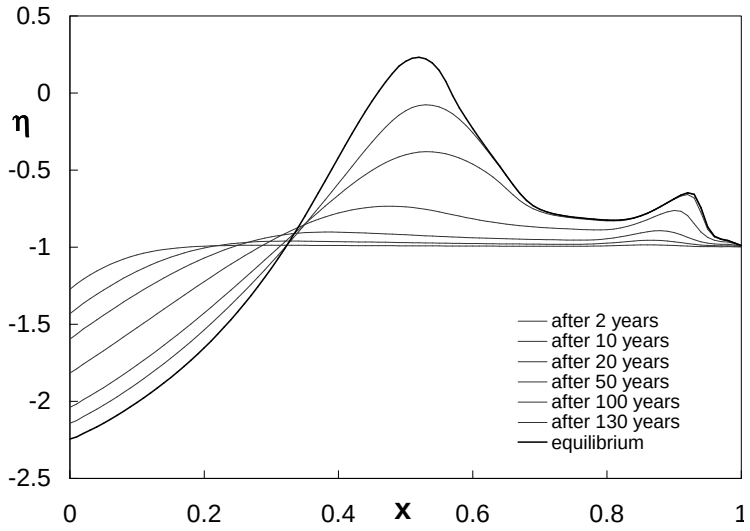

Figure 5.3: The long-term evolution of the bottom profile of a long convergent estuary. $[L_e^* = 480km,\ L_b^* = 120km,\ D_0^* = 10m,\ a_0^* = 4m,\ C_h = 20,\ d_s^* = 10^{-1}mm;\ ]$.

Before analysing in detail the parameters that influence the different behaviours in the morphological evolution of a tidal channel, as the tidal amplitude, the initial water depth, the Chézy coefficient, the presence of overtides, it is useful to make some remarks on the characteristics of the sediment transport. As already said, the propagation of the tidal wave into a channel strongly influences its morphological evolution. Actually the long term erosion/deposition process in tidal channels is determined by the residual sediment transport, which is mainly related to the degree of asymmetry between the flood and the ebb peak values of flow velocity, due to the non-linear dependence of sediment transport on flow velocity. In tide-dominated estuaries, in which the channel convergence can be very strong and determine a distortion in the tidal wave, flood velocities typically exceed ebb velocities but are characterized by a shorter duration. A parameter that represents a measure of such tidal distortion is the degree of asymmetry α that is defined as:

$$\alpha(x) = \log \frac{|U_{flood\,max}(x)|}{|U_{ebb\,max}(x)|}. \tag{5.6}$$

In literature, there are different ways to define this parameter according to the variables taken into account. An equivalent definition refers to the duration of the ebb and flood phases instead of the absolute values of the peak velocities:

$$\alpha(x) = \log \frac{|Duration_{ebb}(x)|}{|Duration_{flood}(x)|}. \tag{5.7}$$

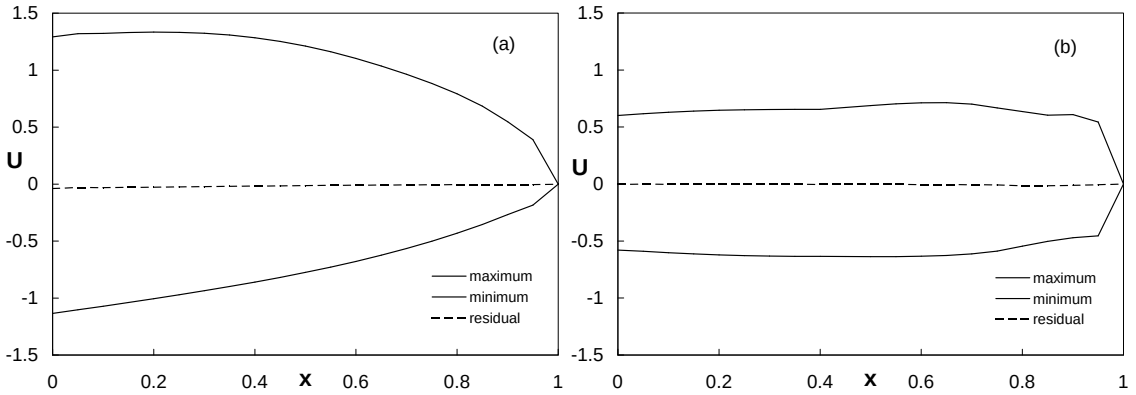

Figure 5.4: Maximum, minimum and residual values of flow velocity along the estuary at the beginning of the simulation (a) and at equilibrium (b) for a short estuary [$L_e^* = 40km$, $L_b^* = 20km$, $D_0^* = 10m$, $a_0^* = 4m$, $C_h = 20$, $d_s^* = 10^{-1}mm$].

In response to this flood-dominance, in most tide-dominated estuaries there is a net landward sediment transport that continues to the tidal node (Dronkers, 1986; Wells, 1995). This net landward sediment transport tends to vanish when the bottom profile reaches its equilibrium configuration, that is characterized by an almost constant bottom slope (e.g. Friedrichs and Aubrey, 1994; Toffolon, 2002). In Figure 5.4 the peaks and the residual values of the velocity U, evaluated when the bottom profile has achieved an equilibrium configuration, are compared with those corresponding to the beginning of the simulation. At equilibrium, the maximum and the minimum value of the velocity are almost equal in absolute value in every point of the estuary and the asymmetry between flood and ebb phase has almost disappeared. This tendency towards a symmetric configuration is clear if the the velocity and the sediment flux during one tidal cycle are plotted at the beginning of the simulation and at equilibrium at the mouth ($x = 0$) and in the middle of the estuary ($x = 0.5$) (Figure 5.5 and 5.6). It is interesting to note that at equilibrium the differences among the various sections of the domain not only in the peak values but also in the shape of velocity and sediment flux are mitigated if compared with those at the beginning of the simulation, as it can be seen in Figure 5.5 and 5.6. The peak values, in fact, keep almost constant along the estuary, as it is observed in some real estuaries.

It is useful to note that the equilibrium reached by the system is dynamical, since it is achieved only in terms of the residual values of velocity and sediment transport. In fact, during the tidal cycle the velocity is free to vary but its residual value has to vanish everywhere.

The reason for which at equilibrium the net sediment transport tends to zero is con-

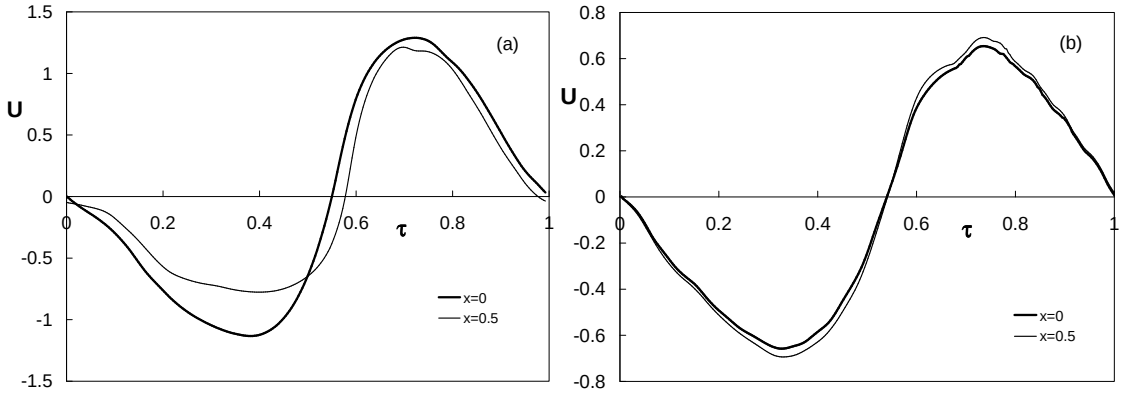

Figure 5.5: Flow velocity in a tidal cycle at the mouth ($x = 0$) and in the middle of the channel ($x = 0.5$) at the beginning of the simulation (a) and at equilibrium (b) [$L_e^* = 40km$, $L_b^* = 20km$, $D_0^* = 10m$, $a_0^* = 4m$, $C_h = 20$, $d_s^* = 10^{-1}mm$].

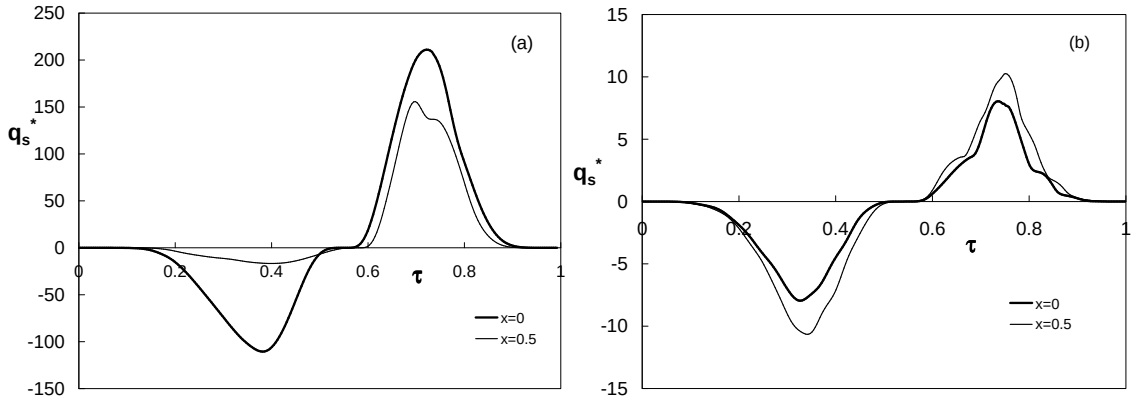

Figure 5.6: Sediment flux in a tidal cycle at the mouth ($x = 0$) and in the middle of the channel ($x = 0.5$) at the beginning of the simulation (a) and at equilibrium (b) [$L_e^* = 40km$, $L_b^* = 20km$, $D_0^* = 10m$, $a_0^* = 4m$, $C_h = 20$, $d_s^* = 10^{-1}mm$].

nected with the choice of the boundary condition; it is useful to remark that in these numerical simulations a reflecting barrier condition is imposed at the landward end of the estuary. When the tidally averaged asymptotic condition is achieved and the mean bed level keeps constant, i.e. $\eta_{,t} = 0$, the sediment continuity equation (4.19), written in terms of the residual sediment transport, recalling also the equation (5.5), reads:

$$\frac{\partial \langle q_s \rangle}{\partial x} - \gamma \langle q_s \rangle = 0 \tag{5.8}$$

where the square brackets denote tidal average. The solution in terms on the residual sediment flux can be written as:

$$\langle q_s \rangle = \langle q_{s0} \rangle \exp(\gamma x) , \tag{5.9}$$

where $\langle q_{s0} \rangle$ represents the average value of the sediment flux at the mouth of the estuary. Since at the landward boundary (i.e. at $x = 1$) the sediment flux vanishes due to the reflecting barrier condition, the only possibility for the residual sediment flux to have an equilibrium configuration is to become negligible in every point of the domain.

However, the Engelund and Hansen formula (4.7) used to evaluate the sediment flux does not contain a threshold value below which the sediment transport could vanish. The residual velocity and consequently the residual sediment flux asymptotically tend to zero in every section of the domain, but they cannot exactly achieve this value. This can be seen in Figure 5.7, where the temporal evolution of the residual sediment flux at the mouth and in the middle of the estuary are plotted. The equilibrium configuration is achieved only asymptotically because the residual sediment flux, however small, implies a non vanishing sediment transport also after a long period of time. The equilibrium configuration reached by the estuary is actually a quasi-equilibrium configuration. For this reason, it is necessary to define a threshold value for the bottom variation in a fixed period of time below which the equilibrium can be considered reached and the numerical simulation can be stopped. In all the results presented in this work, the threshold value has been fixed equal to $10^{-2} mm/year$. The time necessary to reach the equilibrium configuration is usually of the order of a thousand years; in the example reported in Figure 5.7 the morphological time scale T_b^* is equal to 110 years and the equilibrium configuration is reached in in a dimensionless time τ of about ~ 10 that corresponds approximately to 1000 years. Moreover it is interesting to notice that at the mouth of the estuary the residual sediment flux is smaller than in the middle of the channel during the whole simulation. This means that at the mouth the velocity is more symmetrical, as it can be seen also in Figure 5.5

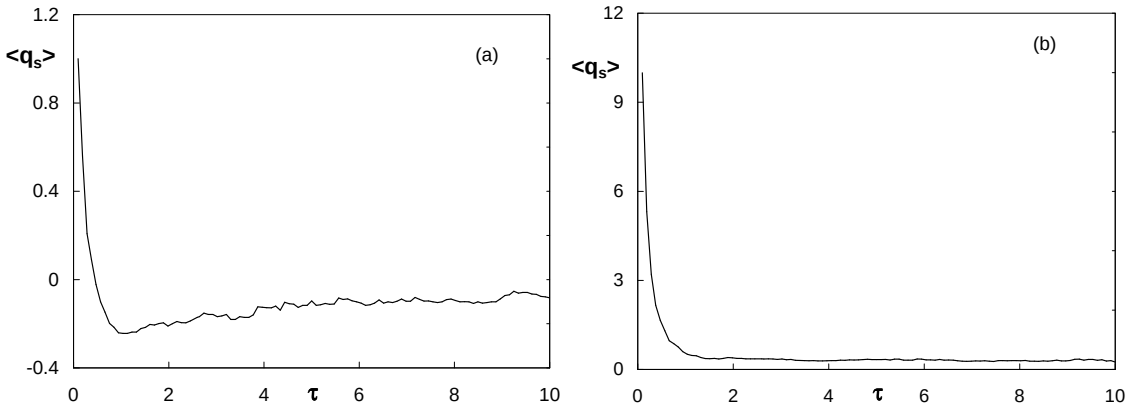

Figure 5.7: Temporal evolution of the residual sediment flux at the mouth ($x = 0$) (a) and in the middle of the estuary ($x = 0.5$) (b) [$L_e^* = 40km$, $L_b^* = 20km$, $D_0^* = 10m$, $a_0^* = 4m$, $C_h = 20$, $d_s^* = 10^{-1}mm$]

and 5.6.

The channel convergence is able to enhance the distortion of the tidal wave and the flood-dominance in an estuary. The influence of the degree of convergence clearly emerges if the peaks and the residual values of the velocity U and the sediment flux q_s are plotted at the initial stage of evolution, when the bed is still horizontal (Figure 5.8). The more the channel is convergent, the more the flood-dominated character is enhanced, since the asymmetry is positive in the entire length of the estuary. When the channel is weakly convergent, both the peak values of the velocity and the sediment flux monotonically decrease landward. On the contrary, when the convergence becomes strong enough, they show a peak inside the estuary, that explains the reason for which the sediment front stops at a certain distance from the mouth and the beach is formed inside the domain.

The influence of the convergence on the hydrodynamics implies a strongly effect also on the morphological response of a tidal channel since the flow field determines the sediment transport and then the evolution of the bottom profile. In fact, the final length L_a^* of the estuary, that is defined as the distance between the mouth and the position of the beach at equilibrium, is strongly dependent on the degree of convergence; this is pointed out in Figure 5.9 that summarizes the outcomes of the numerical simulations corresponding to different values of the physical length imposed to the system in the initial configuration and of the convergence length, L_b^*. Each point corresponds to the result of a simulation characterized by a given degree of convergence; moving along the line, the physical dimension of the domain L_e^* increases. When the channel is not sufficiently long, that is for small values of L_e^*, the equilibrium length L_a^* coincides with the physical dimension

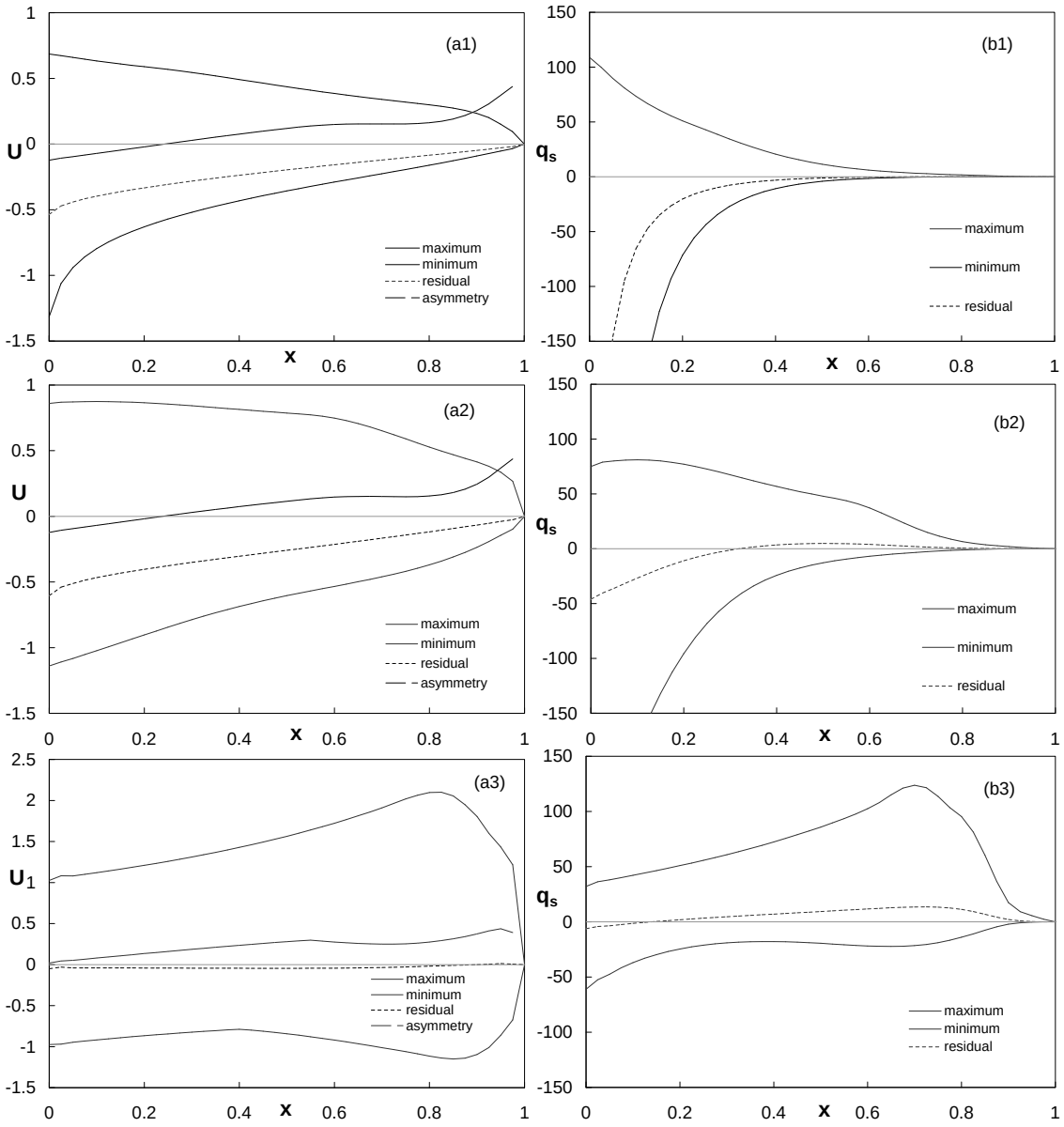

Figure 5.8: Degree of asymmetry α, maximum, minimum and residual values of flow velocity (a) and of sediment flux (b) along the estuary, at the beginning of the simulation, for different values of the convergence length: $L_b^* \to \infty$ (a_1, b_1), $L_b^* = 160km$ (a_2, b_2), $L_b^* = 10km$ (a_3, b_3) [$L_e^* = 160km$, $D_0^* = 10m$, $a_0^* = 4m$, $C_h = 20$, $d_s^* = 10^{-1}mm$].

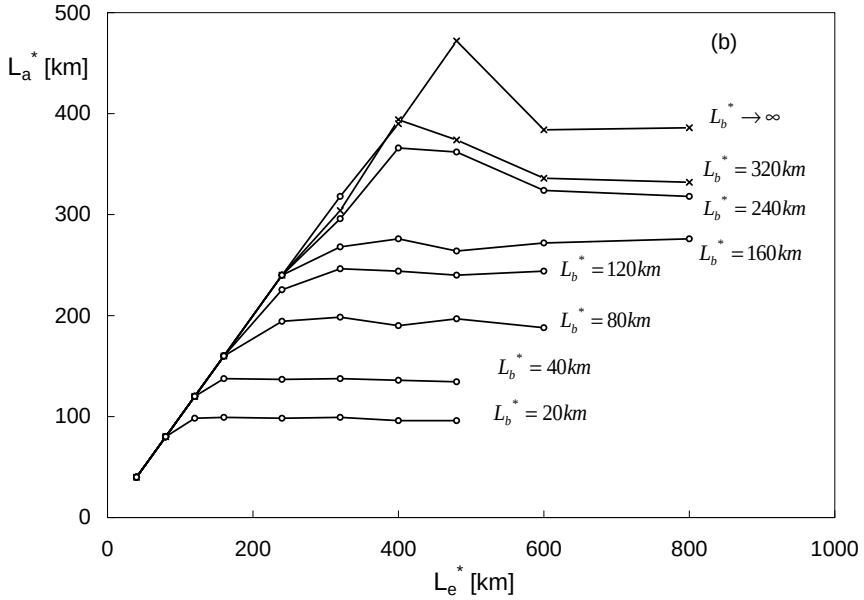

Figure 5.9: Equilibrium length of the estuary L_a^* as a function of the initial length L_e^*, for different values of convergence length [$D_0^* = 10m$, $a_0^* = 4m$, $C_h = 20$, $d_s^* = 10^{-1}mm$].

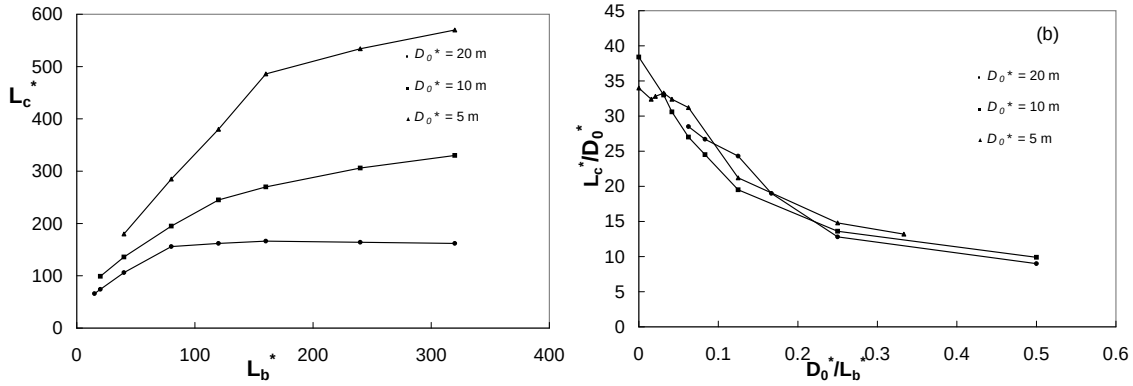

Figure 5.10: Equilibrium length L_c^* as a function of the convergence length L_b^*, for different values of D_0^* and a_0^* but the same $\varepsilon = 0.4$ (a); equilibrium length L_c^*/D_0^* as a function of the dimensionless degree of convergence D_0^*/L_b^* (b) [$C_h = 20$, $d_s = 10^{-1}mm$].

imposed to the system: the corresponding points fall on the bisector line of the graph. On the contrary, when the channel is long enough the system can reach an equilibrium length which becomes independent of the physical dimension of the domain. This asymptotic value L_c^* depends on the degree of convergence of the channel: the stronger is channel

convergence (i.e. small values of L_b^*), the shorter is the equilibrium length L_c^* (Figure 5.10a). The dependence of L_c^* on the depth D_0^* can be ruled out once it is scaled with the initial depth D_0^*, as shown in Figure 5.10b.

Numerical results also suggest that a transition zone occurs close to the bisector line, in which L_a^* still depends on the initial physical dimension, beyond which the asymptotic value of the equilibrium length L_c^* is reached, for a given value of L_b^*. Notice that the width of the transition zone increases as the convergence length increases. Furthermore in weakly convergent channels or in constant width channels the beach does not always emerge. However, a suitable equilibrium length can be defined also in this case in terms of the distance of the leading edge of bottom profile from the mouth (the corresponding points are denoted by an 'x' in Figure 5.9).

It is useful to remark that all the simulations presented in Figure 5.9 are characterized by the same value of the initial dimensionless tidal amplitude ε and of the initial depth at the mouth. Given the definition of the parameter ε:

$$\varepsilon = \frac{a_0^*}{D_0^*} \tag{5.10}$$

it follows that all the simulations are characterized also by the same tidal amplitude a_0^*, which is the external forcing. On the contrary, the value of the water depth and consequently of the dimensionless tidal amplitude changes during the morphological evolution. For this reason it is important to point out that this definition of ε refers to the initial depth at the mouth of the channel.

5.1.1 The effect of boundary conditions

To understand the importance of the seaward boundary condition, two different assumptions at the mouth of the channel are investigated: the first corresponds to a vanishing sediment inflow and the second to an incoming sediment flux that equals the transport capacity associated with the local and instantaneous flow conditions at the mouth. The influence of the seaward boundary condition on sediment transport is clarified in Figure 5.11 and 5.12. When sediment inflow is set equal to zero, sediment transport must vanish at the mouth in order to reach a stable configuration, which implies a smaller velocity and hence a larger scour at the entrance. On the contrary, when sediment inflow balances the equilibrium transport capacity associated with local hydrodynamic condition, the sediment transport can maintain a non-vanishing peak value even at equilibrium. It is useful to remark that at equilibrium the flood and the ebb phase tend to a more symmetric con-

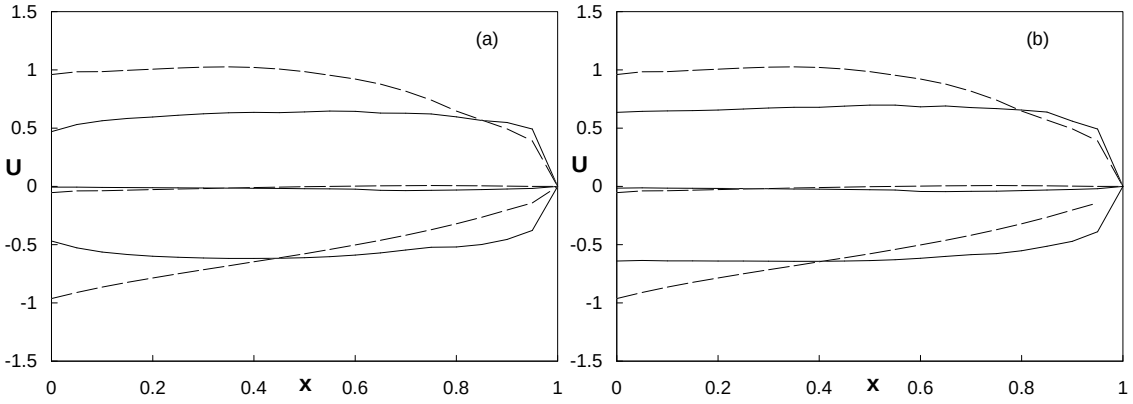

Figure 5.11: Maximum, minimum and residual values of flow velocity U along the estuary after one cycle (dashed line) and at equilibrium (continuous line), for different boundary conditions at the seaward end: (a) vanishing sediment flux; (b) equilibrium sediment flux [$L_e^* = 40km$, $L_b^* = 20km$, $D_0^* = 5m$, $a_0^* = 2m$, $C_h = 20$, $d_s^* = 10^{-1}mm$].

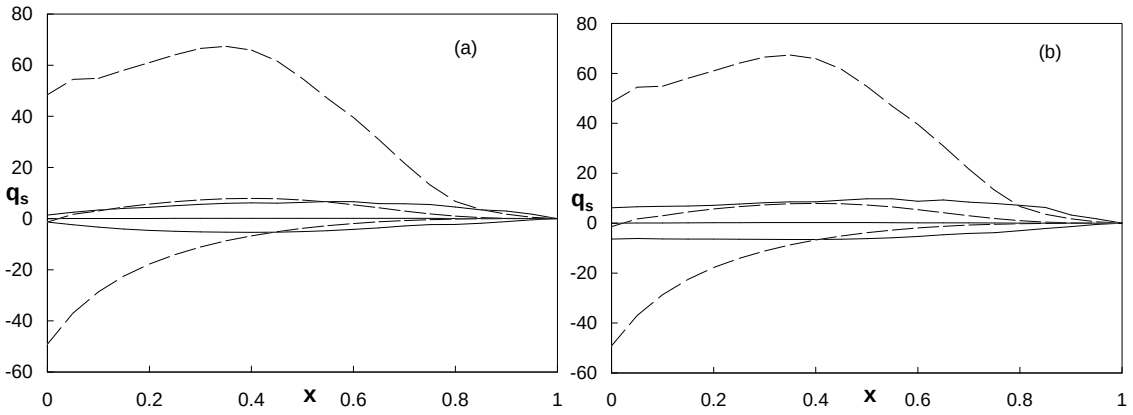

Figure 5.12: Maximum, minimum and residual sediment flux q_s along the estuary after one tidal cycle (dashed line) and at equilibrium (continuous line), for different boundary conditions at the seaward end: (a) vanishing sediment inflow; (b) sediment flux in equilibrium [$L_e^* = 40km$, $L_b^* = 20km$, $D_0^* = 5m$, $a_0^* = 2m$, $C_h = 20$, $d_s^* = 10^{-1}mm$]

figuration that implies a vanishing net sediment flux as it is obvious to expect; moreover this is a dynamical equilibrium since it is achieved only in terms of net transport.

In Figure 5.13 the difference in the bottom profiles obtained with these two different boundary conditions can be observed: the former condition (dashed line), that corresponds to a vanishing sediment inflow, implies a larger scour at the mouth. Furthermore for short channels, which are characterized by a bottom equilibrium profile that coincides with the

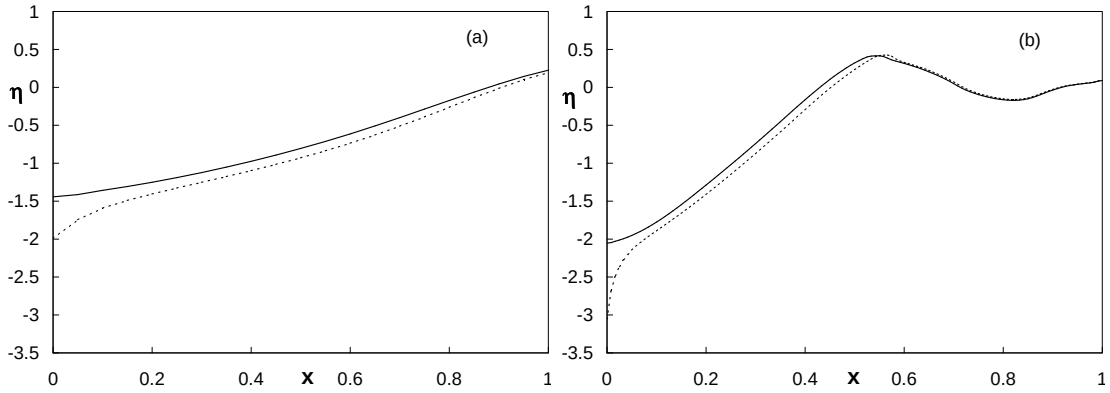

Figure 5.13: The equilibrium bottom profiles in short (a) and long (b) channels with vanishing sediment flux (dashed lines) and equilibrium sediment flux (solid lines) at the mouth of the channel [$D_0^* = 10m$, $a_0^* = 4m$, $C_h = 20$, $d_s^* = 10^{-1}mm$; $L_e^* = 160km$, $L_b^* = 120km$ (a); $L_e^* = 240km$, $L_b^* = 40km$ (b)].

entire length of the estuary, this condition causes also a slight increase in the equilibrium slope; in longer channels the position of the beach at equilibrium slightly migrates landward without a variation in the bottom slope.

5.2 Influence of the external parameters on the solution

In the previous paragraphs, the attention has been mainly focused on the dependence of the morphological evolution on the degree of convergence. Now the the attention is concentrated on how other relevant parameters are able to influence the equilibrium configuration of the estuarine channel.

5.2.1 The role of the initial depth at the mouth

First of all, the role of the initial depth at the mouth, D_0^*, is investigated. This external parameter actually represents the initial condition for the whole system whose initial bed is horizontal. Since the bottom profile evolves in time until the equilibrium configuration is reached, the water depth at the mouth is not constant, differently from Schuttelaars and de Swart (2000) who force the bottom elevation at the mouth of the estuary to keep artificially constant.

It is natural to expect the solution to be only weakly dependent on this parameter, for a given tidal forcing. This is confirmed by the results obtained for a short estuary reported in Figure 5.14, where the equilibrium profiles corresponding to four different values of

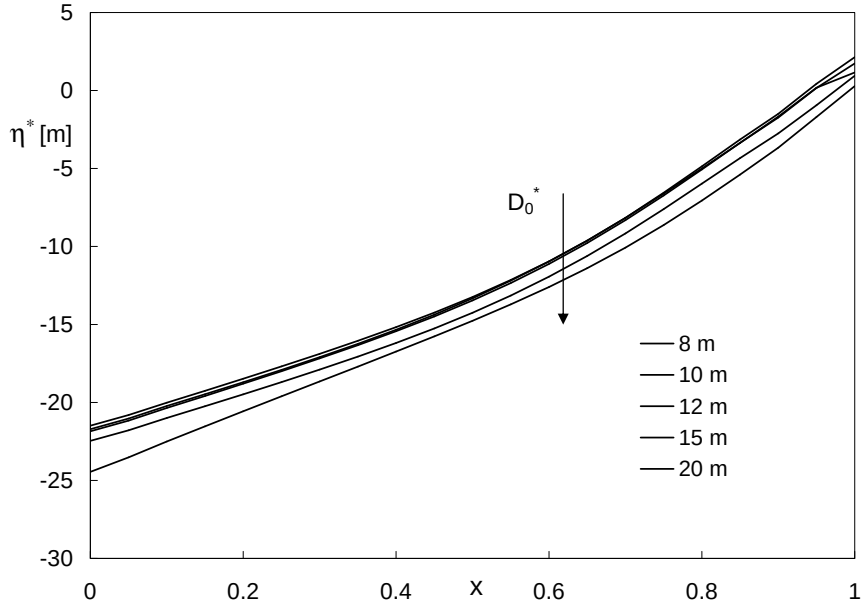

Figure 5.14: Equilibrium bottom profiles for different values of D_0^* in a short estuary [$L_e^* = 40km$, $L_b^* = 20km$, $a_0^* = 4m$, $C_h = 20$, $d_s = 10^{-1}mm$.]

the initial depth for the same dimensional tidal amplitude a_0^* are plotted. The resulting profiles are quite similar. The equilibrium bottom profiles in a long estuary are plotted in Figure 5.15: when the the initial depth D_0^* is not very high there are not great differences between the equilibrium bed profiles; on the contrary, in initially extremely deep channels the morphological evolution is so slow that it takes a very long time to realize. The bottom profile of a deep channel is indeed approaching the equilibrium profiles corresponding to smaller values of the initial depth but with such a small velocity that probably it will never reach the equilibrium configuration in a morphologically reasonable time.

5.2.2 The role of the tidal amplitude

In principle it is obvious to expect the equilibrium profiles to be strongly dependent on the external forcing. In fact the tidal amplitude a_0^* has a strong influence on the solution, since it controls the scale of velocity U_0^* in the estuary (e.g. Toffolon, 2002); furthermore, the propagation of the tidal wave along the channel determines its hydrodynamical and morphological behavior. Given the same geometrical conditions, a larger tidal amplitude corresponds to a deeper bottom equilibrium profile, as it is shown in Figure 5.16. In this case the channel is short and the equilibrium length coincides with the physical dimension of the domain; for a longer channel, a larger tidal amplitude implies a seaward shift in the

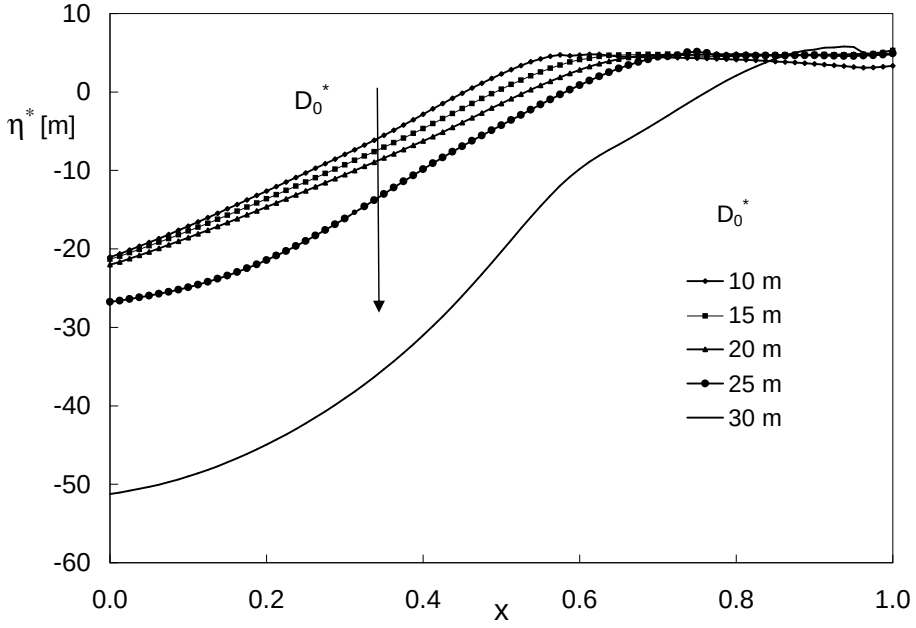

Figure 5.15: Equilibrium bottom profiles for different values of D_0^* in a long estuary. [$L_e^* = 160km$, $L_b^* = 40km$, $a_0^* = 4m$, $C_h = 20$, $d_s = 10^{-1}mm$.]

position of the beach and hence a decrease in the equilibrium length L_a^*, as it can be seen in Figure 5.17.

5.2.3 The role of the Chézy coefficient

Also the other parameters that are used to describe the system, as the Chézy coefficient C_h and the sediment diameter d_s^*, exert an influence on the solution. A correct estimation of the Chézy coefficient is necessary for a proper description of the sediment transport, which depends on the bottom shear stress. It is dimensionless but, for historical reasons, the dimensional form:

$$C^* = C_h\sqrt{g^*} = k_s^* R_h^{*1/6} = \frac{1}{n^*}R_h^{*1/6} \tag{5.11}$$

is often used, where k_s^* is the Gauckler-Strickler coefficient (unit of measurement $m^{1/3}s^{-1}$) and n^* is the Manning coefficient ($n = 1/k_s^*$). Typical values of the Chézy coefficients in tide-dominated estuaries range between 14 and 30, as it can be inferred from Table 2.1.

To investigate the effect of the Chézy coefficient on the morphological evolution, the comparison between two equilibrium bottom profiles corresponding to different values of this coefficient is made. When the flow resistance is increased, the correspondent equilibrium length becomes smaller, as it can be seen in Figure 5.18. Speer and Aubrey (1985) find

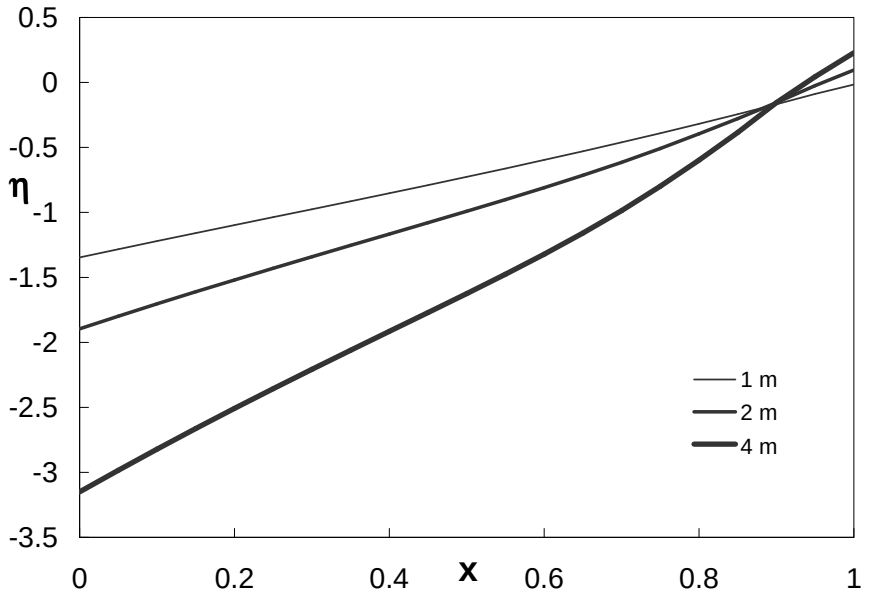

Figure 5.16: Bottom equilibrium profiles for different values of the tidal amplitude $a_0^*\,(1, 2, 4m)$ in a short estuary [$L_e^* = 40km$, $L_b^* = 20km$, $D_0^* = 10m$, $C_h = 20$, $d_s^* = 10^{-1}mm$]

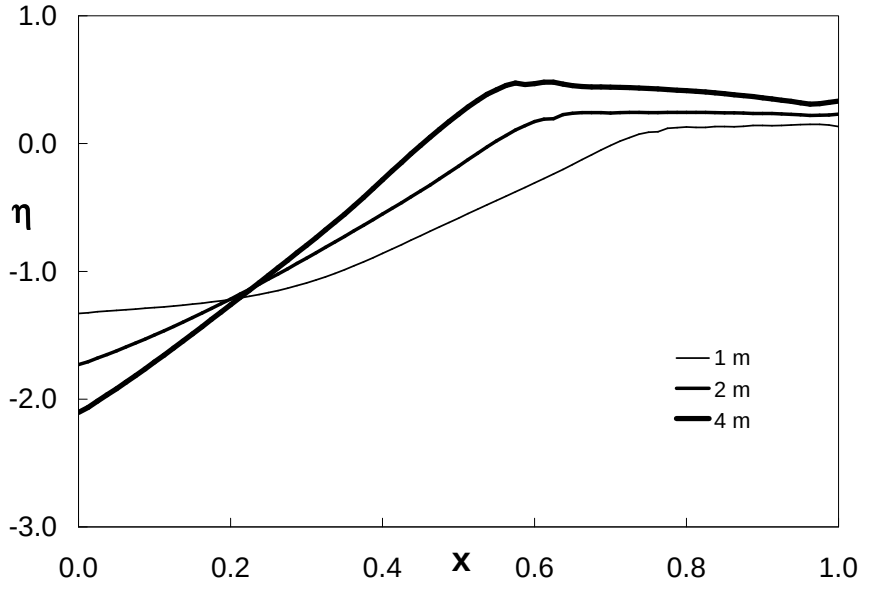

Figure 5.17: Bottom equilibrium profiles for different values of the tidal amplitude $a_0^*\,(1, 2, 4m)$ in a long estuary [$L_e^* = 160km$, $L_b^* = 40km$, $D_0^* = 10m$, $C_h = 20$, $d_s^* = 10^{-1}mm$]

that the flood-dominance is enhanced by stronger frictional effects. The flood-dominance character is accentuated (see Figure 5.8) also for large values of the degree of convergence, a situation that also corresponds to shorter equilibrium lengths (Figure 5.9). Therefore these results are coherent.

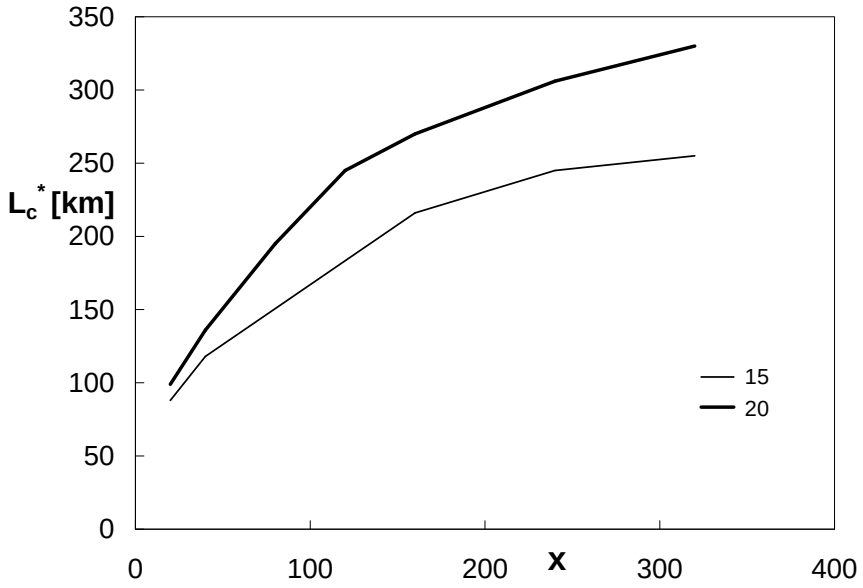

Figure 5.18: Equilibrium length L_c^* as a function of the convergence length L_b^* for different values of the Chézy coefficient $C_h(15, 20)$ $[a_0^* = 4m,\, D_0^* = 10m,\, d_s^* = 10^{-1}mm]$

5.2.4 The role of the overtide M_4

Although the tidal forcing at the mouth of the estuary may be primarily at the semidiurnal frequency , the non linear terms in continuity and momentum equations (4.18-4.17) almost always produce the distortion of tidal wave that can be represented by the growth of significant higher harmonics (Prandle, 1991). Fields observations of estuarine tides often indicate a rich spectrum of forced motions (e.g. Speer and Aubrey, 1985) ranging from high frequency (i.e. greater than semi-diurnal) to low frequency (e.g. fortnightly). In particular, the interaction between the M_2 and its first harmonic M_4 explains the general features of observed tidal asymmetries. The type of tidal distortion depends on the relative phasing of M_4 to M_2. Defining the M_2 and M_4 constituents as:

$$A_{M_2} = \varepsilon \sin(2\pi t - \phi_1) \tag{5.12}$$

$$A_{M_2} = \varepsilon_2 \sin(4\pi t - \phi_2)\,, \tag{5.13}$$

where $\varepsilon_2 = a_2^*/D_0^*$ is the dimensionless amplitudes of the M_4 tide, the relative M_2-M_4 phase is defined as:

$$\Delta\phi = 2\phi_1 - \phi_2 \tag{5.14}$$

This relative phase determines the sense of asymmetry: phases between the 0° and 180° indicate flood-dominance, while phases between the 180° and 360° indicate ebb-dominance.

Tidal forcing at the seaward boundary usually consists of the only semidiurnal M_2 constituent, since along much of the world's coastlines the offshore is dominated by this harmonic component. The overtides are internally generated as the tidal wave propagates into the estuary. Nevertheless, it interesting to investigate whether the prescription of an overtide in addition to the M_2 component in the boundary condition affects the morphological evolution of the estuary. When a M_4 constituent is added to the tidal forcing, the boundary condition at the mouth of the channel (4.28) can be rewritten as :

$$H(t)|_{x=0} = \varepsilon \sin(2\pi t) + \varepsilon_2 \sin(4\pi t - \phi)\,. \tag{5.15}$$

In Figure 5.19 different overtides with different amplitude and phase are shown; their effect on the morphological evolution can be seen in Figure 5.20. Given the same ε_2, when the phase ϕ is positive, the ebb dominance is enhanced and the bottom profile is characterized by a lower elevation. The difference between bed profiles corresponding to positive and negative phases increases if the M_4 amplitude increases, as it is obvious to expect since the tidal wave is distorted in a more marked way.

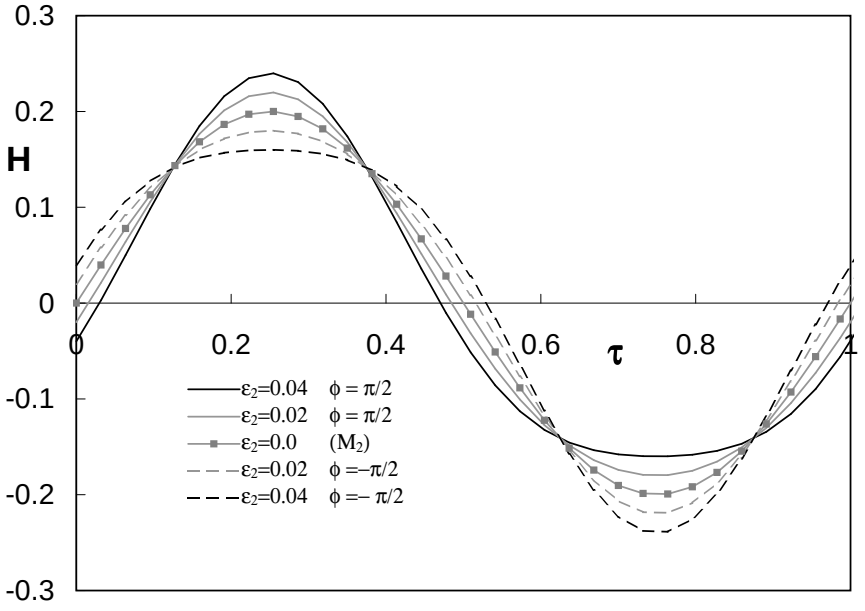

Figure 5.19: Different overtides M_4 imposed at the seaward boundary condition $a_2^* = (0.2m, 0.4m)$, $\phi* = (-\pi/2, \pi/2)$ $[a_0^* = 2m]$.

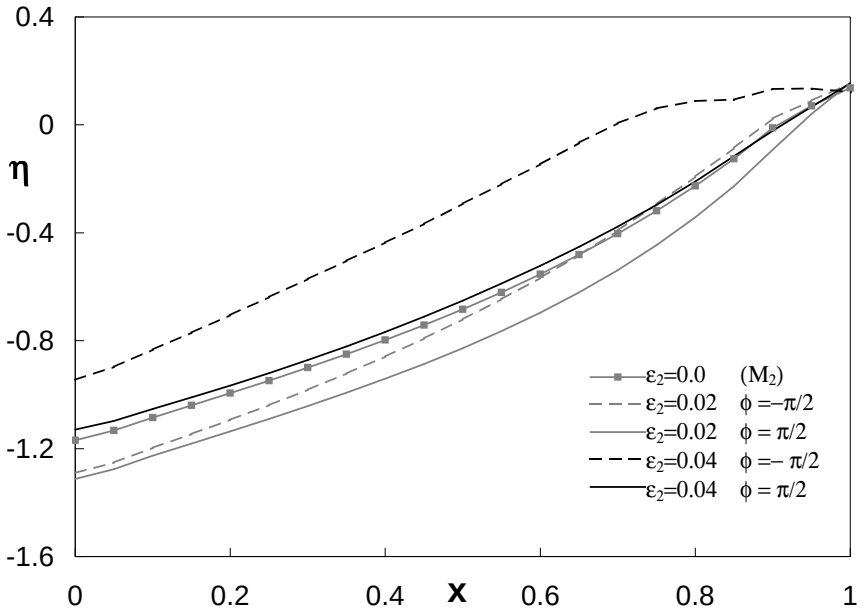

Figure 5.20: Bottom equilibrium profiles for different overtides M_4 $[L_e^* = 40km$, $L_b^* = 20km$, $D_0^* = 10m$, $C_h = 20$, $d_s^* = 10^{-1}mm$, $a_0^* = 2m]$.

5.3 The role of the fresh water discharge

A special attention has to be paid to the study of the effects of a non negligible freshwater discharge which has been neglected in previous works, while being a typical feature of most typical estuaries (see Table 2.14). Despite the fact that in tide-dominated estuaries, the volume of freshwater delivered within a tidal cycle typically keeps an order of magnitude smaller than the tidal prism, however it is interesting to investigate which influence this parameter is able to exert on the morphological evolution of a tidal channel.

5.3.1 Negligible tidal amplitude: analytical solution

Assuming a constant discharge Q^* and looking for the equilibrium bed profile, it is possible to consider a steady state and neglect time derivatives. In this case, the Exner equation (4.4) implies that the total sediment transport $B^*q_s^*$ is constant along the channel. Assuming a simplified sediment transport formula

$$q_s^* = kU^{*n}\,, \tag{5.16}$$

where $n = 5$ for the Engelund-Hansen relationship, the sediment transport is everywhere equal to

$$q_s^* B^* = k\left(\frac{Q^*}{B_r^* D_r^*}\right)^n\,, \tag{5.17}$$

where B_r^* and D_r^* are the width and the depth in a given section, say the upstream end of the channel. Thus, it is possible to relate the depth and the width locally:

$$D(x)^* = D_r^*\left[\frac{B_r^*}{B(x)^*}\right]^{\frac{n-1}{n}}\,. \tag{5.18}$$

The momentum equation (4.1), with constant Q^* and steady condition, gives the variation of the free surface elevation

$$\frac{\partial H^*}{\partial x^*} = \frac{Q^{*2}}{C_h^2 g^* B^{*3} Y^{*3}}\left[B^* + C_h^2 D^*\frac{\partial B^*}{\partial x^*} + C_h^2 B^*\frac{\partial D^*}{\partial x^*}\right]\,. \tag{5.19}$$

Substituting from (5.18) into (5.19) gives

$$\frac{\partial H^*}{\partial x^*} = \frac{Q^{*2}}{g^* D_r^{*2}}\left[\frac{B_r^{*\left(-3\frac{n-1}{n}\right)} B^{*\left(1-\frac{3}{n}\right)}}{C_h^2 D_r^*} + \frac{B_r^{*\left(-2\frac{n-1}{n}\right)} B^{*\left(-1-\frac{2}{n}\right)}}{n}\frac{\partial B^*}{\partial x^*}\right]\,. \tag{5.20}$$

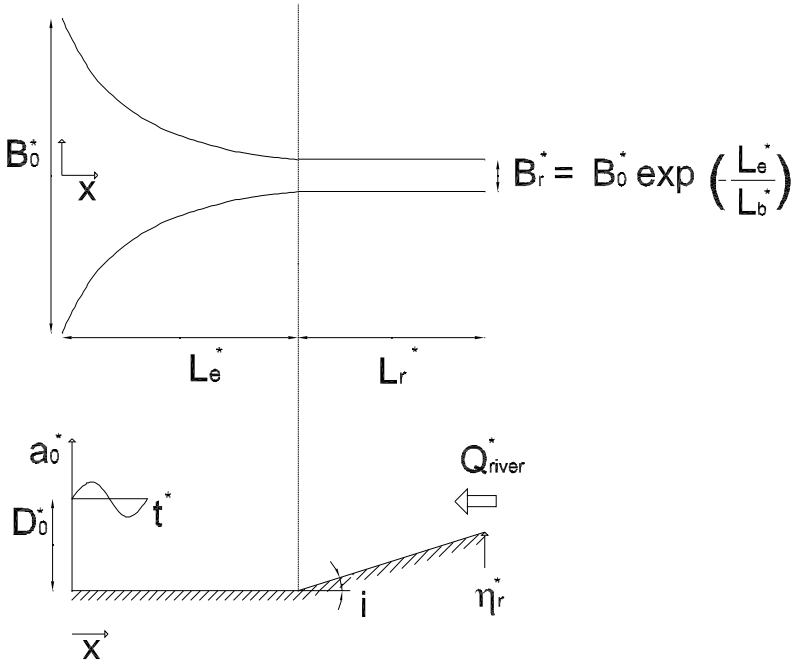

Figure 5.21: Sketch of the plan view and a lateral section of the estuary with a constant width channel at the end of funnel-shape estuary.

To reduce the influence of the landward boundary condition, a new schematization is adopted. A channel separated in two reaches is considered: a constant-width channel of length L_r^* and width B_r^* upstream; a channel of length L_e^* and width $B^* = B_0^* \exp(-x^*/L_b^*)$ downstream. The coordinate x^* is directed upwards, so that the former channel is in the range $x^* \in (0, L_e^*)$ and the latter $x^* \in (L_e^*, L_e^* + L_r^*)$. In order to avoid discontinuities, the width at the junction ($x^* = L_e^*$) must be

$$B^*(L_e^*) = B_0^* \exp(-L_e^*/L_b^*) = B_r^* \,. \tag{5.21}$$

The boundary conditions are chosen as follows: at the downstream end the free surface is prescribed ($H^*(0) = H_0^*$); at the upstream end the discharge per unit width $q^* = Q^*/B_r^*$ is imposed and the bed elevation $\eta^*(L_e^* + L_r^*)$ is fixed. The width B_0^* is imposed downstream and B_r^* can evaluated through (5.21) when L_b^* and L_e^* are chosen. In Figure 5.21 a sketch of the plan view and of a longitudinal section is shown.

In the upstream reach the width is constant ($B^* = B_r^*$) and (5.18) obviously gives $D^* = D_r^*$, i.e. uniform flow holds. Moreover, (5.20) is equivalent to the free surface slope

in uniform flow and the free surface is linearly increasing upstream:

$$H^*(x^*) = H^*(L_e^*) + \frac{Q^{*2}}{C_h^2 g^* B_r^{*2} D_r^{*3}} (x^* - L^*) \, . \tag{5.22}$$

The bottom elevation in this reach can be evaluated as $\eta^* = H^* - D_r^*$. Note that D_r^* and $H^*(L_e^*)$ are not known at the moment, nor the bottom slope is determined.

In the downstream reach the width varies exponentially and the depth is determined by (5.18) as

$$D^*(x^*) = D_r^* \exp\left[-\frac{(n-1)(L_e^* - x^*)}{nL_b^*}\right] . \tag{5.23}$$

The free surface can be obtained integrating (5.20), with the boundary condition that $H^*(0) = H_0^*$:

$$\begin{aligned} H^*(x^*) \quad &= H_0^* + \frac{Q^{*2}}{g^* B_r^{*2} D_r^{*2}} \left\{ \frac{1}{2} \left[\exp\left(-2\frac{L_e^*}{nL_b^*}\right) - \exp\left(-2\frac{(L_e^* - x^*)}{nL_b^*}\right)\right] + \right. \\ &\left. + \frac{nL_b^*}{C_h^2 D_r^* (n-3)} \left[\exp\left(-L_e^* \frac{(n-3)}{nL_b^*}\right) - \exp\left(-\frac{(L_e^* - x^*)(n-3)}{nL_b^*}\right)\right]\right\} \end{aligned} \tag{5.24}$$

The bed profile is given by $\eta^*(x^*) = H^*(x^*) - D^*(x^*)$ with the relations (5.23)-(5.24).

If we impose the bottom elevation η_r^* at $x^* = L_e^* + L_r^*$, from (5.22) we can derive the relation

$$H^*(L_e^*) = \eta_r^* + D_r^* - \frac{Q^{*2} L_r^*}{C_h^2 g^* B_r^{*2} D_r^{*3}} (x^* - L^*) \, , \tag{5.25}$$

which expresses $H^*(L_e^*)$ as a function of the unknown D_r^*. By comparing (5.25) with the value of $H^*(L_e^*)$ obtained through equation (5.24), it is possible to write an implicit relationship for the only unknown D_r^*,

$$\begin{aligned} &\frac{Q^{*2}}{g^* B_r^{*2} D_r^{*2} 2} \left\{ \frac{1}{2} \left[\exp\left(-2\frac{L_e^*}{nL_b^*}\right) - 1\right] + \frac{nL_b^*}{C_h^2 D_r^* (n-3)} \left[\exp\left(-L_e \frac{(n-3)}{nL_b^*}\right) - 1\right]\right\} + \\ &+ H_0^* - \eta_r^* - D_r^* + \frac{Q^{*2} L_r^*}{C_h^2 g^* B_r^{*2} D_r^{*3}} (x^* - L^*) = 0 \, , \end{aligned} \tag{5.26}$$

which can be solved numerically. An example of the resulting profiles of $H^*(x^*)$ and $\eta^*(x^*)$ is drawn in Figure 5.22 and compared with the results of the numerical simulation, showing an excellent agreement.

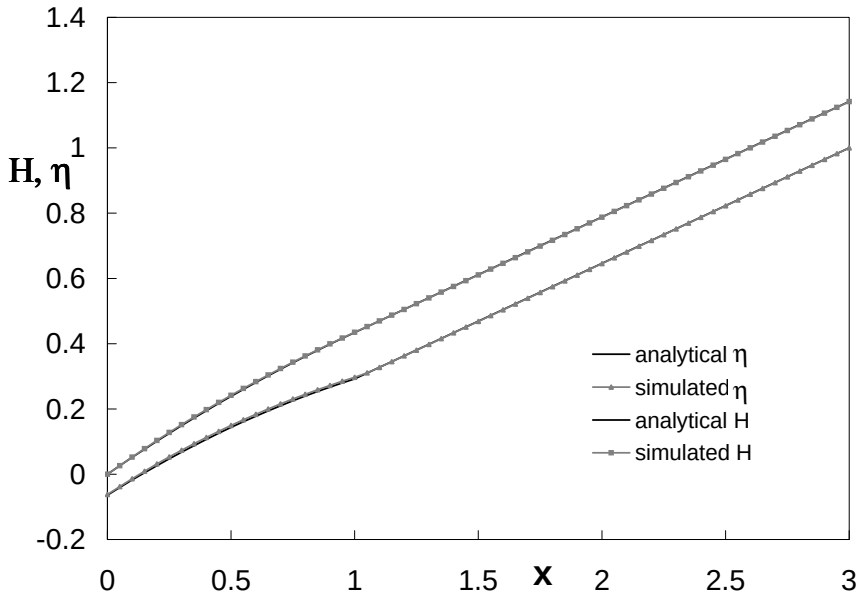

Figure 5.22: Comparison between the bottom elevation and the water surface elevation profiles obtained with the analytical solution and the numerical simulation [$L_e^* = 40km$, $L_b^* = 20km$, $L_f^* = 80km$, $D_0^* = 10m$, $C_h = 20$, $d_s^* = 10^{-1}mm$, $z_f^* = 10m$, $Q_{river}^* = -676m^3/s$]

5.3.2 Non negligible tidal amplitude

Starting from the same schematization used in the previous paragraph, a tidal forcing is imposed at the seaward boundary. Given the same river discharge, the bottom equilibrium profiles for different values of the tidal amplitude a_0^* are reported in Figure 5.23; when the tidal action is not strong enough compared to the river discharge, the bottom profile is characterized by a smaller slope. When the tidal action becomes more important, the bottom slope is larger and more similar to the profiles obtained with a reflecting barrier condition.

The tidal action can be described using a parameter called the tidal prism P^*, which is defined as the total volume of water exchanged between the estuary and the open sea during the flood or the ebb phase:

$$P^* = \int_{T_{ebb}, T_{flood}} |Q^*| \, dt \, . \tag{5.27}$$

which, in the case of short estuaries, can be approximated as:

$$P^* = 2a_0^* L_0^* B_0^* \, . \tag{5.28}$$

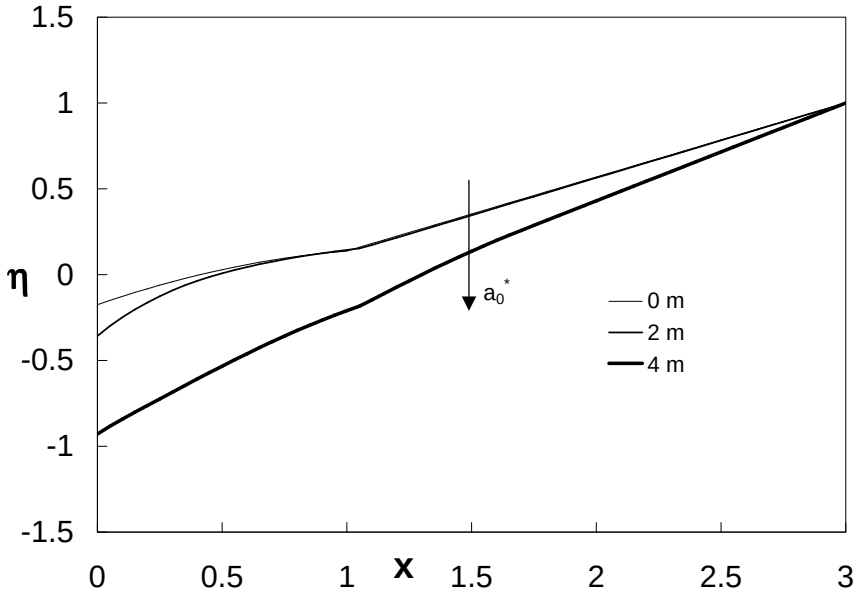

Figure 5.23: Bottom equilibrium profile for different values of the tidal amplitude $a_0^* = (0, 2, 4m)$ [$L_e^* = 40km$, $L_b^* = 40km$, $L_f^* = 80km$, $D_0^* = 10m$, $B_0^* = 1000m$, $C_h = 20$, $d_s^* = 10^{-1}mm$, $z_f^* = 10m$, $Q_{river}^* = -1840m^3/s$].

The relative importance of the river discharge effect with respect to the tidal action can then be described by the ratio p:

$$p = \frac{|Q_{river}^*|}{P^*} \frac{T_0^*}{2} \,. \tag{5.29}$$

When the tidal action is dominant with respect to the river discharge, this parameter p is small. The equilibrium bottom profile in Figure 5.23 that corresponds to a negligible tidal amplitude is characterized by a value of p that tends to infinity while the bottom profile corresponding to the largest tidal amplitude is equal to 0.12.

Given the same tidal amplitude, the equilibrium bottom profiles for different values of the river discharge are compared in Figure 5.24. Also in this case, when the river discharge is able to balance the tidal action, as in the curve characterized by the largest value of the discharge in which the ratio p is equal to 0.12, the equilibrium bottom profile is characterized by a smaller slope.

The addition of a constant width channel at the end of the domain simulates the behaviour of a river that flows into the estuary and prevents the wave reflection due to the impermeable barrier condition. Nevertheless, the number of parameters that have to be fixed in this case increases. In fact, it is necessary to choose the bottom elevation of the

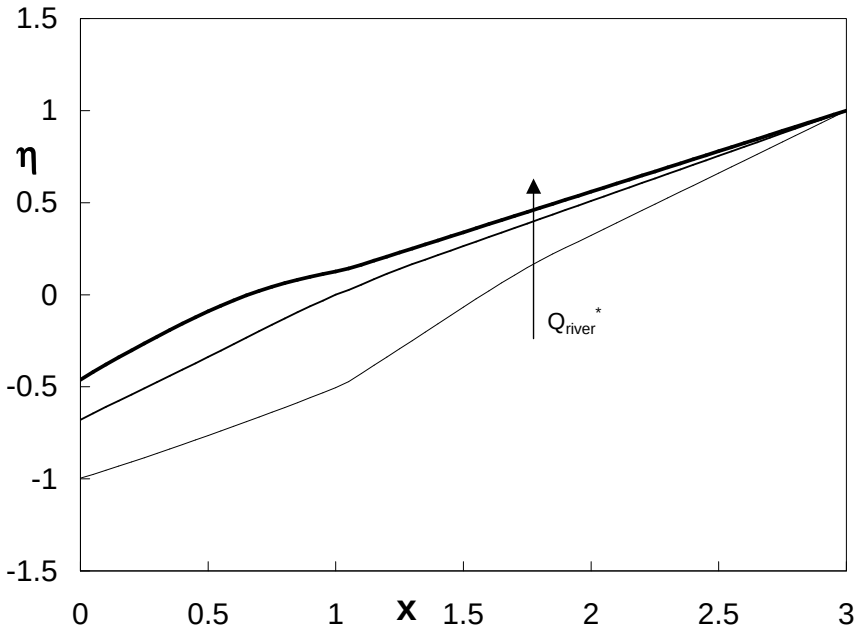

Figure 5.24: Bottom equilibrium profile for different values of the freshwater river discharge $Q^*_{river} = (-184, -368, -735 m^3/s)$ [$L^*_e = 40km$, $L^*_b = 20km$, $L^*_f = 80km$, $D^*_0 = 10m$, $B^*_0 = 1000m$, $C_h = 20$, $d^*_s = 10^{-1}mm$, $z^*_f = 10m$, $a^*_0 = 2m$].

last section and the length of the river channel or alternatively its bottom slope. For this reason, the response of the numerical model is tested when a non negligible river discharge is imposed at the end of the estuarine channel at the position $x = 1$ (Figure 5.21). This condition forces the discharge to assume a constant value that cannot be influenced by the tidal action. In Figure 5.25 a comparison among equilibrium bottom profiles in a short estuary are plotted corresponding to different values of the freshwater discharge. For small values of the river discharge the sediments tend to be collected in the inner part of the estuary while for larger values the sediments do not have the possibility to reach the landward boundary but are carried out of the estuary. Although it appears to be quite hard to compare these result with those presented in Figure 5.24, since the computational domain and above all the boundary conditions are very different, it is possible to notice that also in this case the bottom slope in the case of large freshwater discharge is milder.

When a freshwater discharge is imposed at the landward boundary, the morphological evolution of the channel is very different from the case of negligible river inflow; in fact the sediment flux does not tend to make emerge a beach inside the estuary. In fact, the formation of a beach is inhibited since there is always a non negligible water depth in every cell of the domain. The role of the water discharge is investigated also in the case

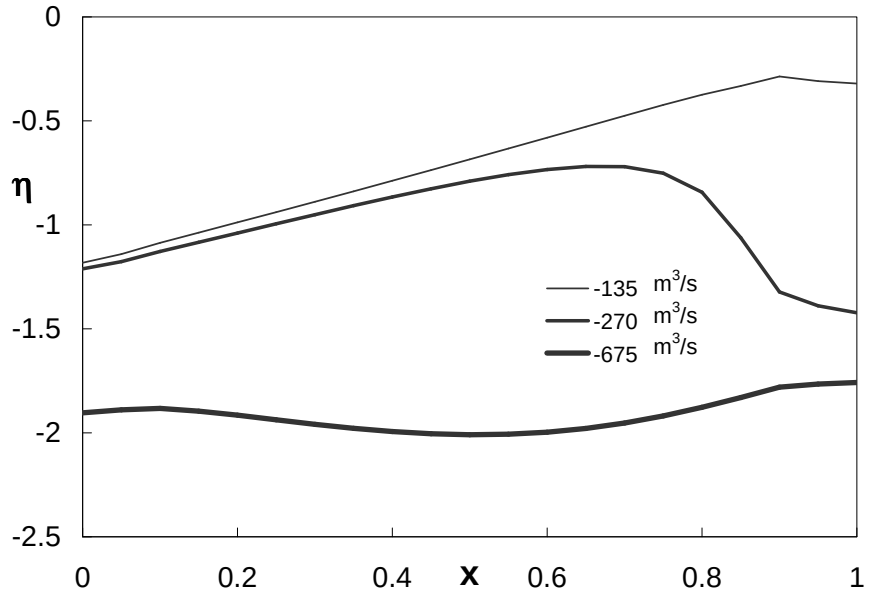

Figure 5.25: Bottom equilibrium profiles for different values of the fresh water discharge Q^*_{river} [$L^*_e = 40km$, $L^*_b = 20km$, $D^*_0 = 10m$, $C_h = 20$, $d^*_s = 10^{-1}mm$, $Q^*_{river} = (-135, -270, -675\, m^3/s)$]

of a long estuary, where, with a reflecting barrier condition, the beach were formed inside the domain. The results are reported in Figure 5.26, where the equilibrium profiles corresponding to two channels with different lengths and different characteristic parameters are shown. Also in the case of a long estuary, for high values of the river discharge the equilibrium bottom slope tends to be mild (p in fact assume a larger value in the example reported in Figure 5.26a).

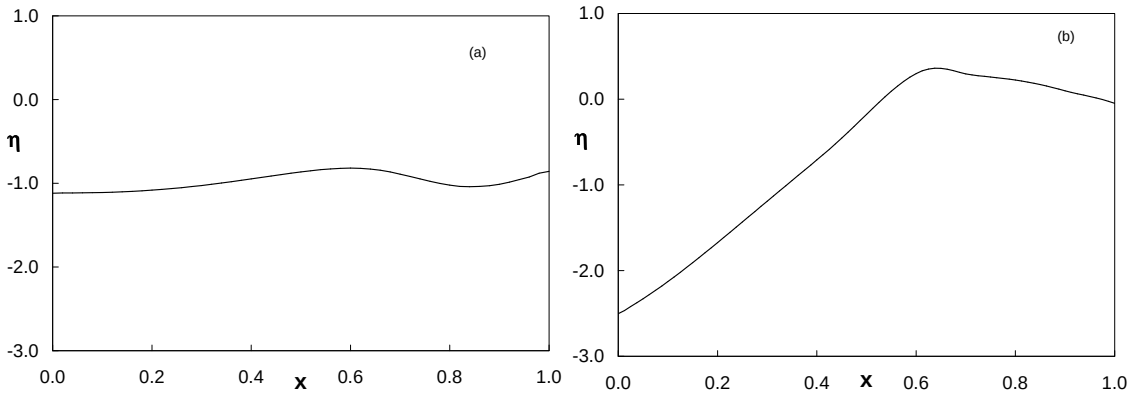

Figure 5.26: Bottom equilibrium profiles for two different long channels: $L_e^* = 100km$, $L_b^* = 40km$, $a_0^* = 1m$, $Q_{river}^* = -328m^3/s$ (a); $L_e^* = 160km$, $L_b^* = 40km$, $a_0^* = 1m$, $Q_{river}^* = -183m^3/s$ (b)[$D_0^* = 10m$, $C_h = 20$, $d_s^* = 10^{-1}mm$].

5.4 Discussion

In this chapter, the long-term morphological evolution of a tide-dominated estuary is investigated with the use of a relatively simple one-dimensional numerical model, which neglects the presence of intertidal areas and in which only the bed is considered erodible.

In this simplified schematization, a tide-dominated estuary is described as a channel with a rectangular cross-section whose width is supposed to follow an exponential law and in which a reflecting barrier condition is imposed at the landward boundary. The equilibrium bottom profile is defined as the configuration in which the tidally averaged sediment flux vanishes everywhere or, alternatively, the bottom elevation attains a constant value. To be more precise, given the Engelund and Hansen transport formula, this condition can be achieved only asymptotically; when the variation of the bottom elevation in a defined period of time is smaller than a threshold value, the equilibrium configuration can be considered attained. The equilibrium is dynamical, since it is achieved only in tidally averaged terms.

As pointed out by Dronkers (1986), the long-term erosion/deposition process is determined by the residual sediment transport, which is mainly related to the degree of asymmetry between the flood and the ebb peak values of flow velocity, due to the non-linear dependence of sediment transport on flow velocity. The effect of degree of convergence is not limited to the hydrodynamics but it represents a fundamental element to characterize the morphological evolution. The morphological response occurs in a fairly long period of time, say of the order of the centuries.

As described above, the final equilibrium length of the channel is found to depend mainly on two parameters, namely the physical length of the channel and the degree of convergence. If the estuary is relatively short and weakly convergent, a beach is formed at the landward end and the equilibrium bottom profile involves the entire length of the estuary. If the initial length of the channel exceeds a threshold value, the beach is formed inside the domain and it is possible to define a final equilibrium length, that is smaller than the initial one, as the distance between the beach and the mouth. In this case, this equilibrium length is independent of the physical dimension that is imposed to the system but it is a function of the degree of convergence: it decreases if the convergence increases.

As it obvious to expect, the equilibrium length is influenced also by the other parameters that characterize the system as the friction coefficient, the sediment diameter, the tidal forcing and the freshwater discharge. The latter parameters have been analyzed in more detail. The tidal action tends to produce larger bottom slopes in the equilibrium profiles, while the effect of the river discharge is opposite and tends to decrease the equilibrium bed slopes. The convergence, in fact, causes the distortion of the tidal wave and forces the sediments to move towards the inner part of the estuary until the bottom slope is large enough to cancel the tidal asymmetry and to establish an equilibrium configuration. On the contrary, the presence of a river discharge enhances the ebb dominance so that the bottom slope is not forced to increase to reach the equilibrium bottom profile.

6 Long-term evolution of tide-dominated estuaries with erodible banks

In the previous chapter, the attention has been focused on the characterization of the bottom evolution of a convergent estuary with fixed banks. The typical planimetric funnel shape of a tide-dominated estuary has been characterized with an exponential variation law along the longitudinal coordinate. In this kind of approach, two big limitations can be pointed out. The first one is obvious and inherent in the use of such kind of model: a fixed banks model is not able to explain the origin and the reasons for which tidal channels are convergent. The second limitation is represented by the fact that the slopes of the equilibrium bottom profiles are quite large if compared with those of real estuaries, where the bed profile in some cases shows an almost vanishing slope (Figures 2.19, 2.21, 2.23).

In fact, the morphological evolution obtained with the fixed banks model tends inevitably to the emergence of a beach which is not closely correspondent to what is found in natural tidal channels. The fixed bank approach is essentially based on the assumption that the time scale of bed development is much faster than that of bank, such that bed adjustment is driven by the channel planimetric geometry. The discrepancies between prediction and observations concerning the emergence of a beach could be related to neglection of the effect of other factors that has been discarded. Furthermore, these discrepancies may also indicate that the mutual interaction between bed and banks development in tidal channels cannot be completely neglected as it happens when performing the fixed banks simulation, at least when the time scales of the two processes are not so far apart.

For these reasons, the assumption of fixed banks has been removed in the present Chapter and the channel banks have been let free to vary with time. The sought outcome herein is a quite ambitious but at the same time fascinating goal and deals with understanding the reasons why tidal channels are convergent and defining the conditions under which the exponential law for width variation, so often observed in nature, occurs. In fact, most of the models in literature, which are described in the introductive chapter, do

not allow the bank evolution with time. Actually, various attempts to reproduce the equilibrium cross section of tidal channels have been pursued in previous works (e.g. Gabet, 1998; Fagherazzi and Furbish, 2001). However, the above analyses are focused on a local scale and hence they do not consider the full coupling with the morphological evolution of the channel in a global scale.

On the other hand, several contributions already exist in the case of rivers. Indeed, as it has been briefly described in Chapter 3, most of the works that study the evolution of the river cross-section provide numerical models to describe the bank erosion, by identifying the failure mechanism that is responsible for the lateral erosion process. For instance, a numerical model of widening and bed deformation has been proposed by Darby and Thorne (1996a) who considered both planar and rotational failures and calculated channel widening by coupling bank stability with flow and sediment transport algorithms. Other works investigate the dimensions of a stable channel by testing some empirical equations that relate the wetted perimeter with the bankfull discharge (e.g Savenije, 2003). A lack in the knowledge of the mechanisms able to reproduce the funnel shape in the class of tide-dominated estuaries emerges from the close examination of the literature. This is certainly the most important reason that has encouraged the study the problem of the width adjustment in a tidal channel; the work described in the present Chapter represents a promising starting point for more complex investigations.

Actually, the possible causes for the estuarine funnel shape could be manifold; the coastlines are very complex environments that can experience changes in the sea-level because of either a global sea level change or local coastal uplift. Fluctuating sea level and wave erosion can strongly influence the coastline morphology. Besides the one-dimensional or bi-dimensional dynamics that take place inside the estuary could play an important role in the determination of the planimetric shape. This work adopt a very simplified approach and focus the attention only on the one-dimensional processes that take place inside the channel. Furthermore, still within this one-dimensional framework, only the effects related to flow and sediment transport processes within the tidal channel are retained, while further ingredients, such as the control exerted by tidal flats or the direct effect of sea currents in the outer part of the estuary, are discarded. The lateral erosion is taken into account and computed as a function of bed shear stress, provided it exceeds a threshold value within the cross section. The effect of different initial and boundary conditions on the widening process of the channel are tested, along with the role of the incoming river discharge.

6.1 A model for width change

To investigate the long term morphological evolution of a tidal channel whose width can vary in time it is necessary to supplement the governing problem with a bank erosion law suitable for a tidal context, whose definition is not obvious in a one-dimensional framework. Differently from the bed-erosion process, which can be treated in a satisfactory, albeit simplified, way within a one-dimensional framework, width changes are inherently influenced by the hydrodynamic behavior close to the banks, which can differ significantly from the cross-sectionally averaged flow.

6.1.1 Constant width-to-depth ratio

A first possibility is to abridge the transverse behavior into the concept of asymptotic equilibrium shape of the cross-section, assuming that the width-to-depth ratio of the channel may attain a given value β. Consequently, the bank erosion can be modelled in the following form

$$\frac{\partial B^*}{\partial t^*} = \gamma^* \left(B^*_{eq} - B^* \right) , \tag{6.1}$$

where the equilibrium width

$$B^*_{eq} = \beta D^*_{av} \tag{6.2}$$

is related to the tidally averaged depth D^*_{av} (Figure 6.1). The parameter γ^* represents the inverse of the time scale of width evolution. In fact, if B^*_{eq} is fixed, the solution of equation (6.1) can be written as

$$B^*(t^*) = B^*_{eq} + \left(B^*|_{t^*=t^*_0} - B^*_{eq} \right) \exp\left[-\gamma^* (t^* - t^*_0) \right] . \tag{6.3}$$

As a first approximation, β is supposed to be constant along the entire channel, though this is quite a crude simplification (Lawrence et al., 2004; D'Alpaos et al., 2005). At the beginning of the simulation, the bed profile is supposed to be horizontal and, given an initial depth D^*_0, the width B^*_0 is supposed to be equal to βD^*_0. The morphological evolution is computed by using the model presented in Chapter 4 to which the equation 6.3 for width adjustment has been added; the average water depth D^*_{av} and the correspondent equilibrium width B^*_{eq} are evaluated after every tidal cycle. In Figure 6.2 two examples of the bottom and banks equilibrium profiles, evaluated according to the above assumption with two different values of the width-to-depth β, are shown: in both cases the bottom

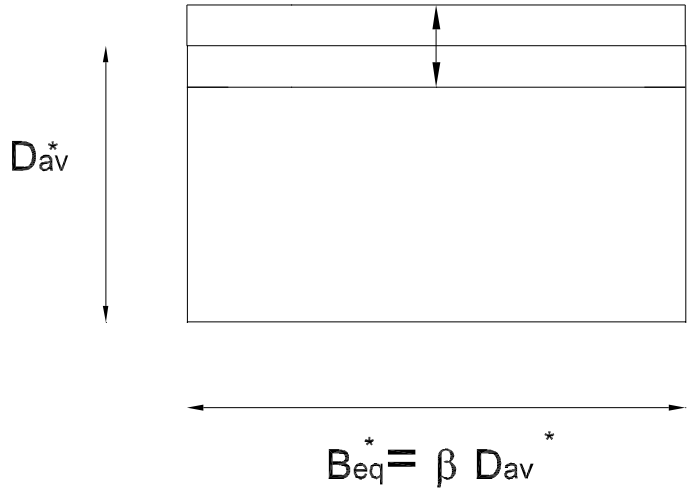

Figure 6.1: Sketch of the channel cross-section with a fixed width-to-depth ratio, β.

profile is linearly increasing landward and consequently, through equation (6.2), the tidally averaged depth and the bank profile exhibit the same shape. It is possible to note that the bottom evolution is not influenced in a significant way by the value of the parameter β: in fact the bed profiles are quite similar although the different values of the width.

This formulation does not prove to be useful if the aim is to explain the exponential law typical of tide-dominated estuaries. Furthermore the assumption of a constant β along the whole channel represents a strong approximation. A more realistic solution would require an improved morphological model able to estimate the width-to-depth ratio β in equation (6.2) on the basis of hydrodynamic and geometrical conditions. The degree of uncertainty affecting the above estimate along with the constraint imposed by the application of equation (6.2) suggest the opportunity to search for a more physically-based erosion law.

6.1.2 Physically-based erosional law

As briefly explained in Chapter 3, in the case of rivers several existing models can be found in the literature, whereby width adjustment is essentially related to the excess bed shear stress with respect to some threshold value. Following Darby and Thorne (1996a), it is possible to assume the channel widening to occur in a given section provided the bottom shear stress $\sigma^* = \rho \left(U^*/C_h\right)^2$ exceeds a threshold value σ^*_{cr}. The simplest choice is a first order law:

$$\frac{\partial B^*}{\partial t^*} = k^* \left(\frac{\sigma^*}{\sigma^*_{cr}} - 1 \right) . \tag{6.4}$$

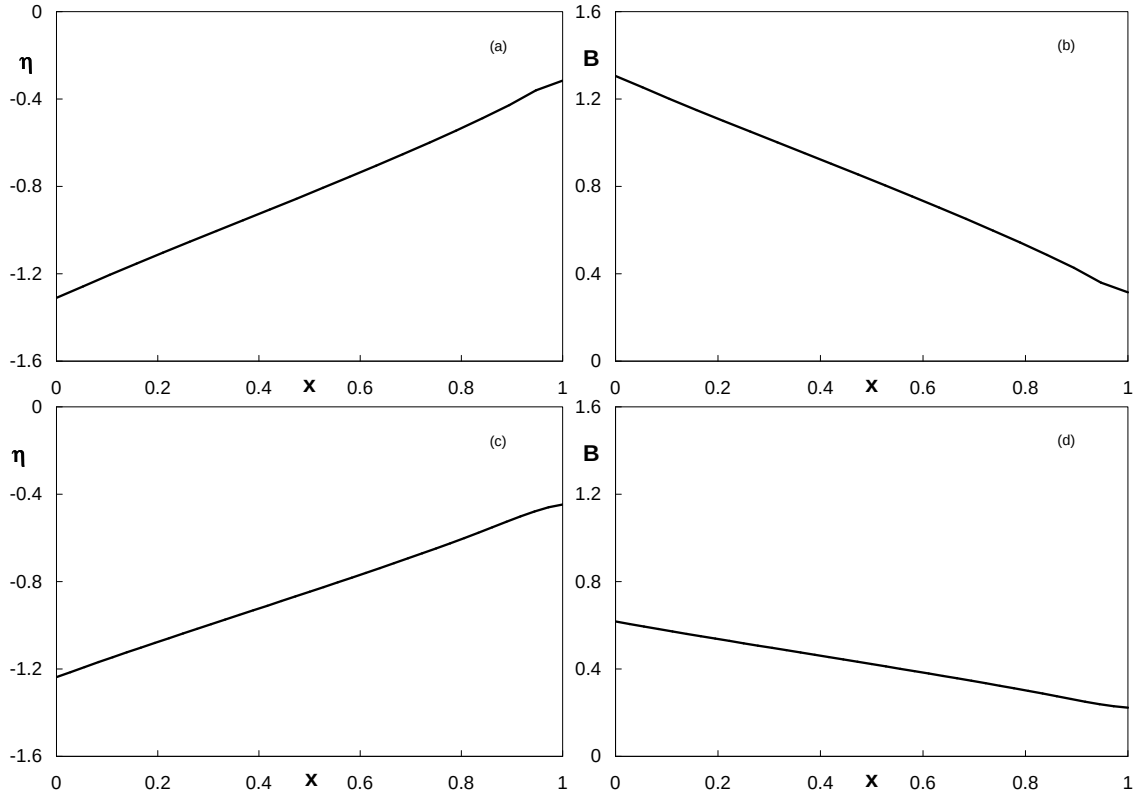

Figure 6.2: Bank erosion evaluated assuming β as constant using equation (6.1); the long-term configuration of: the bottom profile $\eta(x)$ (a) and (c); the width profile $B(x)$ (b) and (d) for β=20 (upper part) and β=10 (lower part) respectively [L_e^*=20 km, D_0^*=5 m, B_0^*=100m, a_0^*=1 m, C_h=20, $d_s^* = 10^{-4}$ m, $\gamma^* = 10^{-8} s^{-1}$].

Equation (6.4) can be written in dimensionless form to obtain:

$$\frac{\partial B}{\partial \tau} = k \left(\frac{U^2}{U_{cr}^2} - 1 \right) , \qquad if \quad U > U_{cr} \tag{6.5}$$

in which $k = k^* T_b^* / B_0^*$. It is worth noting that equation (6.4) represents a pure erosional law and does not provide for banks reconstruction: indeed the reconstruction process is more difficult to model since it occurs on a slower time scale with respect to erosion (Todeschini et al., 2005).

This width adjustment law is characterized by two parameters, σ_{cr}^* and k^* that have to be estimated. In the simulations presented here a value of $0.1\, N/m^2$ of the critical bed shear stress σ_{cr}^* is adopted which represents the critical value for a particle of diameter $10^{-4} m$. The definition of a suitable range of values for the lateral erosion rate k^* poses

an important and non trivial problem, since only few contributions can be found in the literature dealing with bank erosion processes in tidal channels. Darby and Thorne (1996a) propose for rivers an empirical relationship to evaluate lateral erosion rate which is a function of the critical bed shear stress σ^*_{cr}, of the unit weight of the soil and of an initial rate of soil erosion, derived with another empirical expression. Substituting the critical bed shear stress $0.1\,N/m^2$ and the sediment diameter $10^{-4}m$ it is possible to obtain an estimate value for k^* of the order of $10^{-8}m/s$. Another estimate for k^* can be deduced from Gabet (1998), who investigated the process of bank erosion of a saltmarsh creek, reporting a lateral migration rate of the order of $10^{-11}m/s$. An intermediate value $k^* = 10^{-10}m/s$ is adopted in the following numerical simulations where equation (6.5) is solved using an explicit scheme:

$$B_i^{t+1} = B_i^t + k\left(\frac{U_i^{t\,2}}{U_{cr}^2} - 1\right)\Delta t \tag{6.6}$$

6.2 Bottom and banks equilibrium profiles

Before analysing the results obtained with the use of the simple one-dimensional model formulated in the previous section, some considerations about the concept of equilibrium need to be done. In the case of fixed banks model the equilibrium was defined by means of a threshold value for the bottom variation within a certain period of time, below which it was possible to assume that a quasi-equilibrium configuration had been achieved. However the dynamical equilibrium was achieved only in terms of the residual sediment flux while peak values of flow velocity kept non negligible in the whole estuary (Figures 5.5, 5.6). Also in the case of erodible banks at equilibrium the peak values of the velocity and consequently of the sediment flux are non negligible, as it can be seen in Figure 6.3 and 6.4 . The evolution of bottom elevation η depends on the tidally average values of the sediment flux through equation (4.19). On the contrary, the lateral erosion rate is a function of the absolute value of the velocity through equation (6.5) and not of its residual value. In order to reach the stability of the banks, the peak values of the velocity should be smaller than the critical value U_{cr} in every point of the domain. This condition do not occurs even at equilibrium given that the peak velocities keep larger than the critical value despite the widening of the banks. For this reason, within this one-dimensional approach it is not obvious to define the conditions which determine the stability of the banks, since there is no mechanism ensuring that an equilibrium configuration can be reached. Thus, while the bottom configuration becomes relatively stable after a period of time comparable with the morphological time scale, the width continues to increase. An example of this evolution

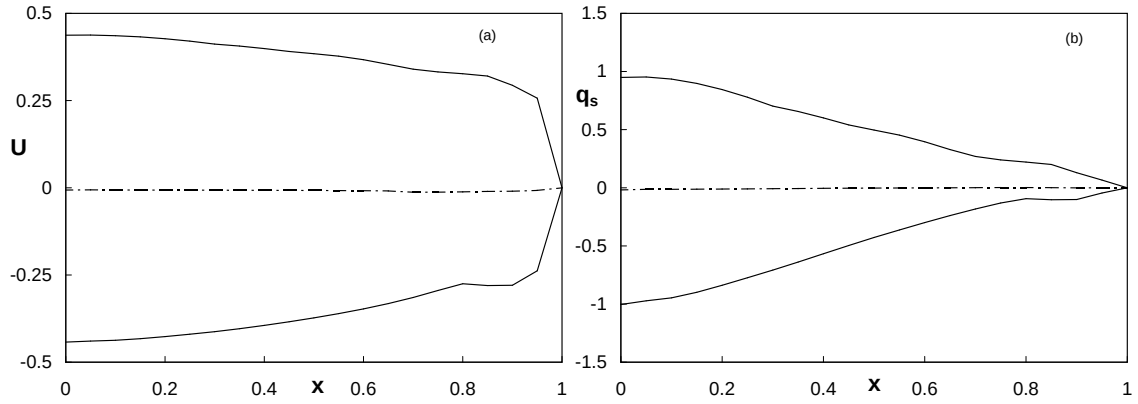

Figure 6.3: Maximum, minimum and residual values of flow velocity (a) and sediment flux (b) along the estuary at equilibrium [L_e^*=20 km, D_0^*=5 m, B_0^*=50 m, a_0^*=1 m, C_h=20, $k^* = 10^{-10}$ m/s, $d_s^* = 10^{-4}$ m, U_0^*=0.7 m/s, T_b^*=157 years].

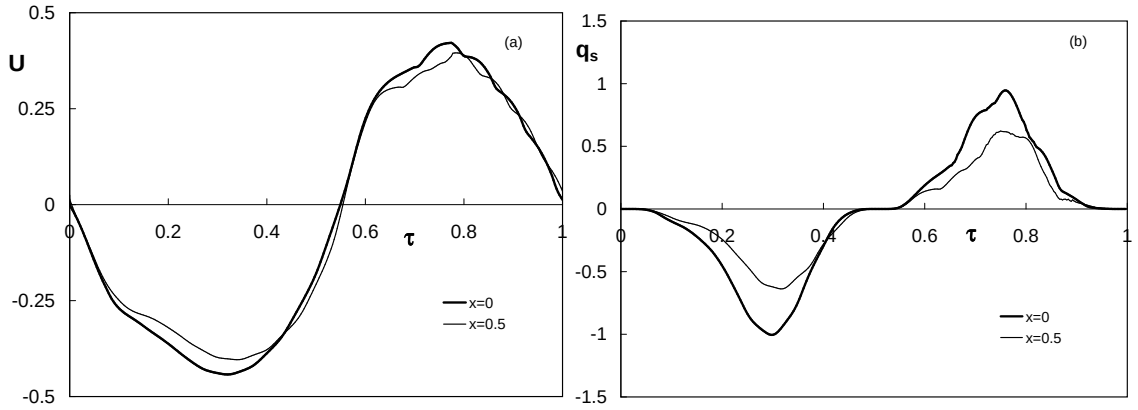

Figure 6.4: Flow velocity (a) sediment flux in a tidal cycle at the mouth ($x = 0$) and in the middle of the channel ($x = 0.5$) when the bottom profile has achieved an equilibrium configuration [L_e^*=20 km, D_0^*=5 m, B_0^*=50 m, a_0^*=1 m, C_h=20, $k^* = 10^{-10}$ m/s, $d_s^* = 10^{-4}$ m, U_0^*=0.7 m/s, T_b^*=157 years].

in a short channel can be seen in Figure 6.5 and in Figure 6.6, where the differences in the adaptation process of bottom elevation and width are quite evident: the bottom evolution is concentrated in a smaller period of time, which is required to let the sediment wave to reach the last section of the channel; on the contrary channel widening proceeds with a velocity that is roughly constant in time. When bottom attains a quasi-equilibrium configuration, it is assumed that the bank profile has achieved a sort of characteristic configuration, which determines the planimetric shape and the numerical simulation is stopped. The same remarks about the different temporal evolution between the bottom

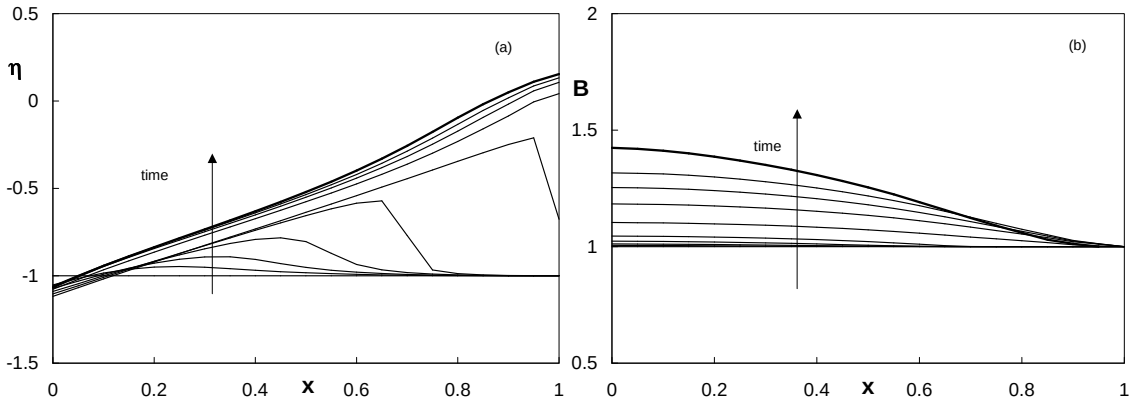

Figure 6.5: The long-term evolution of a short estuary: (a) the bottom profile $\eta(x)$; (b) the width profile $B(x)$ [L_e^*=20 km, D_0^*=5 m, B_0^*=50 m, a_0^*=1 m, C_h=20, $k^* = 10^{-10}$ m/s, $d_s^* = 10^{-4}$ m, U_0^*=0.7 m/s, T_b^*=157 years].

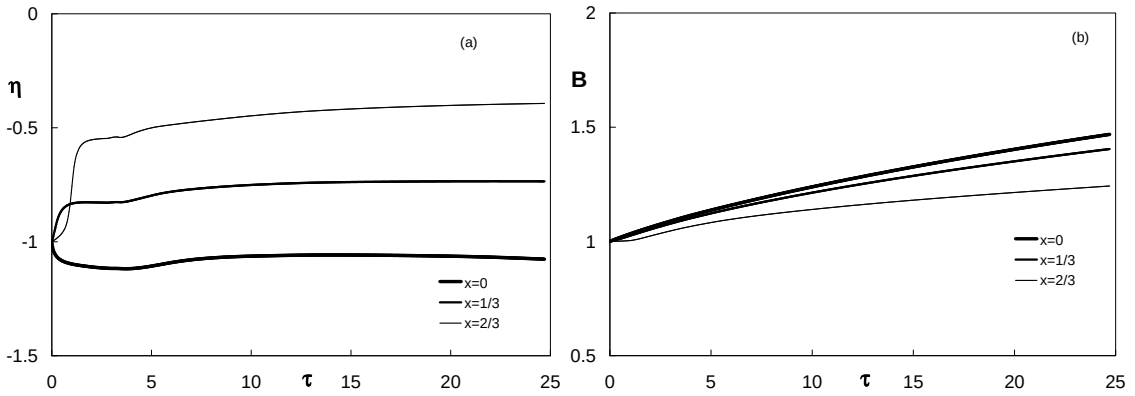

Figure 6.6: Temporal evolution of: (a) the bottom elevation $\eta(\tau)$; (b) the width $B(\tau)$, at x=0, x=1/3 and x=2/3 [L_e^*=20 km, D_0^*=5 m, B_0^*=50 m, a_0^*=1 m, C_h=20, $k^* = 10^{-10}$ m/s, $d_s^* = 10^{-4}$ m, U_0^*=0.7 m/s, T_b^*=157 years].

and the width profile can be made in the case of a long estuary; an example of evolution in a long estuary is shown in Figure 6.7. A beach is formed inside the domain as in the case of convergent channel with fixed banks; in the landward part of the channel the width evolution is reduced since the cells are emerged for a large part of the tidal cycle and the residual velocity is very small.

6.2.1 The role of the parameters

Analogously to what has been done in the case of fixed banks, the dependence of the solution on the parameters that describe the system, as the tidal amplitude a_0^*, the ini-

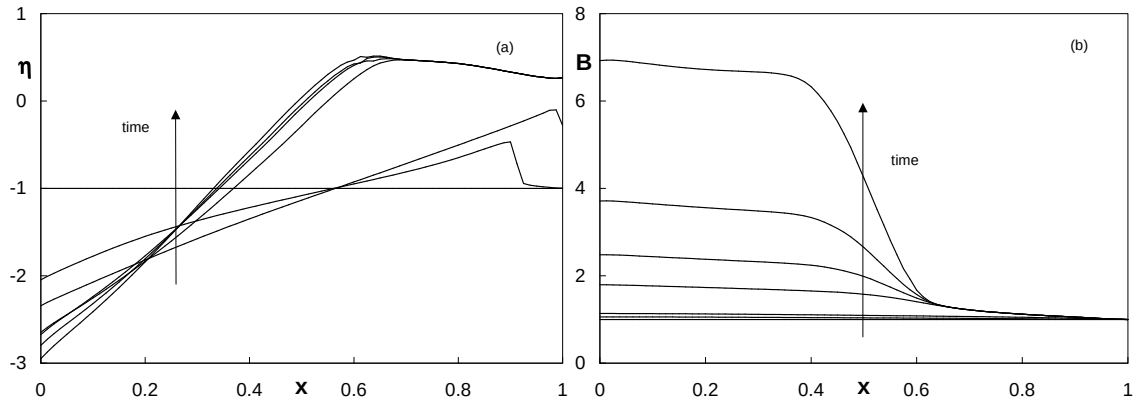

Figure 6.7: The long-term evolution of a long estuary: (a) the bottom profile $\eta(x)$; (b) the width profile $B(x)$ [L_e^*=160 km, D_0^*=10 m, B_0^*=50 m, a_0^*=4 m, C_h=20, $k^* = 10^{-10}$ m/s, $d_s^* = 10^{-4}$ m, U_0^*=1.1 m/s, T_b^*=272 years].

tial depth at the mouth D_0^*, the sediment diameter d_s^* and the Chézy coefficient C_h, is investigated.

It is possible to expect the equilibrium profiles to be mainly dependent on the tidal forcing. In fact the sediment transport and consequently the morphological evolution is determined by the flow velocity field in the estuary whose scale is controlled by the tidal amplitude a_0^*. A larger tidal amplitude determines larger velocities and larger landward sediment flux. Hence, as in the case of fixed banks, larger bottom slopes correspond to larger tidal amplitudes. Moreover, given the same geometrical conditions, larger velocities in (6.5) imply a larger rate of widening (see Figure 6.8).

It is interesting to investigate the role of the initial depth at the mouth D_0^* on the solution. Indeed, it is useful to remark that this parameter represents the initial condition for the system. It is possible to expect the solution to be only weakly dependent on this parameter, for a given tidal forcing. This is confirmed quite clearly by the results reported in Figure 6.9, where the equilibrium profiles corresponding to four different values of the initial depth are plotted for the same dimensional tidal amplitude a_0^*. The resulting profiles do not substantially differ.

A special attention has to be paid in the choice of the constant k^* which controls the lateral erosion rate of the banks. As pointed out before, it is very difficult to obtain a reliable estimate of this parameter; on the other hand its value deeply influences the solution. Imposing different values of the parameter k^*, different equilibrium bottom profiles and consequently different bank configurations are achieved (Figure 6.10). This implies that k^* plays a non negligible role, not only in the transient phase of evolution

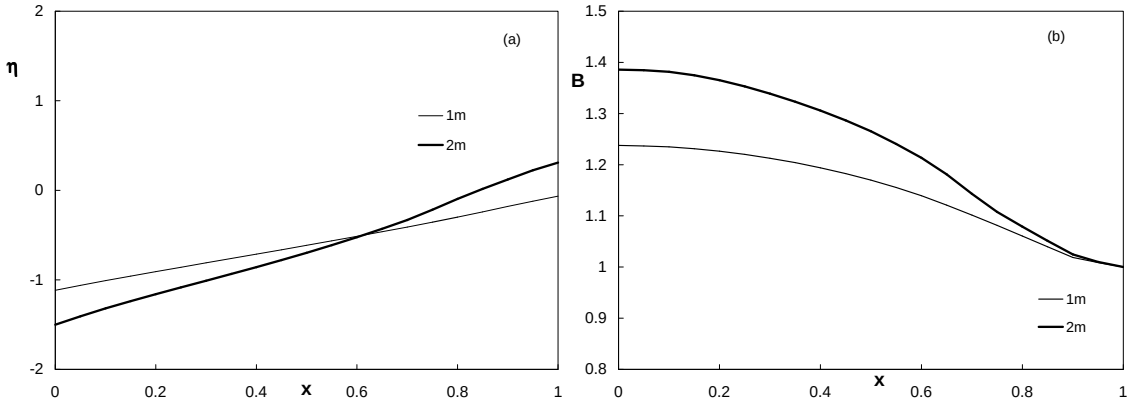

Figure 6.8: The long-term configuration of: (a) the bottom elevation scaled with the tidal amplitude η^*/a_0^*; (b) the width profile $B(x)$, for different values of tidal amplitude $a_0^*(1, 2m)$ [L_e^*=50 km, D_0^*=10 m, B_0^*=50 m, C_h=20, $k^* = 10^{-10}$ m/s, $d_s^* = 10^{-4}$ mm].

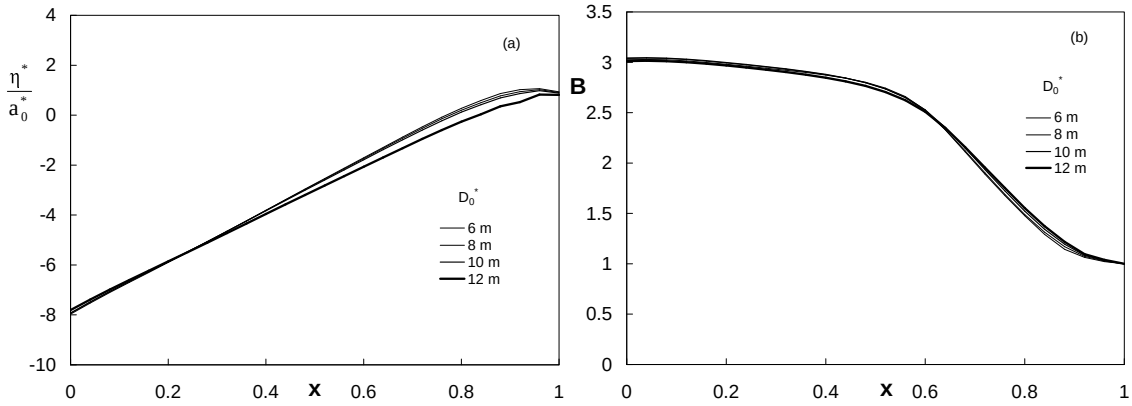

Figure 6.9: The long-term configuration of: (a) the bottom elevation scaled with the tidal amplitude η^*/a_0^*; (b) the width profile $B(x)$, for different values of initial depth at the mouth, D_0^* [L_e^*=50 km, a_0^*=1 m, B_0^*=50 m, C_h=20, $k^* = 10^{-10}$ m/s, $d_s^* = 10^{-4}$ mm].

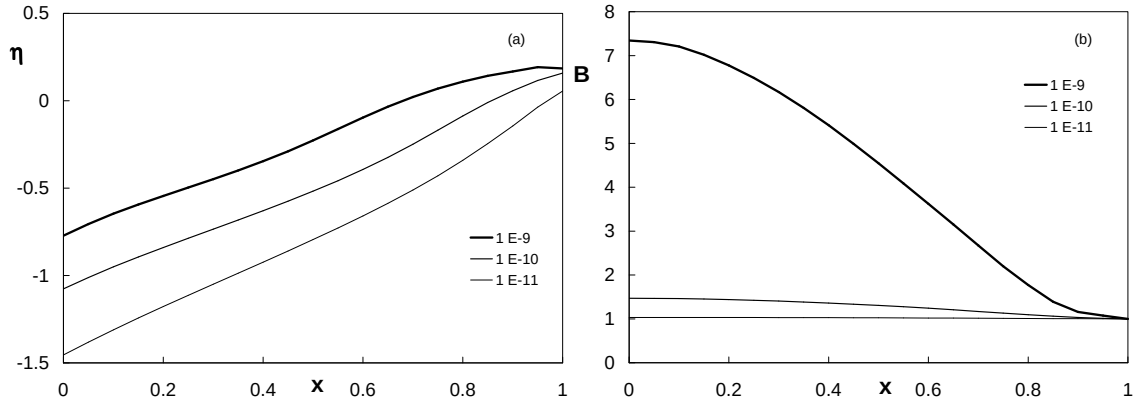

Figure 6.10: The long-term configuration of: (a) the bottom profile $\eta(x)$; (b) the width profile $B(x)$, for different values of the constant k^* used in the lateral erosion law $(1 \cdot 10^{-11}, 1 \cdot 10^{-10}, 1 \cdot 10^{-9} m/s)$ [L_e^*=20 km, D_0^*=5 m, a_0^*=1 m, B_0^*=50 m, C_h=20, $d_s^* = 10^{-4}$ m].

but also in the equilibrium profiles, though the bottom and the banks evolve on different time scales. The degree of widening influences the bottom profile until it has reached an equilibrium configuration, while it is no longer relevant when the residual sediment transport that governs the bottom evolution becomes negligible.

6.3 Considerations about the concave shape of the width profile

An important remark on the results presented up to now has to be made: all the equilibrium width profiles $B(x)$ are characterized by a concave shape in the seaward part of the estuary (i.e. with a seaward widening rate) and by a significant bottom slope; on the other hand observed bank profiles in tide dominated estuaries, like those presented in Figure 2.19, 2.21 and 2.23, display a convex shape (i.e. with an increasing rate of widening seaward) while the bottom slope keeps relatively small. It is interesting to investigate if the divergence between model results and field observations is due to the role of some factors that have been neglected until now and that could be important in the determination of the solution.

In order to understand the role of the bottom profile on the bank shape the model has been tested imposing a fixed horizontal bed. Two resulting bank profiles $B(x)$ are plotted for different values of τ in Figure 6.11, characterized by two different tidal forcing: a simple M_2 tide for the first one, a M_2 with an overtide M_4 in the second one. It appears

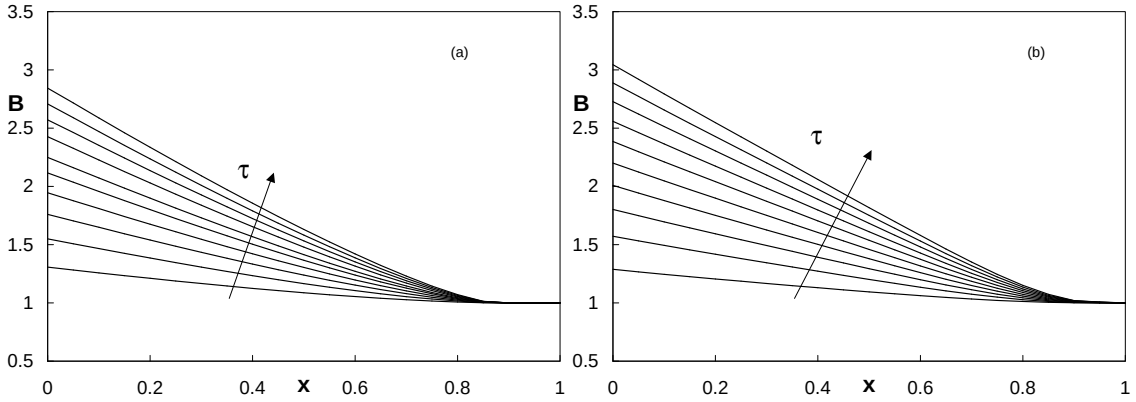

Figure 6.11: Bank profile $B(x)$ obtained with fixed bed at τ varying from 2 to 20 with no overtide (a) and with a M_4 with amplitude a_2^*=0.8m and $\phi=-\pi/2$ (b) [L_e^*=20 km, D_0^*=5 m, a_0^*=1 m, B_0^*=50 m, C_h=20, $d_s^* = 10^{-4}$ m, $k^* = 10^{-10}$ m/s, U_0^*=0.7 m/s, T_b^*=157 years].

that in both these cases the width profile is characterized by a convex shape and tendency toward the establishment of an exponential law for the bank profile can be reproduced. The difference with the case of mobile bed is even more evident if the width profile of Figure 6.11 is compared with the one reported in Figure 6.5: the comparison, at time $\tau = 20$, is shown in Figure 6.12. In order to point out the role of the bottom slope

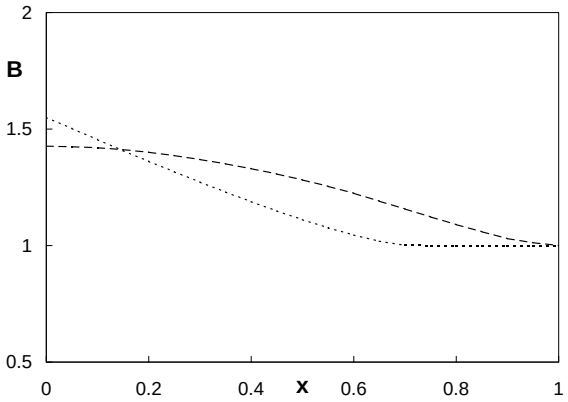

Figure 6.12: Bank profile $B(x)$ obtained with fixed bed at τ varying from 2 to 20 with no overtide (dotted line) and with mobile bed (dashed line) [L_e^*=20 km, D_0^*=5 m, a_0^*=1 m, B_0^*=50 m, C_h=20, $d_s^* = 10^{-4}$ m, $k^* = 10^{-10}$ m/s, U_0^*=0.7 m/s, T_b^*=157 years].

on the shape of the banks profile, the model is tested with different fixed bed profiles corresponding to different bottom slopes. The comparison is shown in Figure 6.13: it

emerges that the convex shape is reproduced only from negligible or mild bottom slopes while, when the bottom slope begins to increase, the width profiles become concave as in the case of moveable bed. An almost horizontal bottom profile seems to be a necessary condition for the banks profile to be convex. However, the hypothesis of fixed bed is not

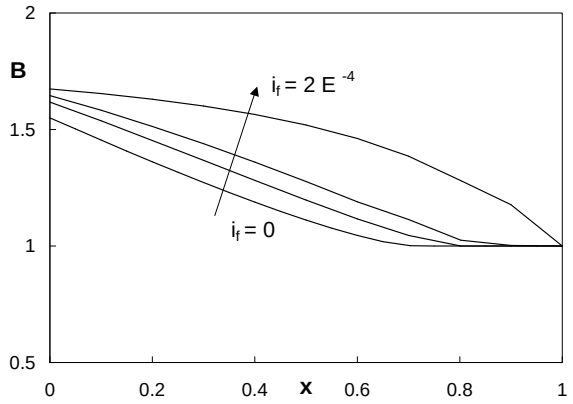

Figure 6.13: Bank profile $B(x)$ obtained with fixed bed at $\tau = 20$ for different values of the bottom slope i_f: (0, $5\,E^{-5}$, $1\,E^{-4}$, $2\,E^{-4}$) [L_e^*=20 km, D_0^*=5 m, a_0^*=1 m, B_0^*=50 m, C_h=20, $d_s^* = 10^{-4}$ m, $k^* = 10^{-10}$ m/s, U_0^*=0.7 m/s, T_b^*=157 years].

realistic; in fact, the time scale that characterizes the bottom evolution, T_b^*, is much faster than the time scale that governs the banks evolution, B_0^*/k^*: for example, in the case reported in Figure 6.5 the morphological time scale $T_b =^*$ is about 157 years while B_0^*/k^* is a hundred times larger. The ratio between the two temporal scales is always a small parameter unless a very large value but not very physically meaningful for the constant k^* is adopted in the lateral erosion law. For typical values of this constant, the bottom evolution is faster and tends to collect sediment in the inner part of the estuary so that the bed profile becomes characterized by a significant slope. As it propagates into the estuarine channel, the tidal wave is distorted and a flood-dominance in generated inside the estuary. This asymmetry causes a net landward sediment transport. At equilibrium the bottom profile is forced to attain a non negligible bottom slope to compensate this flood-dominance, until the asymmetry is cancelled (Figure 6.4).

It is possible to examine the effect of an overtide which enhances the ebb dominance character of the tidal wave in order to understand whether it is sufficient to alter the sediment transport and to decrease the bottom slope. Two examples of the long-term equilibrium bottom and banks profiles with two different prescribed overtides M_4 are plotted in Figure 6.14. As it can be seen, the overtides do not decrease the bottom slopes

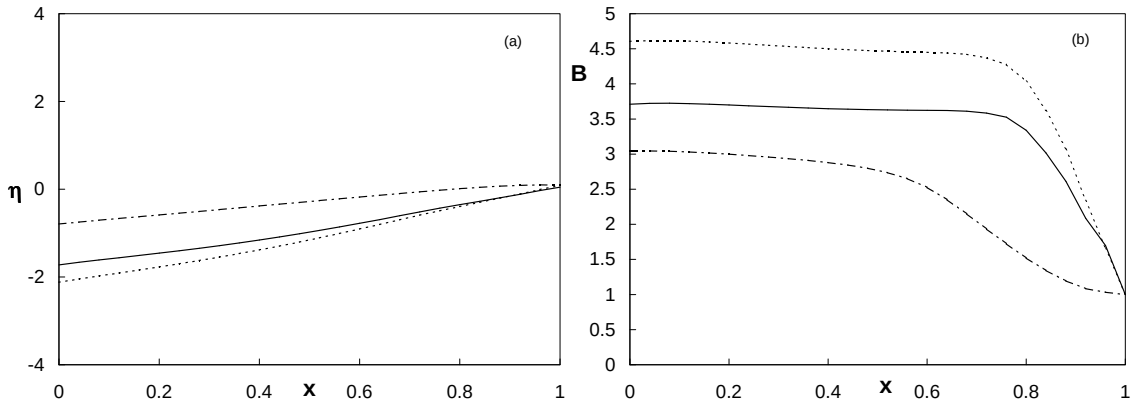

Figure 6.14: The long-term configuration of: (a) the bottom elevation scaled with the tidal amplitude η^*/a_0^*; (b) the width profile $B(x)$, for two different values of M_4 amplitude (dash-dotted line: no overtide) [L_e^*=50 km, D_0^*=10 m, B_0^*=50 m, C_h=20, L_e^*=50 km, $k^* = 10^{-10}$ m/s, $d_s^* = 10^{-4}$ mm].

and the width profiles are characterized also in this case by a concave shape.

6.3.1 The role of the freshwater discharge

Among the other factors that can affect the morphological evolution of tidal channels, a non vanishing freshwater discharge could oppose this tendency and help the bottom profile to keep quite flat. Indeed, in Chapter 5 it has been shown that, in the case of fixed banks and convergent estuaries, a non negligible river discharge induces a milder bottom slope in the equilibrium bed configuration.

This has suggested to incorporate the presence of a non negligible freshwater discharge, which has been neglected in the simulations with erodible banks presented herein. The boundary condition is imposed in $x = 1$ without the addition of a constant width channel in order to decrease the number of parameters that need to be fixed. When a non-vanishing freshwater discharge is imposed at the landward boundary, the formation of a beach within the estuary is inhibited and the bottom profile can be significantly different. In Figure 6.15 the equilibrium profiles in the case of a closed end (the example reported in Figure 6.10 for $k^* = 10^{-10}\, m/s$) are compared with the ones in case of a non-negligible value of the river discharge ($Q^* = -100\, m^3/s$, which corresponds to a value of p of about 0.5). In the latter case the equilibrium bottom profile is characterized by a smaller slope and a larger depth because the discharge contrasts with the landward directed sediment transport due to the tidal wave. The corresponding width profile has a convex shape that resembles the exponential profile of the real estuaries. However in this case the value chosen for the river

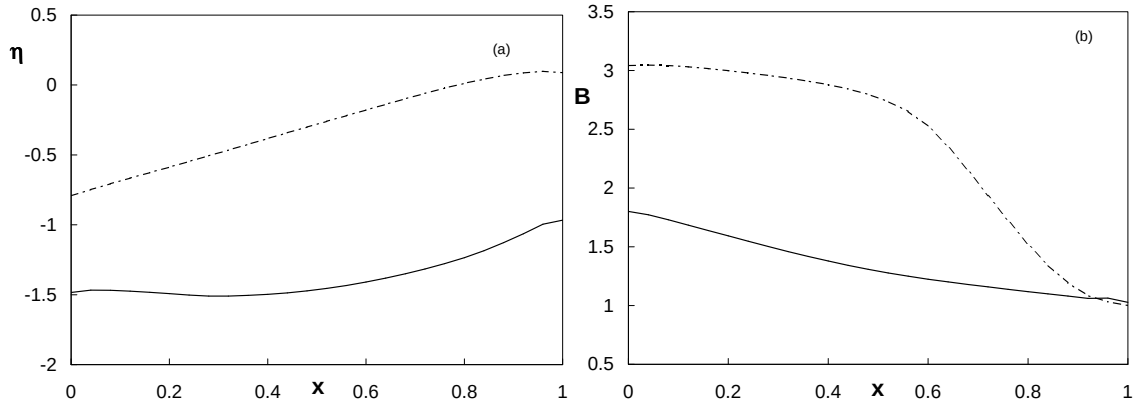

Figure 6.15: Comparison between the long-term configurations of: (a) the bottom profile $\eta(x)$; (b) the width profile $B(x)$, for a vanishing river discharge (dash-dot lines) and a non negligible value of the river discharge at the landward boundary, $Q^*_{river} = -100m^3/s$ (continuous lines) [L^*_e=50 km, D^*_0=10 m, a^*_0=1 m, B^*_0=50 m, C_h=20, $d^*_s = 10^{-4}$ m, $k^* = 10^{-10}$ m/s, $U^*_0 = 1$ m/s].

discharge is quite large since it turn out to be of the same order of magnitude of the tidal prism ($p \simeq 0.5$).

The presence of a freshwater discharge changes significantly the pattern of sediment transport, as it can be seen in Figure 6.16; the residual sediment fluxes, that govern the bed evolution, assume negative values all along the estuary even at the beginning of the simulation and the tendency toward a landward sediment transport is removed.

It is interesting to understand whether the convex shape, that is expected in the case of tide-dominated estuaries occurs for every value of the the river discharge; for this purpose two long-term configurations of the bottom and banks profiles corresponding to different values of this parameter are compared in Figure 6.17. As it can be seen, when the effect of the freshwater discharge is small if compared with the tidal action, the equilibrium planimetric shape is concave, analogously with the case of the reflecting barrier condition. This situation corresponds to the curve in Figure 6.17 characterized by the smallest value of the discharge and by a value of p smaller than 0.1. In the other curve, where the river discharge is higher, the ratio p assumes a value of about 0.2 and the width profile shows a convex shape. The presence of a freshwater river discharge is able to induce a convex shape in the width profile, if the ratio between the discharge and the tidal prism is not too small. In some examples reported in this chapter, however, this value is quite high and the river discharge and the tidal prism turn out to be approximately of the same order of magnitude.

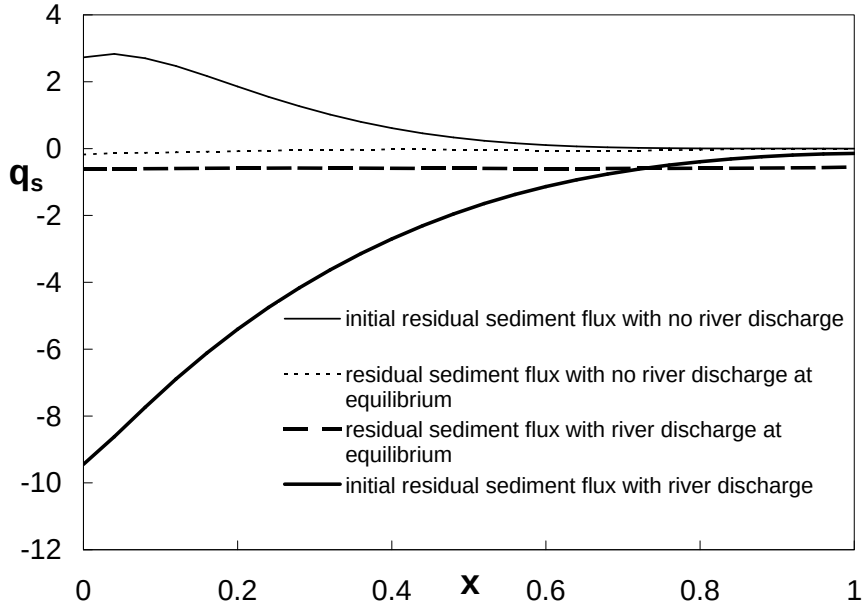

Figure 6.16: Comparison between the residual sediment flux at the beginning of the simulation (continous line) and at equilibrium (dashed line) in the case of a non negligible river discharge and the case of a reflecting barrier condition [L_e^*=50 km, D_0^*=10 m, a_0^*=1 m, B_0^*=50 m, C_h=20, $d_s^* = 10^{-4}$ m, $k^* = 10^{-10}$ m/s, $U_0^* = 1$ m/s].

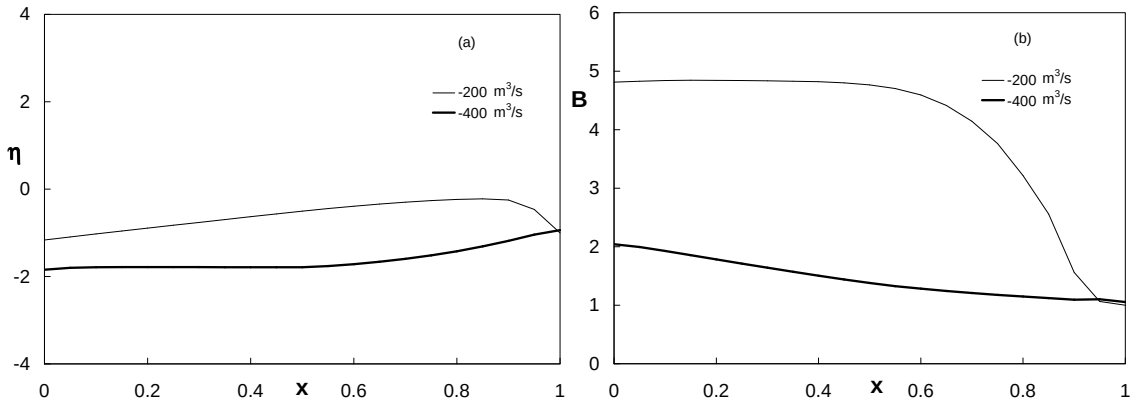

Figure 6.17: The long-term configurations of: (a) the bottom profile $\eta(x)$; (b) the width profile $B(x)$, for the different values of the river discharge $Q_{river}^* = (-200, -400 m^3/s)$ [L_e^*=40 km, D_0^*=10 m, a_0^*=2 m, B_0^*=200 m, $d_s^* = 10^{-4}$ m, $k^* = 10^{-10}$ m/s, $U_0^* = 1$ m/s].

6.3.2 The role of other parameters

The importance of the tidal forcing and its effect on the morphological evolution of the estuary is tested and represented in Figure 6.18. Also in this case, when the tidal action becomes predominant with respect to the river discharge and the tidal prism becomes very large, the bottom profile is characterized by a significant bottom slope while the width profile becomes concave.

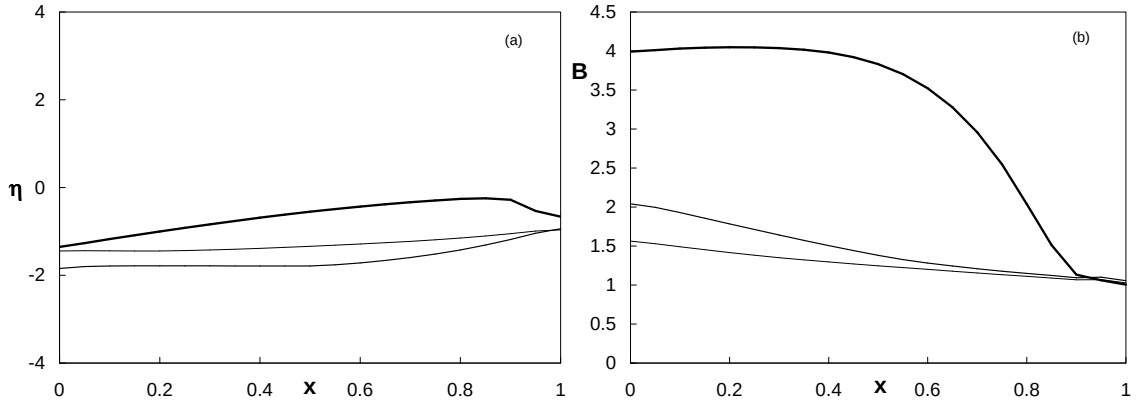

Figure 6.18: The long-term configurations of: (a) the bottom profile $\eta(x)$; (b) the width profile $B(x)$, in the case of a non negligible river discharge for different values of the tidal amplitude a_0^*: (1m, 2m and 3m) [L_e^*=40 km, D_0^*=10 m, a_0^*=1.5 m, B_0^*=50 m, $d_s^* = 10^{-4}$ m, $k^* = 10^{-10}$ m/s, $U_0^* = 1$ m/s, $Q_{river}^* = -400m^3/s$].

The role of the Chézy coefficient is shown in Figure 6.19, where the long-term bottom and width profiles, corresponding to different values of this parameter, are plotted.

As it can be seen, for larger values of the Chézy coefficient, that means for smaller friction coefficients, the velocity and so the erosive power is enhanced and at equilibrium the banks are wider. The slope of the bottom profile is larger for smaller values of the Chézy coefficient that correspond to a larger flood-dominance. Besides, when the Chézy coefficient is small, the width profile shows a more accentuated concave shape in the whole estuary.

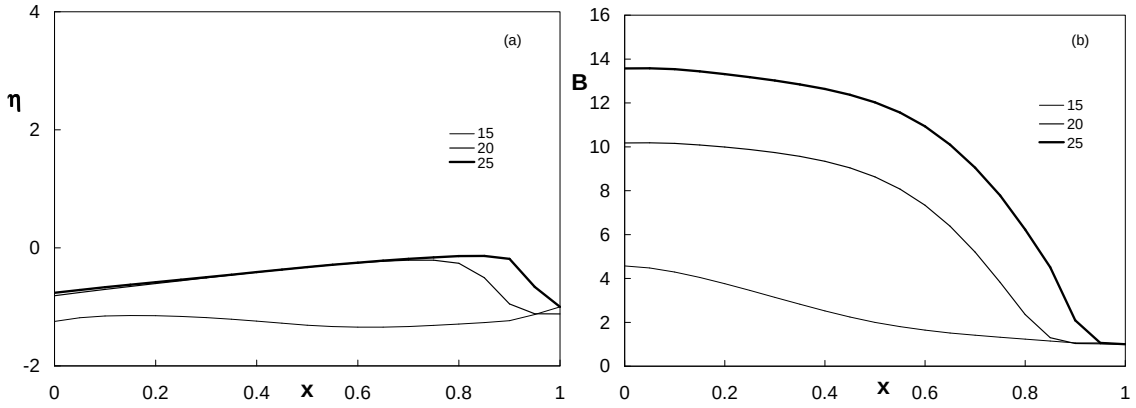

Figure 6.19: The long-term configurations of: (a) the bottom profile $\eta(x)$; (b) the width profile $B(x)$, in the case of a non negligible river discharge for different values of the Chézy coefficient: (15, 20 and 25) [L_e^*=40 km, D_0^*=10 m, a_0^*=1.5 m, B_0^*=50 m, $d_s^* = 10^{-4}$ m, $k^* = 10^{-10}$ m/s, $U_0^* = 1$ m/s, $Q_{river}^* = -400 m^3/s$].

6.4 Discussion

In nature tide-dominated estuaries are characterized by a funnel-shape, negligible river discharge and small bottom slopes. In this chapter, the long-term evolution of an estuarine channel, whose width is allowed to vary with time, is investigated through the use of a one-dimensional numerical model. The choice of the banks erosion law, however, is not a trivial question. Two ways to model this phenomenon have been explored. Firstly, the idea of the existence of an equilibrium cross-section described by the width-to-depth ratio β as in (6.1)-(6.2) has been considered. Though this can be regarded as a phenomenological description, it hides the problem of determining the values of β along the estuary; on the other hand, considering a constant value of this parameter gives the unrealistic results that the width is tightly related to the depth.

As a second conceptual scheme, a physically-based law (6.4) has been adopted, which relates the velocity of bank erosion to the excess of the bottom shear stress with respect to a threshold value, as it is common in the formulation of the bed erosion due to sediment transport. However, besides the problem to determine the correct value of the parameter k^* that controls the intensity of erosion, the adopted relationship hinders the possibility to reach a stable bank configuration because a purely erosive law vanishes only when the bottom shear stress reaches its critical value. This problem could have been avoided considering a process of bank reconstruction, which usually occurs on a large time scale. Instead of using an unrealistic instantaneously varying depositional law, this process could

be modelled with a fixed rate of reconstruction due to vegetation activity, for instance. On the other hand, through the simple law (6.4) it is possible to examine the influence of the width on the velocity. In fact, differently from the case of the bed evolution, where the bottom profile has a strong influence on the values of the velocity developing within the channel, the width seems to control the flow field mainly through the influence of the channel convergence rather than through the local value of the width in a given section. For instance, when an exponential variation of the width and fixed banks are assumed, the solution is independent of the local value of the width (Todeschini et al., 2003). In this way, even large variations of channel width do not change the values of velocity significantly.

Despite of the uncertainties in the bank erosion law, an interesting result is shown by the present analysis. The typical funnel shape of most estuaries seems to be related to the occurrence of a small longitudinal slope of the bottom, which can results from the effect of an incoming discharge at the head of the estuary. However, it is possible to expect that other features, like bi- or three-dimensional circulations within the channel, the formation of large scale bed forms or the exchange with the outer sea, which have not been considered in this analysis, could play a role in the long-term planimetric evolution of estuaries; they certainly should be the subject of further research.

There are several other factors which can affect the morphological aspect of tidal channels. Here the attention is focused on the role of the river discharge, which has been neglected in previous simulations but can be easily included in a one dimensional model. The presence of a discharge, imposed at the landward end, determines a width profile $B(x)$ with a convex shape, which resembles the exponential profile of real estuaries. Although these simulations are not enough to draw general conclusions on this issue, anyway we can infer that the river discharge influences the solution in a significant way. In particular, its presence induces a morphological evolution that makes the planimetric shape of the channels more similar to that typical of real estuaries. The biggest limitation is represented by the fact that the ratio between the river supply and the tidal prism at the mouth assumes relatively large values that in some cases are beyond those typical of the class of tide-dominated estuaries.

7 Conclusions

This Ph.D thesis has comprehensively tackled the issue of the problem of the long-term morphological evolution of a tide-dominated estuary. Tide-dominated estuaries are characterized by a typical funnel shape and mild bottom slopes, as revealed by the analysis of the bathymetries of some natural estuaries; the interest for the study of such class of estuaries is motivated by the fact that they are very common in nature.

In the first part of the work, the estuary is schematized as a convergent channel with fixed banks and rectangular cross-section area. A one-dimensional model is used to investigate the role of the different parameters that characterize the system on the equilibrium configuration. It is known that the morphological evolution of a convergent estuary is characterized by the formation of a sediment front that migrates landward and tends to emerge (e.g. Lanzoni and Seminara, 2002, Todeschini et al., 2003). The net landward sediment transport is due to the flood-dominance which is enhanced by strong convergence (e.g. Dronkers, 1986). The bottom profile evolves assuming a longitudinal slope until the asymmetry between the flood and ebb phase disappears and an equilibrium configuration is achieved.

The equilibrium configuration is achieved in terms of the residual value of velocity and sediment flux and for this reason it is reached only asymptotically. It is characterized by the presence of a beach whose position depends on the initial length of the channel and on the degree of convergence. If the estuary is relatively short and weakly convergent, a beach is formed at the landward end and the equilibrium bottom profile involves the entire length of the estuary. If the initial length of the channel exceeds a threshold value, the beach is formed inside the domain and it is possible to define a final equilibrium length as the distance between the position of the beach and the mouth. This scenario suggests to define "long channels" those whose equilibrium length is independent of the physical dimension that is imposed to the system as it is a function of the degree of convergence: it reduces if the convergence increases.

The equilibrium length of a tide-dominated estuary is influenced also by the other

parameters as the friction coefficient, the sediment diameter, the tidal forcing and the freshwater discharge, whose effect has been thoroughly analysed in more detail. The tidal amplitude enhances the flood-dominance and it tends to produce larger bottom slopes in the equilibrium profiles, an effect which is counterbalanced by the presence of a non negligible river discharge. Numerical simulations show that freshwater discharge enhances the ebb dominance and tends to produce smaller bed slopes so that the bottom profile is not forced to attain relatively large values of the longitudinal slope to achieve an asymptotic balance between the ebb and the flood phase.

The morphological evolution obtained in the case of a fixed banks model, characterized by the emergence of a beach inside the domain, is not closely correspondent to what is found in natural estuaries. Moreover the fixed banks model is unable to explain why tide-dominated estuaries are convergent. For these reasons, in the second part of the work the assumption of fixed banks has been removed; the one-dimensional model has been solved incorporating an equation that describes the lateral bank erosion in order to investigate the widening process. The few models that have appeared in the literature with the aim to reproduce the equilibrium channel cross-section are only focused on a local scale and do not consider the full coupling between bed and banks evolution. One of the main novel features of the present work is its ability to cover a large spatial scale while including the full coupling between bed and banks morphodynamics, incorporating some useful ideas that were previously applied in the case of rivers.

The choice of the banks erosion law is not a trivial question; the present model adopts a physically-based relationship whereby the lateral erosion rate is function of the excess of the bottom shear stress. The definition of an equilibrium configuration for the width profile is not obvious, given the purely erosional law that has been adopted. In fact, at equilibrium the residual sediment transport vanishes everywhere and the bottom configuration becomes stable. This is not true for the width profile whose evolution is related to the absolute value of the velocity that keeps larger than the critical values for a large part of the tidal cycle. For this reason it is necessary to assume that a characteristic configuration is achieved when the bottom becomes stable even though the widening process is not in equilibrium.

The model is able to reproduce the funnel shape typical of tide dominated estuaries and represents a powerful tool to investigate the conditions that determine its occurrence.

The funnel shape seems to be related to the occurrence of small longitudinal slopes of the bottom profile; increasing the fixed bed slope indeed determines an evident transition towards a concave shape. It has been observed that mobile simulations with vanishing discharge at the landward boundary reproduce equilibrium width profiles with a concave

shape which differ from the exponential law of tide-dominated estuaries obtained assuming a fixed horizontal bed. Therefore the presence of a freshwater discharge, able to enhance ebb-dominance and thus to reduce the equilibrium bottom slope, appears as another important condition that determines the occurrence of a convex, funnel shape of the estuary. Results indicate that for a non negligible freshwater discharge, the bank profile displays a convex shape which closely resembles the exponential profile of the real estuaries. Such convex shape is reproduced, in some cases, provided the volume of freshwater contributed by the river within a tidal cycle is not negligible with respect to the tidal prism. Data (e.g. Dalrymple et al., 1992) indicate that the river contribution is not invariably negligible in every tide-dominated estuary, thus positively supporting the present findings.

Another important result is that a relatively gentle bottom slope is almost invariably associated with the funnel shape of real estuaries: while such mild values of the bottom slope can be due to the presence of a river discharge, an important role could be played by other factors that have not been the subject of the present work. An example is given by the presence of tidal flats flanking the main channel that has been observed to determine stronger ebb-currents (e.g. Speer and Aubrey, 1985) and whose role would be interesting to incorporate in the model. Another factor that has been neglected up to now but that could represent a improvement of the present model is the reconstruction process of the river bank, which usually occurs on a large time scale and whose effect would be interesting to investigate.

References

J. R. L. Allen. Morphodynamics of holocene salt marshes: a review sketch from the atlantic and southern north sea coasts of europe. *Quat. Sci. Rev.*, 19(17-18):1155–1231, 2000.

M. Bolla Pittaluga. *Long term morphodynamic equilibrium of tidal channels*. PhD thesis, University of Genoa, December 2002.

M. Bolla Pittaluga, N. Tambroni, C. Zucca, L. Solari, and G. Seminara. Long term morphodynamic equilibrium of tidal channels: preliminary laboratory observations. In *Proceedings of 2nd RCEM Symposium*, pages 423–432, Obihiro (Japan), 10-14 September 2001.

A. D'Alpaos, S. Lanzoni, M. Marani, S. Fagherazzi, and A. Rinaldo. Tidal network ontogeny: Channel initiation and early development. *Journal of Geophysical Research*, 110(F2):F02001 10.1029/2004JF000182, 2005.

R. Dalrymple, R. Knight, B. Zaitlin, and G. Middleton. Dynamics and facies model of a macrotidal sand-bar complex, Cobequid Bay-Salmon River estuary (Bay of Fundy). *Sedimentology*, 37:577–612, 1990.

R. Dalrymple, B. Zaitlin, and R. Boyd. Estuarine dacies models: conceptual basis and stratigraphi implications. *Journal of Sedimentary Petrology*, 62(6), 1992.

S. E. Darby and C. R. Thorne. Numerical simulation of widening and bed deformation of straight sand-bed rivers. i: Model development. *Journal of Hydraulic Engineering*, 122 (4):184–193, April 1996a.

S. E. Darby and C. R. Thorne. Numerical simulation of widening and bed deformation of straight sand-bed rivers. i: Model evaluation. *Journal of Hydraulic Engineering*, 122 (4):194–202, April 1996b.

H. J. de Vriend. Mathematical modelling of meso-tidal barrier inland coasts. part i: Empirical and semi-empirical models. In P. L. F. Liu, editor, *Advances in coastal and ocean engineering*, volume 2, pages 115–149, 1996.

A. Defina. Two dimensional shallow flow equation for partially dry areas. *Water Resources Research*, 36(11):3251–3264, 2000.

J. Dronkers. Tidal asymmetry and estuarine morphology. *Netherlands Journal of Sea Research*, 20(2/3):117–131, 1986.

K. R. Dyer. *Estauries, a physical introduction.* Wiley, London, 1997.

F. Engelund and E. Hansen. *A monograph on sediment transport in alluvial streams.* Danish Technical Press, 1967.

S. Fagherazzi. Basic flow field in a tidal basin. *Geophys. Res. Letters*, 29(8):1221, 2002.

S. Fagherazzi and D. J. Furbish. On the shape and widening of salt-marsh creeks. *J. Geophys. Res.*, 106(C1):991–1003, January 15 2001.

C. Friedrichs. Stability shear stress and equilibrium cross-sectional geometry of sheltered tidal channels. *J. Coast. Res.*, 11(4):1062–1074, 1995.

C. Friedrichs and D. Aubrey. Tidal propagation in strongly convergent channels. *J. Geophys. Res.*, 99:3321–3336, 1994.

C. T. Friedrichs, B. D. Armbrust, and H. E. de Swart. *Hydrodynamics and equilibrium sediment dynamics of shallow, funnel-shaped tidal estuaries*, pages 315–327. Balkema, Rotterdam, 1998.

E. J. Gabet. Lateral migration and bank erosion in a saltmarsh tidal channel in san francisco bay, california. *Estuaries*, 21(4B):745–753, December 1998.

C. Hirsch. *Numerical Computation of Internal and External Flows. Volume 1.* John Wiley & Sons, 1990a.

C. Hirsch. *Numerical Computation of Internal and External Flows. Volume 2.* John Wiley & Sons, 1990b.

J. T. Jarret. Tidal prism-inlet area relationship. In *Gen. Invest. Tidal Inlets, Rep. 3*, page 32. U.S. Army Corps Coastal Eng. Res. Center, Vicksburg, Miss., 1976.

S. Lanzoni and G. Seminara. On tide propagation in convergent estuaries. *Journal of Geophysical Research*, 103(C13):30793–30812, 15 December 1998.

S. Lanzoni and G. Seminara. Long term evolution and morphodynamic equilibrium of tidal channels. *J. Geophys. Res.*, 107:1–13, 2002.

D. S. L. Lawrence, J. R. L. Allen, and G. M. Havelock. Salt marsh morphodynamics: an investigation of tidal flows and marsh channel equilibrium. *Journal of Coastal Research*, 20(1):301–316, 2004.

M. Marani, E. Belluco, , A. D'Alpaos, A. Defina, S. Lanzoni, and A. Rinaldo. On the drainage density of tidal networks. *Water Resources Research*, 39(2):105–113, 2003.

M. Marani, S. Lanzoni, D. Zandolin, G. Seminara, and A. Rinaldo. Tidal meanders. *Water Resources Research*, 38(11):1225–1239, 8 November 2002.

D. S. McLusky. *The estuarine ecosystem*. Blackie, 1989.

J. Murray and A. Hawkins. Sediment transport in the Severn Estuary during the past 8000-9000 years. *J. Geol. Soc. London*, 132:385–398, 1977.

R. M. Myrick and L. B. Leopold. Hydraulic geometry of a small tidal estuaty. *Geological Survey Professional Paper*, 422-B:18 pp., 1963.

M. P. O'Brien. Equilibrium flow areas of inlets on sandy coasts. *J. Waterw. Harbors Coastal Eng. Div., Am. Soc. Civ. Eng.*, 95(303-3):43–52, 1969.

G. M. E. Perillo. *Geomorphology and sedimentology of estauries*. Elsevier, 1995.

J. E. Pizzuto. Numerical simulation of gravel river widening. *Water Resources Research*, 26(9):1971–1980, September 1990.

D. Prandle. Tides in estuaries and embayments. In B. B. Parker, editor, *Tidal hydrodynamics*, pages 125–152. John Wiley & Sons, 1991.

D. Prandle. Relationship between tidal dynamics and bathymetry in strongly convergent estuaries. *J. Physical Oceanography*, 33(12):2738–2750, 2003.

A. Rinaldo, S. Fagherazzi, S. Lanzoni, M. Marani, and W. E. Dietrich. Tidal Networks 2. Watershed delineation and comparative network morphology. *Water Resources Research*, 35(12):3905–3917, December 1999a.

A. Rinaldo, S. Fagherazzi, S. Lanzoni, M. Marani, and W. E. Dietrich. Tidal Networks 3. Landscape-forming discharges and studies in empirical geomorphic relationships. *Water Resources Research*, 35(12):3891–3904, December 1999b.

H. H. G. Savenije. A simple analytical expression to describe tidal damping or amplification. *Journal of Hydrology*, 243:205–215, 2001.

H. H. G. Savenije. The width of a bankfull channel; lacey's formula explained. *Journal of Hydrology*, 276:176–183, 2003.

H. M. Schuttelaars and H. E. de Swart. An idealized long-term morphodynamic model of a tidal embayment. *Eur. J. Mech. B/Fluids*, 15(1):55–80, 1996.

H. M. Schuttelaars and H. E. de Swart. Initial formation of channels and shoals in a short tidal embayment. *J. Fluid Mech.*, 127:15–42, 1999.

H. M. Schuttelaars and H. E. de Swart. Multiple morphodynamic equilibria in tidal embayments. *J. Geophys. Res.*, 105:24105–24118, 2000.

G. Seminara, S. Lanzoni, M. Bolla Pittaluga, and L. Solari. Estuarine patterns: an introduction to their morphology and mechanics. In *Fluid Mechanical Problems in Geomorphology, Lecture Notes in Physics*. Springer, December 2001.

S. R. G. Shetye and A. D. Gouveya. On the role of geometry of cross-section in generating flood dominance in shallow estuaries. *Estuarine, Coast. and Shelf Sci.*, 35:113–126, 1992.

P. E. Speer and D. G. Aubrey. A study of non-linear tidal propagation in shallow inlet/estuarine systems. Part ii: Theory. *Estuarine, Coast. and Shelf Sci.*, 21:207–224, 1985.

The Open University. *Waves, tides and shallow-water processes*. Pergamon, 1989.

I. Todeschini, M. Toffolon, and M. Tubino. Long-term evolution of self-formed estuarine channels. In *Proceedings of 4th RCEM Symposium*, pages 161–170, Urbana (Illinois, USA), 7-10 October 2005.

I. Todeschini, M. Toffolon, G. Vignoli, and M. Tubino. Bottom equilibrium profiles in convergent estuaries. In *Proceedings of 3rd RCEM Symposium*, pages 710–722, Barcelona (Spain), 1-5 September 2003.

M. Toffolon. *Hydrodynamics and morphodynamics of tidal channels*. PhD thesis, PhD thesis, University of Padova, 2002.

M. Toffolon, G. Vignoli, and M. Tubino. Large amplitude effects on tidal amplification in convergent estuaries. In *Proceedings, 3rd IAHR Symposium on River, Coastal and Estuarine Morphodynamics*, volume 2, pages 761–772, Barcelona (Spain), 1-5 September 2003.

A. R. van Dongeren and H. J. de Vriend. A model of morphological behaviour of tidal basins. *Coastal Engineering*, pages 287–310, 1994.

L. C. van Rijn. Sediment transport. Part II: Suspended load transport. *Journal of Hydraulic Engineering, ASCE*, 110(11):1613–1641, November 1984.

Z. B. Wang, B. Karssen, R. J. Fokkink, and A. Langerak. A dynamic-empirical model for estuarine morphology. In Dronkers and Scheffers, editors, *Physics of Estuaries and Coastal Seas*, pages 279–286. Balkema, Rotterdam, 1998.

J. T. Wells. Tide-dominated estuaries and tidal rivers. In G. M. E. Perillo, editor, *Tidal hydrodynamics*, pages 179–205. Elsevier, 1995.

L. Wright, J. Coleman, and B. Thom. Processes of channel development in a high-tide-range environment: Cambridge Gulf-Ord River delta, Western Autralia. *J. Geol.*, 81: 15–41, 1973.

List of Figures

List of Tables